Modelling of the electrode-auditory nerve fibre interface in cochlear prostheses

by

Tania Hanekom

Submitted as partial fulfilment of the requirements for the degree

Philosophiae Doctor

in the

Faculty of Engineering, Built Environment and Information Technology

University of Pretoria, Pretoria

June 2001

Modelling of the electrode-auditory nerve fibre interface in cochlear prostheses

by

Tania Hanekom

Advisor : Prof PJ Cilliers

Departement : Electrical, Electronic and Computer Engneering

Degree : Philosophiae Doctor

KEYWORDS

cochlear implant; intracochlear electrode array; electrode configuration; electrode geometry; modelling; finite element method; potential distribution; neural excitation patterns; multipolar stimulation; three-dimensional

ABSTRACT

The objective of this thesis is to provide additional insight into the electrode array-nerve fibre interface that exists in the implanted cochlea and to facilitate investigation of new electrode arrays in interaction with the cochlea and auditory nerve fibres. The focus is on potential distributions and excitation profiles generated by different electrode array types and factors that could have an influence on these distributions and profiles.

Research contributions made by the thesis are the creation of a detailed 3-D model of the implanted cochlea that accurately predicts measurable effects in cochlear implant wearers and facilitates effortless simulation of existing and new electrode array variations; the establishment of the important anatomical structures required in a 3-D representation of the implanted cochlea; establishment of evidence that array location is the primary parameter that controls spread of excitation; definition of the critical focussing intensity of intracochlear electrode pairs; confirmation that

monopolar stimulation could deliver focussed stimulation to approximately the same degree than that delivered by widely spaced electrode configurations and that the use of monopolar configurations over bipolar configurations are therefore advantageous under certain conditions; explanation of the effect that encapsulation tissue around cochlear implant electrodes could have on neural excitation profiles; extension of the information available on the focussing ability of multipolar intracochlear electrode configurations; and establishment of evidence that a higher lateral electrode density could facilitate better focussing of excitation, continuous shaping of excitation profiles and postoperative customization of electrode arrays for individual implant wearers.

Modellering van die elektrode-ouditiewe senuweevesel-intervlak in kogleêre prosteses

deur

Tania Hanekom

Promotor	:	Prof PJ Cilliers
Departement	:	Elektriese, Elektroniese en Rekenaar-Ingenieurswese
Graad	:	Philosophiae Doctor

SLEUTELWOORDE

kogleêre inplant; intrakogleêre elektrodeskikking; elektrodekonfigurasie; elektrodegeometrie; modellering; eindige element metode; potensiaalverspreiding; senuweeopwekkingspatrone; multipoolstimulasie; drie-dimensioneel

OPSOMMING

Die doel van hierdie proefskrif is om addisionele inligting omtrent die elektrodeskikking-senuweevesel-intervlak wat in die geïnplanteerde koglea bestaan te voorsien en om die ondersoek van nuwe elektrodeskikkings in wisselwerking met die koglea en gehoorsenuweevesels te fasiliteer. Die fokus is op potensiaalverspreidings en senuweeveselopwekkingspatrone wat deur verskillende tipes elektrodeskikkings geskep word en die faktore wat hierdie verspreidings en patrone kan beïnvloed.

Die navorsingsbydrae wat deur die proefskrif gemaak word kan opgesom word as die skep van 'n gedetailleerde drie-dimensionele model van die geïnplanteerde koglea wat die tendense van meetbare effekte in persone met kogleêre inplantings akkuraat kan voorspel en maklike simulasie van bestaande en nuwe elektrodeskikkingvariasies fasiliteer; bevestiging van die belangrike anatomiese strukture wat nodig is om in 'n drie-dimensionele voorstelling van die geïnplanteerde

koglea in te sluit; vestiging van bewyse dat skikkingposisie die primêre parameter is wat die verspreiding van senuweeveselopwekking beheer; definisie van die kritiese fokuseringsintensiteit van intrakogleêre elektrodepare; bevestiging dat monopolêre stimulasie gefokusde stimulasie kan lewer tot dieselfde mate as wyd gespasieerde elektrodepare en dat dit onder sekere omstandighede voordelig is om monopolêre stimulasie te gebruik eerder as bipolêre stimulasie; verklaring van die effek wat enkapsuleringsweefsel om intrakogleêre elektrodes op senuweeaktiveringspatrone het; uitbreiding van beskikbare inligting oor die fokuserende vermoë van multipoolelektrodekonfigurasies; vestig van bewyse dat 'n hoër laterale elektrodedigtheid beter opwekkingsfokusering, kontinue vorming van opwekkingspatrone en postoperatiewe aanpassing van elektrodeskikkings vir individuele persone kan moontlik maak.

I wish to express my thanks to

My colleague and husband, Johan, for encouragement, love, valuable comments on the work in this thesis and patience with the chaos in our house while at the same time working on his own PhD.

My family who gave up much time that I should have spent with them to enable me to complete this thesis.

Our Heavenly Father for much grace and help.

My mother for patiently editing the language of this manuscript and of the articles that resulted from it.

Contents

List of abbreviations

2-D	two-dimensional
3-D	three-dimensional
AF	activating function
AR	apical reference
BP	bipolar
BP+1	bipolar + 1
BP+2	bipolar + 2
BP+3	bipolar + 3
CFI	critical focussing intensity
CGND	common ground
BL	banded electrode array at lateral location relative to the modiolus
DOF	degree of freedom
FE	finite element
F-fibre	used when referring to results generated with the full nerve fibre model
GSEF	generalized Schwarz-Eikhof-Frijns (nerve fibre model)
LP	lumped parameter
MONO	monopolar
OR	offset radial
BM	banded electrode array in a medial location relative to the modiolus
R	radial
SAS	simultaneous analogue stimulation
SE	Schwarz-Eikhof (nerve fibre model)
T-fibre	used when referring to results generated with the truncated nerve fibre model
UF	unimodal focussing ability

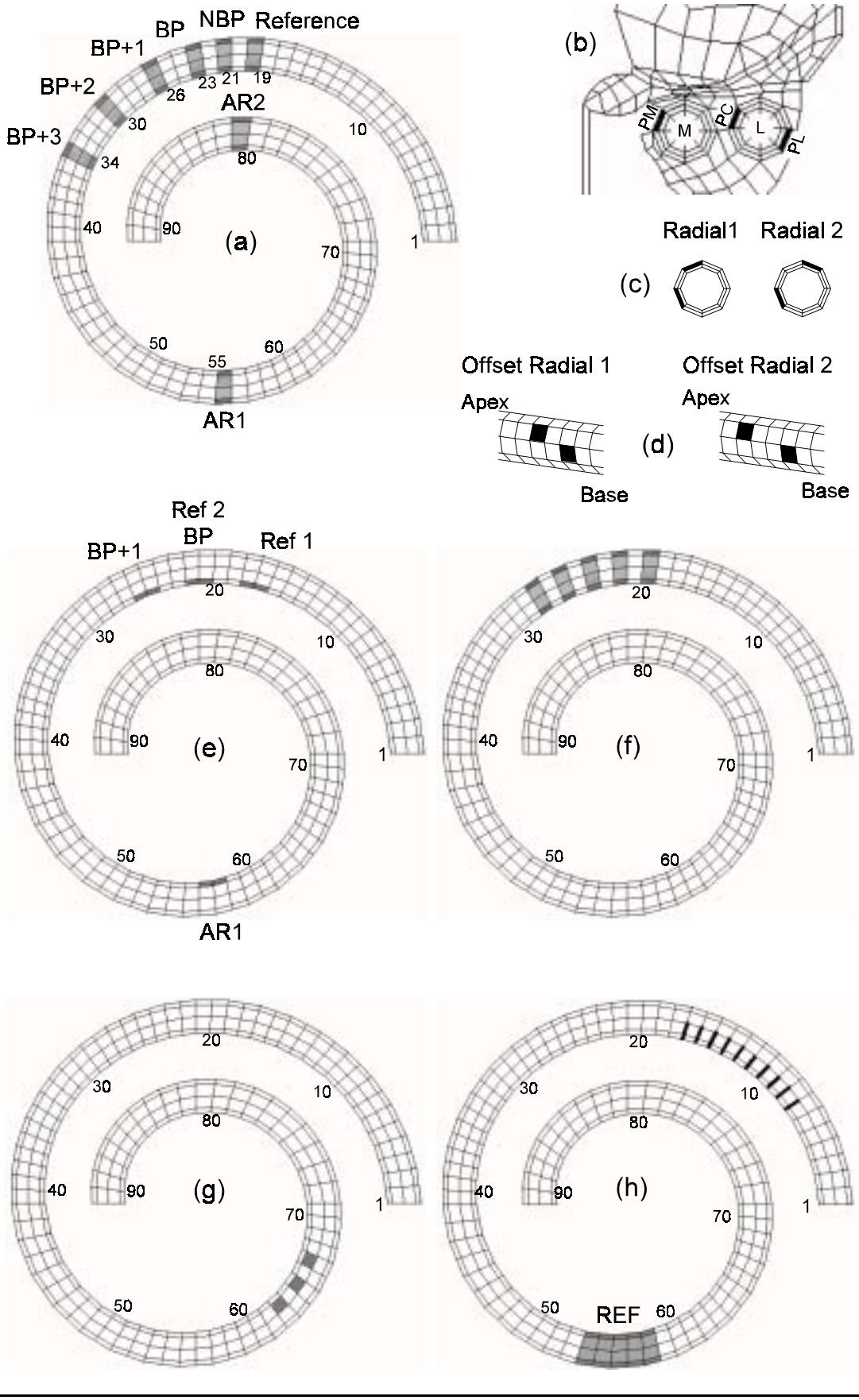

Summary figure of electrode configurations on previous page.

(a) Locations of electrode contacts for NBP, BP, BP+1, BP+2, BP+3, AR1 and AR2 banded (BM and BL) and point (PM, PC and PL) electrode configurations. Electrode contacts for banded electrode configurations are shown. The reference electrode is used as the stimulating electrode for monopolar stimulation. For widely spaced quadrupolar and tetrapolar electrode configurations (Chapter 5), the Reference electrode and BP, BP+1, BP+2 and BP+3 electrodes are used.

(b) Location of electrode contacts for point electrode configurations (PM, PC and PL) on the perimeter of the electrode carriers. The location of the medial (M) electrode array and the lateral (L) electrode array are also indicated.

(c) Location of electrode contacts on perimeter of electrode carrier for radial electrode configurations.

(d) Location of electrode contacts on perimeter of electrode carrier for offset radial electrode configurations.

(e) Location of electrode contacts for Hifocus-like electrode configurations. The BP and BP+1 configurations use Ref 1 as return electrode while AR1 uses Ref 2 as return electrode. Ref 2 is used as the stimulating electrode contact for monopolar stimulation.

(f) Electrode contact locations for the narrowly spaced quadrupolar and tetrapolar electrode configurations studied in Chapter 5.

(g) Location of electrode contacts for the tripolar electrode configurations studied in Chapter 5. The radial electrode configuration is similar to Radial 2 in (b) except that the segments are displaced anticlockwise with one segment.

(h) Location of the electrode contacts (thick lines) for the pseudo-continuous electrode configuration studied in Chapter 5. The reference electrode (REF) for a AR-type return electrode is shaded.

Chapter 1
INTRODUCTION

It is generally accepted that cochlear prostheses can be successfully used to treat profound deafness (National Institutes of Health, 1995). In a study performed by Kou, Shipp and Nedzelski (1994) it was found that the majority of the cochlear implant subjects in the group studied, experienced a substantial improvement in independence and communication confidence after cochlear implantation. This finding was ascribed to an increased ability of implant wearers to communicate via hearing and an increased awareness of environmental sounds. However, much interperson variation in performance still exists and subjects do not all experience the same benefits from their cochlear implants.

The functioning of cochlear implants is still not well understood despite much research that has been done on the interaction between the implant and the target nerve fibres. To improve and ultimately guarantee subject benefits from cochlear implants, the mechanisms underlying the functioning of these devices have to be studied so that improvements can be based on a detailed understanding of the system as a whole.

Chapter 1 serves to place the research described in this thesis concerning the physical interaction between the implant and the target nerve fibres in context with research to date. Specific emphasis is placed on the distribution of electrical potentials in the cochlea and the neural excitation patterns following electrical stimulation. Factors that have an influence on these distributions are also discussed.

1 CONTEXT OF THE PROBLEM

1.1 Basic operation of cochlear implants

The peripheral auditory system consists of three primary parts: the outer ear, the middle ear and the inner ear or cochlea. The cause of profound deafness is in many cases located in the cochlea, where pressure waves caused by sounds have to be transduced to neural signals travelling to the higher auditory centres of the brain. The transducing mechanism between pressure waves and the electrical nerve impulses are hair cells which are located inside the cochlea. Profound deafness is in many cases associated with the loss of hair cells. If the hair cells are damaged or destroyed, no neural information can reach the higher auditory centres in the brain even though the neural pathways from the cochlea to the brain are intact. Deafness caused by hair cell loss can mostly be rehabilitated with a cochlear implant by directly activating the auditory nerve fibres through electrical stimulation (Black & Clark, 1980; Clark, 1996; Clark et al., 1990; Girzon, 1987; Rebscher et al., 1996).

Cochlear implants normally consist of three primary parts: an external signal processing unit, a telemetry system and an implanted stimulator-electrode system. The external signal processing unit detects sounds with a microphone and converts these sounds to an electrical code. This code is transmitted through the skin via a telemetry system to the implanted stimulator. The stimulator circuit uses the code to generate electrical signals that drive the electrode (in the case of single channel devices) or electrode array[1] (in the case of multi-channel devices) which is usually placed close to the residual nerve fibres inside the cochlea. The objective of intracochlear stimulation is to replicate the neural activity produced in the normal ear during acoustic stimulation (Girzon, 1987; Suesserman & Spelman, 1993). When a

[1]In this thesis the term "electrode" is used when reference is made to a single electrode contact. The electrode array, consisting of a silastic electrode carrier, electrode contacts and wires connecting the electrode contacts to the implanted electronics, is referred to as the "electrode array" or simply the "array".

cochlear implant is used, the entire peripheral auditory system up to the nerve fibres is essentially bypassed - the cochlea merely serves as a convenient mounting space for the electrode array since it contains the terminals of the auditory nerve fibres as well as an electrolyte (perilymph) to serve as conduction pathway between the electrodes and the nerve fibres.

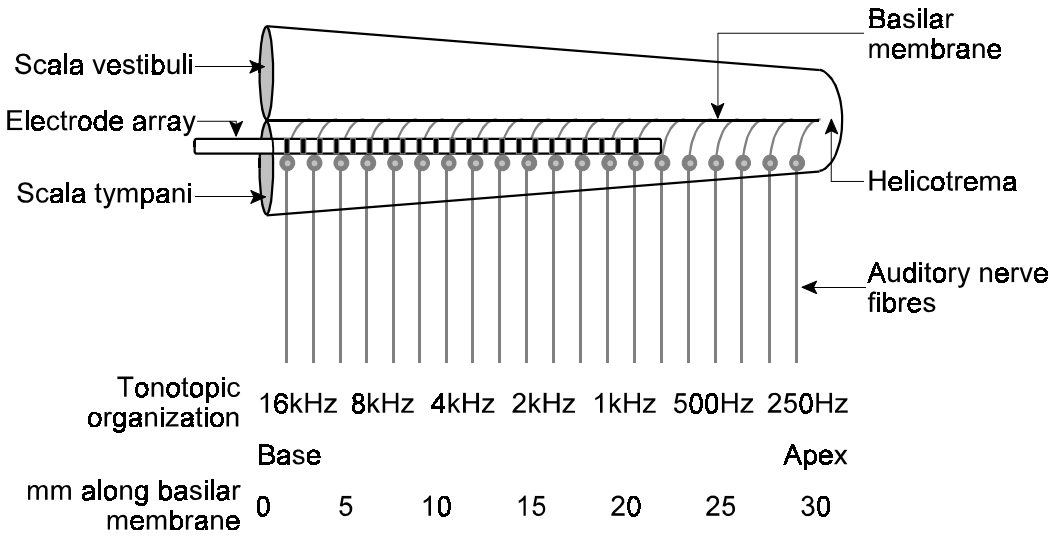

Figure 1.1. A simplified unrolled representation of the cochlea showing the auditory nerve fibres, the tonotopic organization of these nerve fibres and an intracochlear electrode array in the scala tympani.

The auditory nerve fibres inside the cochlea are tonotopically arranged (Figure 1.1) so that those nearest to the base of the cochlea detect high frequencies and those nearest to the apex low frequencies (Eddington et al., 1988; Frijns, 1995). Multichannel implants currently make use of this tonotopic arrangement of the auditory nerve fibres to produce perceptions of changing pitch. By spacing the electrodes along the length of the cochlea (Figure 1.1), different populations of nerve fibres can be excited to produce different perceptions of pitch (Eddington et al., 1988; Frijns, 1995; Rebscher et al., 1996; Suesserman & Spelman, 1993).

1.2 Understanding and improving cochlear implants

Rubinstein (1988) identified three basic processes that have to be understood before a complete theory of the speech information transfer in cochlear implant subjects can be structured. These three processes include conversion of speech into electrical stimuli, the nerve fibre-electrode interface and information processing by the central auditory nervous system. Figure 1.2 shows a diagrammatic representation of the broad research areas concerned with each of the processes.

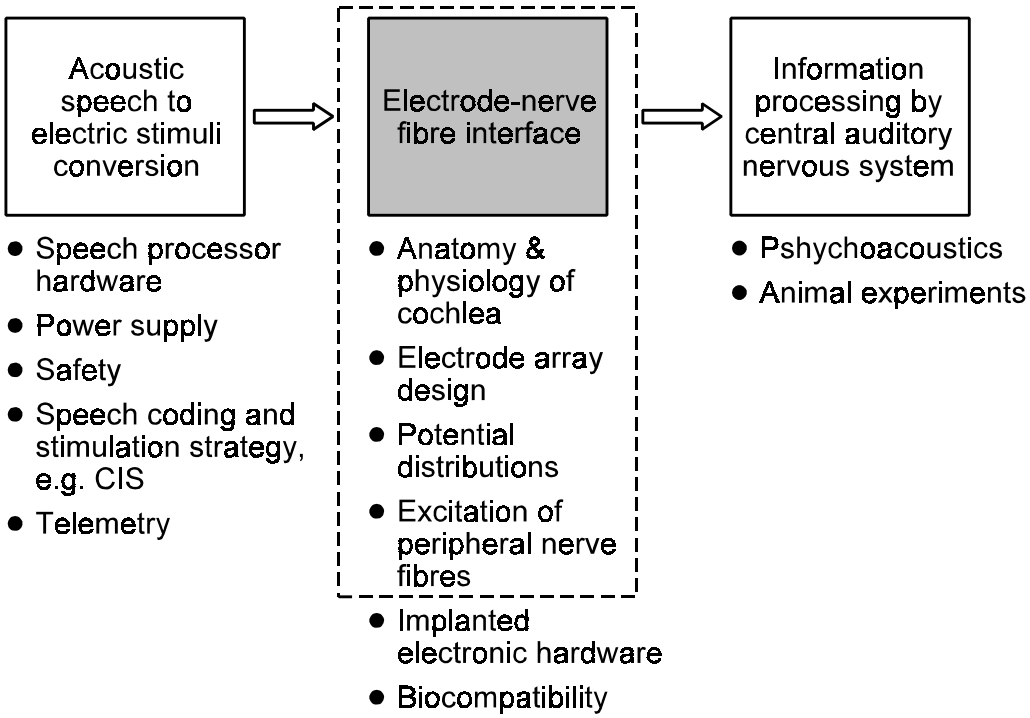

Figure 1.2. Diagrammatic representation of the broad areas in cochlear implant research. The research area addressed in this thesis is indicated with a dashed block.

Vast variations in the hearing sensations experienced by different users of cochlear implants bear witness to the fact that none of these processes is fully understood yet. Variations manifest in aspects such as the unpredictability of the performance of a cochlear implant subject preoperatively (Clark, 1996), the inability of most implant users to perceive music (Fujita & Ito, 1999), and the fact that many users cannot use a telephone or struggle to follow speech in noisy environments (Hirsch, 1993). Perceived auditory sensations vary as a result of complex interactions between

several patient and device related factors, i.e. electrode placement, shape and size of the cochlea, number and distribution of surviving nerve fibres inside the cochlea and tissue reactions to the implanted electrode (Rebscher et al., 1996; Ruddy & Loeb, 1995).

To address variations in perception, Loizou (1999) pointed out that (1) the factors that contribute to variability in performance among patients must be identified, (2) preoperative procedures that can predict how well a patient will perform with a particular type of cochlear implant have to be developed and (3) better electrodes capable of providing a high degree of specificity have to be designed. Activation of sensory nerve fibres by electrical stimulation with a high degree of specificity is regarded as one of the main problems in cochlear prostheses research (Girzon, 1987; Kral et al., 1998; Loizou, 1999; Miller & Spelman, 1990; Ruddy & Loeb, 1995). Researchers active in the field agree that better models of the three-dimensional structure of the cochlea are necessary, that better models of the current distribution are required, and that this knowledge can lead to better electrode designs (Miller & Spelman, 1990; Suesserman & Spelman, 1993).

1.3 Volume conduction models of the implanted cochlea[2]

Girzon (1987), Finley (1990), Frijns et al. (2000; 1995) and Rattay (2000) made important contributions in the field by creating volume conduction models to predict the potential distributions around intracochlear electrode arrays and developed neural models to predict nerve fibre excitation patterns around electrode pairs.

However, existing detailed volume conduction models are limited to spiralling models for either the guinea pig cochlea (much anatomical detail included) (Frijns, Briaire, & Schoonhoven, 2000) or a simplified human cochlea (Rattay, Leao, & Felix, 2000). The models also do not provide an easy method to test structural and geometrical

[2]The phrase "implanted cochlea" is used to refer to a cochlea that contains an implanted electrode array.

variations of the electrode array or variations in the anatomical structure of the cochlea. The degree of anatomical detail that is necessary to include in such models has not yet been established either.

1.4 Potential distributions and neural excitation patterns

1.4.1 Array location, electrode configuration and nerve fibre properties

Electrical potential distributions at the target nerve fibres are dependent on the material, size, shape and impedance of the electrodes, the amplitude and waveform of the electrical stimulus, the distance from the electrode to the nerve fibre and the characteristics of the tissues surrounding the implant (Marsh, Coker, & Jenkins, 1992; Ruddy & Loeb, 1995). Threshold currents at which a nerve fibre will be activated and spread of neural activation are functions of these electrical fields and of the electrical properties of the nerve fibres, their dimensions and survival patterns and higher order processing in the central nervous system. The closer an electrode is to the nerve fibres, the less current is required to elicit a threshold response (Shepherd, Hatsushika, & Clark, 1993), the larger the dynamic range of stimulation is and the more discrete the stimulated nerve populations are (Skinner et al., 1994; Wang et al., 1996).

Experimental data of Pfingst et al. (1995) showed that the intensity of the potential fields generated at a specific stimulation current changes if the electrode configuration is changed. It has been experimentally verified that lower currents are required to reach the psychophysical detection threshold if widely spaced bipolar[3] electrode pairs are used for stimulation than when more narrowly spaced pairs are

[3]The term *bipolar electrode pair* is normally used when referring to the Nucleus electrode array from Cochlear Corporation Ltd. A bipolar (BP) electrode configuration refers to an electrode pair consisting of two neighbouring electrode contacts which are both located inside the cochlea. A bipolar+1 (BP+1) electrode configuration refers to an electrode pair separated by one electrode contact, bipolar+2 (BP+2) by two electrode contacts, bipolar+3 (BP+3) by three electrode contacts, etc. A "widely spaced" bipolar pair refers to a BP+m electrode configuration where m>0.

used (Pfingst, Morris, & Miller, 1995; Shepherd, Hatsushika, & Clark, 1993). Some auditory prostheses make use of electrode spacing to control the loudness of electrical stimulation and to ensure that the device can deliver adequate current to effect stimulation (Pfingst, Morris, & Miller, 1995). The lowest threshold for electrical stimulation is usually obtained with monopolar[4] electrode configurations.

Research contributions in this area can potentially be made by quantification of the discussed observations in terms of parameter variations such as electrode separation, array location and survival patterns of auditory nerve fibres.

1.4.2 Postoperative changes

Changes to the electrode-nerve fibre interface that occur after implantation could influence neural excitation patterns. Such changes could include further degeneration of the nerve fibres and the formation of scar tissue and bone around the electrode array.

Implantation and direct stimulation of the nerve fibres in the cochlea do not cause degradation of these structures if no trauma is caused. Rather, electrical stimulation may preserve existing neural processes and decrease or eliminate the normal sequence of neural degeneration that follows deafness (Leake et al., 1992; Shepherd, Hatsushika, & Clark, 1993). However, it has been shown that trauma to the cochlea is not uncommon during insertion of an electrode array (Welling et al., 1993). It includes scraping or tearing of the endosteum lining the medial wall of the scala tympani, damage to the osseous spiral lamina including fracture, perforation of the basilar membrane, including deviation of the electrode into the scala media or scala vestibuli, and damage to the spiral ligament (Rebscher et al., 1996). Studies in cats have shown that even minimal damage to the spiral ligament, basilar

[4]A monopolar electrode configuration refers to an electrode pair consisting of a stimulating electrode that is located inside the cochlea, normally the scala tympani, and a return electrode that is located outside the cochlea, for example in the temporalis muscle.

membrane or osseous spiral lamina results in direct rapid loss of peripheral dendrites and spiral ganglion cells (Leake et al., 1992).

Trauma to the cochlea during electrode insertion could also cause tissue reactions such as the formation of scar tissue or new bone at the implant-tissue interface (Webb et al., 1988; Zappia et al., 1991). Grill and Mortimer (1994) reported that the resistivity of encapsulation tissue around implanted electrodes is sufficient to alter the shape and magnitude of the electric field generated by such electrodes. Postoperative changes to the cochlea and the implant-tissue interface could be responsible for threshold variations that are frequently observed in the months following implantation (de Sauvage et al., 1997; Pfingst, 1990).

The mechanisms responsible for postoperative changes in threshold currents are not clearly understood yet (Brown et al., 1995; Miller, Morris, & Pfingst, 2000) and require further investigation.

1.5 New electrode arrays

In an NIH report on the development of speech processors for cochlear prostheses Wilson, Lawson and Zerbi (1996) commented on existing cochlear electrode designs and proposed the development of an electrode array with a greater number of electrodes which are spaced closer to the medial wall of the scala tympani as a new generation solution to overcoming deficiencies in existing designs. The design of improved cochlear prostheses requires a better understanding of the factors that dictate the potential distributions and therefore the neural activation patterns inside the implanted cochlea (Girzon, 1987).

Knowledge of the exact location of the electrode array within the cochlea is important to improve electrical stimulation of the auditory nerve (Gstoettner et al., 1999). To control the location of the array, state of the art intracochlear electrode arrays assume a perimodiolar position inside the scala tympani (Schindler & Kessler, 1989; Tykocinski et al., 2000). This has the additional benefits of lowering threshold

currents, limiting spread of excitation and increasing dynamic range (Tykocinski et al., 2000). However, the number of electrode contacts that are currently used is between 16 and 22 which is very few compared to the approximately 30 000 nerve fibres (Allen, 1985) that must be activated by these electrodes. Furthermore, stimuli are mostly delivered nonsimultaneously to electrode pairs to prevent crosstalk between electrode pairs, corrosion of the electrode metal and uncontrollable spread of excitation. Recent advances in the development of intracochlear electrode arrays include better focussing of excitation and limiting of lateral current spread, thus allowing simultaneous stimulation via all electrode pairs (Advanced Bionics Corporation, 2000). Research in this field is continuing and could be complemented by accurate models of the implanted cochlea.

2 RESEARCH GAP

From the deficiencies in the understanding of the functioning of cochlear implants with regard to the nerve fibre-implant interface, the following research gap has been identified:

1) The construction of a *detailed* three-dimensional volume conduction model of the implanted cochlea that can be adapted to investigate potential distributions and neural excitation patterns as a result of
   a) stimulation with existing electrode configurations;
   b) variations in electrode configuration, electrode geometry and array location;
   c) stimulation with new, improved electrode arrays; and
   d) variations in the model structure or current pathways such as the absence or presence of electrode encapsulation and cochlear structures, i.e. the helicotrema and the Organ of Corti.
2) Qualitative and quantitative characterization of the effects of the above-mentioned aspects on auditory nerve excitation patterns to contribute

towards the knowledge base on the implant-nerve fibre interface.

The area within cochlear implant research that is addressed in this thesis is indicated with a dashed block in Figure 1.2.

3 OBJECTIVE AND OVERVIEW OF THIS STUDY

The objective of this study is to provide additional insight into the functioning of current intracochlear electrode arrays and also to facilitate investigation of new electrode arrays. The focus is on potential distributions and excitation profiles generated by different electrode array types and factors that could have an influence on these distributions and profiles.

Chapter 2 deals with the generation of a three-dimensional finite element model of the implanted cochlea to calculate potential distributions on the nerve fibres as a result of electrical stimulation. The interface of the finite element model with an existing nerve fibre model and a modification of the nerve fibre model to represent degenerated nerve fibres are described. In Chapter 3 the effect of electrode geometry and configuration, array location, anatomical structure of the cochlea and peripheral dendrite degeneration are investigated. Chapter 4 illustrates and explains the effect of scar tissue around intracochlear electrodes on excitation patterns while Chapter 5 investigates multi-electrode configurations that could be used for focussing and continuous, simultaneous shaping of the excitation profile of the auditory nerve fibres. The thesis is concluded with a general discussion and a summary of results and findings in Chapter 6.

Chapter 2
BACKGROUND AND MODELLING APPROACH

1 INTRODUCTION

This chapter describes the generation of a three-dimensional (3-D) model of the implanted cochlea. The objective with the model is to estimate the *electrical potential distributions at the target auditory nerve fibres* caused by current injection into the deaf cochlea. The complex 3-D structure of the cochlea had to be conserved so that the effect of cochlear structures, neighbouring cochlear canals and conduction along the fluid-filled canals of the cochlea could be incorporated in the potential estimates (and thus the neural excitation patterns). The proposed model is classified as a volume conduction model. Since the geometry of the cochlea is complex, accurate analytical solutions for the volume conduction problem, i.e. calculation of potential distributions in the implanted cochlea with closed-form equations, do not exist. Analytical models only give a qualitative insight into the fields generated by intracochlear stimulation (Jolly, Spelman, & Clopton, 1996). Numerical methods are required for an accurate description of field distributions (Steele, 1987). The volume conduction problem of the implanted cochlea is addressed by various numerical methods: lumped parameter (LP) models (Johnstone, Johnstone, & Pugsley, 1966; Kral et al., 1998; Rodenhiser & Spelman, 1995; Strelioff, 1973; Suesserman & Spelman, 1993), finite difference methods (Girzon, 1987), boundary element methods (Briaire & Frijns, 2000; Frijns, de Snoo, & Schoonhoven, 1995) and the finite element (FE) method (Finley, Wilson, & White, 1990; Rattay, Leao, & Felix, 2000).

The FE method was selected for this study because of the ease with which different array locations and electrode configurations could be defined without remeshing the volumes. The model described here is a detailed 3-D spiralling representation of the

first one-and-a-half turns of the implanted cochlea. Electrodes and electrode arrays were simply activated or deactivated by changing the material properties of the applicable elements. The FE model is coupled with a nerve fibre model to translate the potential distributions calculated with the FE model into neural excitation patterns. In this chapter the theoretical background pertaining to the volume conduction problem is discussed, the definition and construction of the model are outlined, and verification methods are presented.

2 THE FINITE ELEMENT MODEL

To determine the potential distributions as a result of intracochlear stimulation, a numerical linear field problem must be solved (Steele, 1987) using the FE method (the method selected for this study). The modelling approach can be broken down into four primary categories: definition of the problem, construction and solution of the FE model, data processing and verification of model integrity and results.

2.1 Definition of the problem

2.1.1 Problem domain and fields to be calculated

The problem domain consists of the cochlea embedded into the surrounding tissues, in this case the temporal bone. The cochlea consists of different tissues each having specific material properties. The problem domain can thus be divided into several subdomains each representing a specific tissue. Each subdomain is characterised by a linear, isotropic conductivity (except the peripheral axonal processes that have anisotropic conductivity). The electrical potential distributions as a result of an injected current have to be calculated at the target nerve fibres.

2.1.2 Equations to be solved

The problem is quasi-static since capacitive, propagation and inductive effects can be neglected (Plonsey, 1969; Steele, 1987) based on the approximation of all

cochlear tissues with purely resistive materials. Simulations are thus performed with low-frequency ac current (0 Hz). As a result, the current density ***J***, the electric field ***E*** and the scalar potential are purely spatial variables, which are directly proportional to the excitation current at any moment in time.

If a current source (stimulation current) I_s is applied, its value equals the divergence of the current density vector ***J***

$$I_s = \nabla \cdot \boldsymbol{J} . \tag{2.1}$$

The electric field is obtained by the negative gradient of the scalar potential , i.e.

$$\boldsymbol{E} = -\nabla\Phi . \tag{2.2}$$

According to Ohm's law the current density ***J*** and the electric field ***E*** are related by

$$\boldsymbol{J} = \frac{1}{\rho}\boldsymbol{E} , \tag{2.3}$$

where is resistivity in -m. Combining (2.1) to (2.3)

$$I_s = \nabla\cdot\boldsymbol{J} = \nabla \cdot (-\frac{1}{\rho}\nabla\Phi) = -\frac{1}{\rho}\nabla^2\Phi \tag{2.4}$$

$$\nabla^2\Phi = -\rho I_s \tag{2.5}$$

which is Poisson's equation for a static potential distribution due to a source I_s.

2.1.3 Boundary conditions

The first boundary condition is applied inside the FE model on the boundaries between cochlear structures. This boundary condition states that potentials $_j$ must

be continuous over boundaries, i.e.

$$\Phi_j = \Phi_{j+1} \tag{2.6}$$

The second boundary condition is applied on the outer boundaries of the model, i.e. on the outside of the bone cylinder. Since the model's outer boundaries (represented by surface **S** in Figure 2.1) are not insulating, current can emerge through them. This implies that the current density must be continuous in the direction normal to the surface **S** (Gonzalez & Huerta, 1979), i.e.

$$\boldsymbol{Jn}_j = \sigma_j \boldsymbol{En}_j = \sigma_j \frac{\partial \Phi_j}{\partial S} = \sigma_{j+1} \frac{\partial \Phi_{j+1}}{\partial S} = \sigma_{j+1} \boldsymbol{En}_{j+1} = \boldsymbol{Jn}_{j+1} \tag{2.7}$$

where $_j$ is the electrical conductivity and *S* is the boundary between different materials j and j+1.

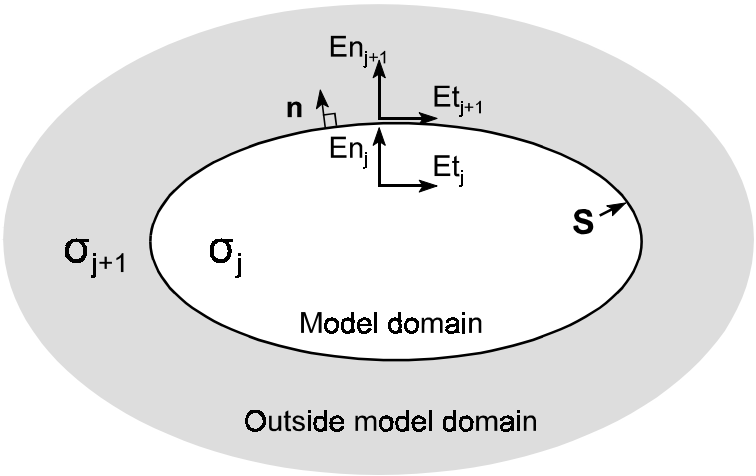

Figure 2.1. Schematic representation of boundary condition on a conducting boundary, i.e. a boundary between two materials where $_j$ and $_{j+1}$ have the same order of magnitude. **n** is a unit vector normal to surface **S**.

The third boundary condition exists on metallic surfaces, i.e. the electrode contacts, in contact with other conducting media, i.e. the cochlear tissues. These surfaces are

defined as equipotential surfaces (Girzon, 1987; Rubinstein, Soma, & Spelman, 1985).

2.2 Construction and solution of the FE model

2.2.1 Software package used

A multi-physics FE software package, *ANSYS*, was used to create the cochlear model. ANSYS uses Poisson's equation (2.5) as the basis for electric field analysis (ANSYS, 1999). Electric scalar potentials are the primary unknowns or nodal degrees of freedom (DOF) that are calculated. A steady-state current conduction analysis was performed to calculate the values of the scalar potential at predefined points on the target nerve fibres as a result of an injected stimulation current.

2.2.2 Elements used

A two-dimensional (2-D) geometry was used to extrude the cochlear structures from (Figure 2.4). This 2-D geometry was generated with 2-D plane elements with four nodes. Since the specific type of element can be used for coupled electrical and thermal analyses, it incorporates both voltage and temperature degrees of freedom at each node. The temperature degree of freedom was not used[1]. Triangular elements could be formed by combining two of the nodes.

The 3-D element used is similar to the 2-D plane element since it also incorporates both temperature and voltage degrees of freedom at its nodes. The temperature degree of freedom was again not active. The 3-D solid element is a brick element defined by 8 nodes and orthotropic material properties. Obtaining prism and tetrahedral element shapes is possible by combining the applicable nodes.

2.2.3 Discretization of model domain

Construction of the cochlear model was performed as follows. A 2-D line drawing of

[1]If the material properties corresponding to a specific degree of freedom are not specified, that degree of freedom becomes inactive.

the geometry of a slice through the cochlea was created through the GUI interface of the FE software package. The geometry is a combination of the geometry used by Finley, Wilson, & White (1990) (Figure 2.2) and a photomicrograph of the cochlea that indicates the position of the spiral ganglion shown in Figure 2.3 (Golden, 1997).

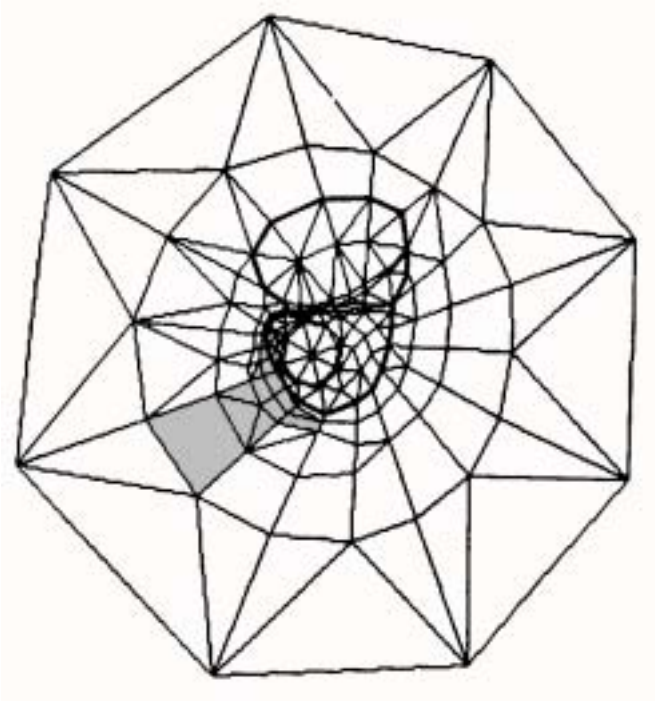

Figure 2.2. 2-D FE geometry used by Finley, Wilson and White (1990).

Different areas, each representing a specific cochlear structure (and thus a tissue), were defined by the lines. The areas were meshed using the plane elements described in section 2.2.2 (Figure 2.4). The 2-D geometry was then extruded into 3-D around the axis of the modiolus (Figure 2.5). To simplify the extrusion process, the diameters of the structures were not tapered toward the apical end of the model. The 3-D solid elements described in section 2.2.2 were used for the extrusion. A cylindrical coordinate system was used for the extrusion and the extrusion parameters are listed in Table 2.1. The first half-turn of the model was generated with 40, the second with 30 and the third with 20 equal *angle* segments.

This produced model segments with approximately equal lengths. Any of the segments could thus be used to construct electrode contacts, allowing the model to be used for different electrode configurations, e.g., pseudo monopolar electrode configurations where the return electrode is located on the opposite side (i.e., in the next half-turn) of the cochlea.

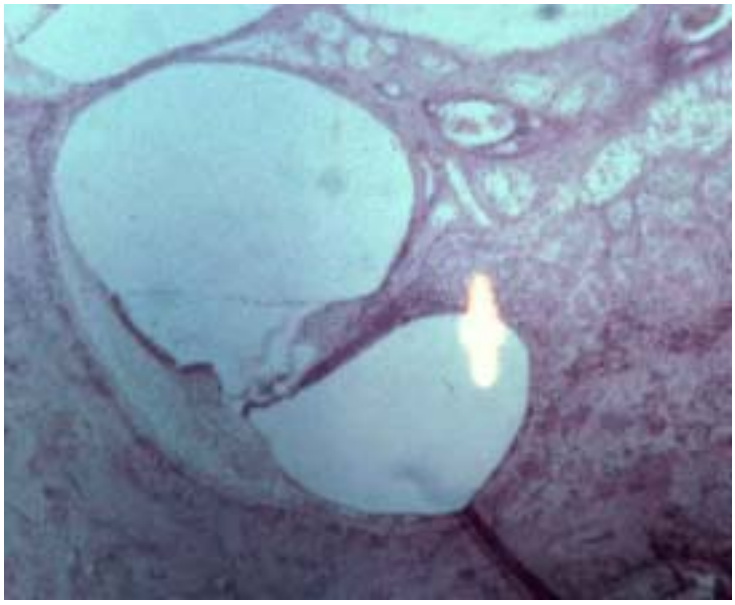

Figure 2.3. Photomicrograph of a section through one turn of the mammalian cochlea (Golden, 1997) that was used in the creation of the 2-D geometry of the FE model.

The method by which the 2-D model in Figure 2.4 was extruded into three dimensions (Figure 2.5) dictated the shape of the modelled spiral ganglion. A layer of axons was created during the extrusion process in the modiolus. The axons were extended so that the nerve fibres originating from the upper half-turn of the model extended downwards to at least below the scala tympani of the lower half-turn of the model. This provided a means of determining which of the axons inside the modiolus might be stimulated as a result of stimulation in the lower turn of the model. To be a true representation of the anatomy the axons should eventually combine into one nerve bundle. In the model this was realized by "filling" the volume enclosed by the medial axonal processes with nerve tissue, i.e. setting the material properties of elements in this volume to that of nerve tissue. The volume of nervous tissue

extends to the end of the bone cylinder thereby creating a low conductance path along the modiolus. Nerve tissue's conductance is approximately twice that of bone. Figure 2.5 does not show the nerve tissue enclosed by the medial axonal processes (which are protruding below the scalae).

2.2.4 Dimensions and anatomical detail of cochlear model

The model approximates the scalae of a human cochlea. However, the location of the modelled spiral ganglion corresponds with the location of the spiral ganglion in a guinea pig cochlea (Figure 2.4). In a human cochlea the spiral ganglion is located more towards the eight o'clock position (Figure 2.2). This inaccuracy should mainly influence absolute threshold current values and not the shape of potential distributions and therefore neural excitation patterns that are calculated with the model.

The modelled width of the scala tympani is 1.46 mm, which is less than 1% smaller than the average width of the human scala tympani measured by Hatsushika et al. (1990). The height of the modelled scala tympani is 1.14 mm, which is within 5% of the average measured height of the human scala tympani[2]. If the model were extruded to two-and-three-quarter turns the total height of the modelled cochlea would have been 6.6 mm and not 5 mm as with a human cochlea (Leeson & Leeson, 1981). The model is therefore approximately 25% higher from base to apex (measured along the modiolus) than a normal human cochlea. The base diameter of the modelled cochlea is approximately 8.5 mm which is within 6% of the 9 mm diameter reported by Leeson and Leeson (1981).

[2]The measured width of a number of scalae tympani in human cochleas varied from 3 mm at the base to 1.24 mm at a point 25 mm from the round window and the height between 2.4 mm and 0.8 mm over the same length of the scala tympani (Hatsushika et al., 1990).

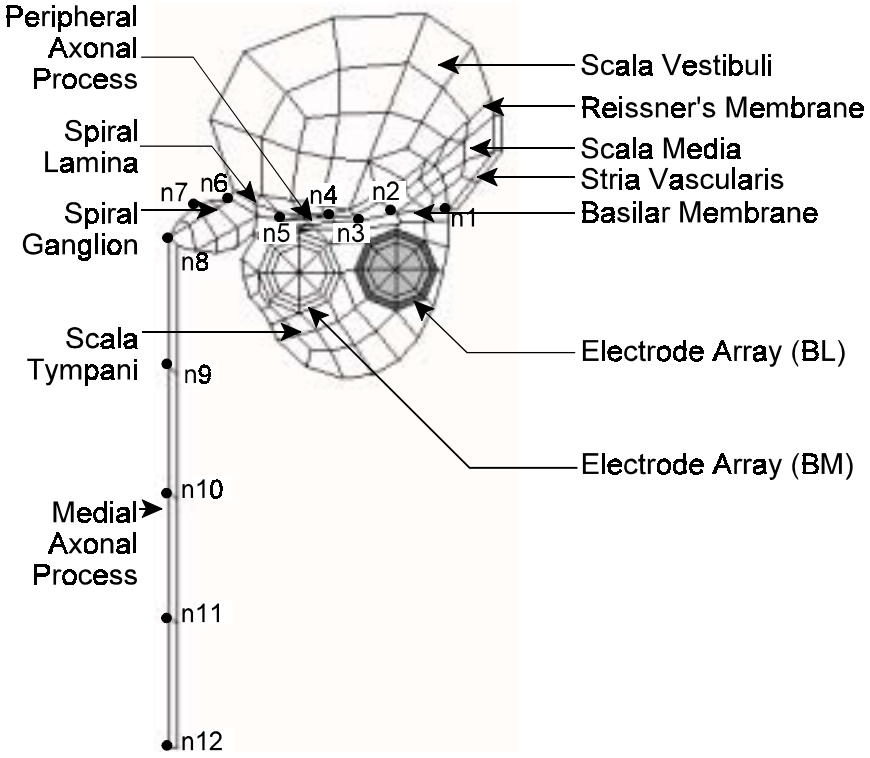

Figure 2.4. 2-D FE model geometry of a plane through one arch of the cochlea. The medial array (marked BM) can be seen as a circular geometry toward the top left of the scala tympani while the lateral array (marked BL) is located toward the top right of the scala tympani and is shaded in this illustration for clarity.

The length of the basilar membrane is 9.2 mm in the first half-turn of the cochlear model, 7.4 mm in the second half-turn and 5.6 mm in the third half-turn (i.e. a total length of 22.2 mm for the first one-and-a-half turns). If the extrusion were to be continued to two-and-three-quarter turns, the total length of the modelled basilar membrane would have been 28.6 mm. Although this is shorter than the average length of the cochlear duct (35 mm reported by Skinner et al. (1994)), Ulehlova, Voldrich and Janisch (1987) reported human cochlear duct lengths of between 28 and 40 mm. It is thus concluded that the dimensions used for the width and height of the cochlear model are representative of a typical human scala tympani.

Table 2.1. Extrusion parameters for 3-D model. Cylindrical coordinates r, and z are used.

[a] The segments per volume refer to the number of sections along the length of the modelled basilar membrane in a single volume extrusion, i.e. in the first half-turn two layers of elements are generated in each 9° volume slice while only one layer of elements is generated in the third half-turn in each volume slice.

Cochlear half-turn	Segments per volume[a]	Total number of volume segments	Total number of segments	r (mm)	(deg)	z (mm)
1st	2	20	40	-0.03	9	0.06
2nd	2	15	30	-0.04	12	0.08
3rd	1	20	20	-0.03	9	0.06

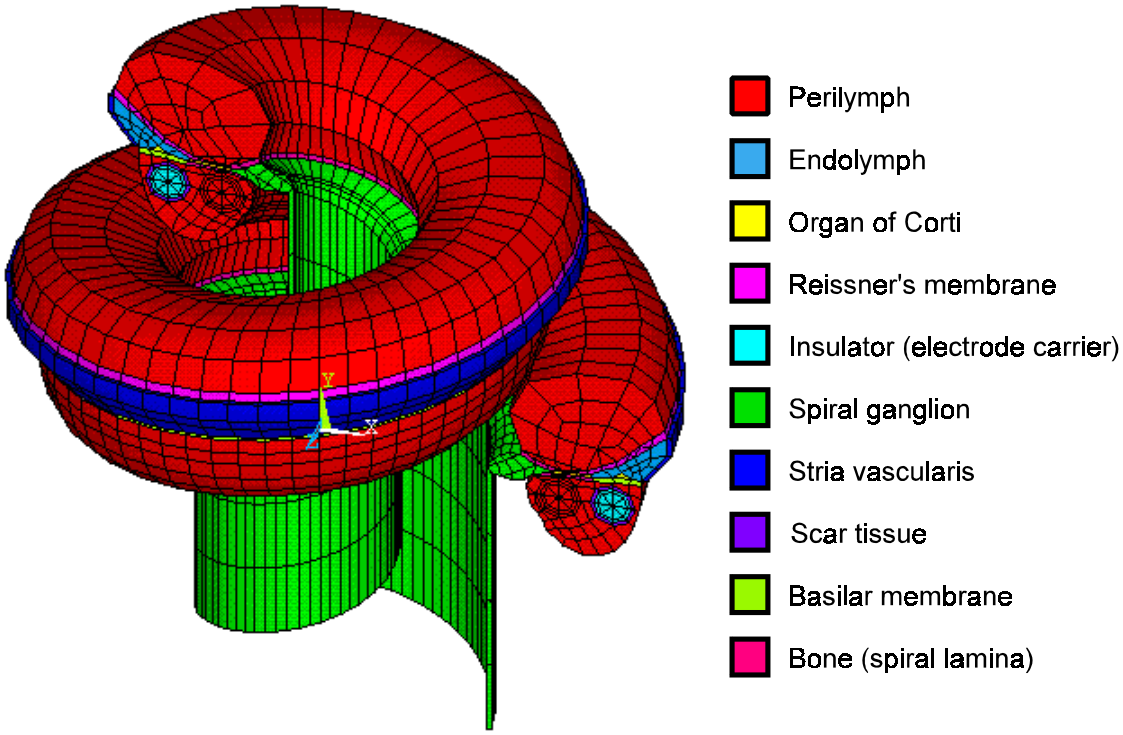

Figure 2.5. 3-D FE model geometry with nerve tissue (that was used to fill the modiolus) and surrounding bone tissue removed. Each colour represents a tissue or material type as indicated in the figure.

Shepherd et al. (1985) recorded insertion depths with a Nucleus electrode in human cadaver cochleas of between 15.5 and 27 mm with a mean insertion depth of 18.6 mm. Since the length of the modelled part of the cochlea is 22.17 mm, it will in most cases represent a cochlea with full electrode insertion. Anatomical studies showed that the straight Nucleus[3] electrode array is positioned approximately 1.0 mm from the modiolus at the extreme base of the scala and 0.8 mm 25 mm from the base (Shepherd, Hatsushika, & Clark, 1993) because of the tapering of the cochlea toward the apex. Other electrodes, e.g. the electrode used in the Clarion implant (Kessler, 1999), are designed to fit snugly around the modiolus. Although such a design does not guarantee a perimodiolar array location, an additional electrode positioner that can force the electrode array to the correct location has recently been developed (Advanced Bionics Corporation, 2000). For this reason the model was designed to allow two possible electrode array locations in the FE model, one close to the modiolus and one at a more lateral location distal to the nerve fibres. The abbreviations for the banded electrode arrays are shown in Figure 2.4 to indicate the two locations: BM indicates the *b*anded *m*edial electrode array and BL indicates the *b*anded *l*ateral electrode array. The distance from the modiolus remained constant over the entire length of the scala tympani for both electrode arrays.

Each electrode in the model consists of a cylindrical core and two external layers (Figure 2.4). Segments of the layer in direct contact with the core were defined as band electrode contacts by setting the resistivity of these segments to that of a conductor. The material properties of the outer layer were set to those of perilymph or scar tissue for this case. The outer layer was also used to create point electrode contacts. Material properties of the remaining part of the outer layer, the inner layer and the core were set to that of an insulator when modelling point electrodes.

[3]The Nucleus implant (Clark, 1996) is a cochlear implant manufactured by Cochlear Corporation.

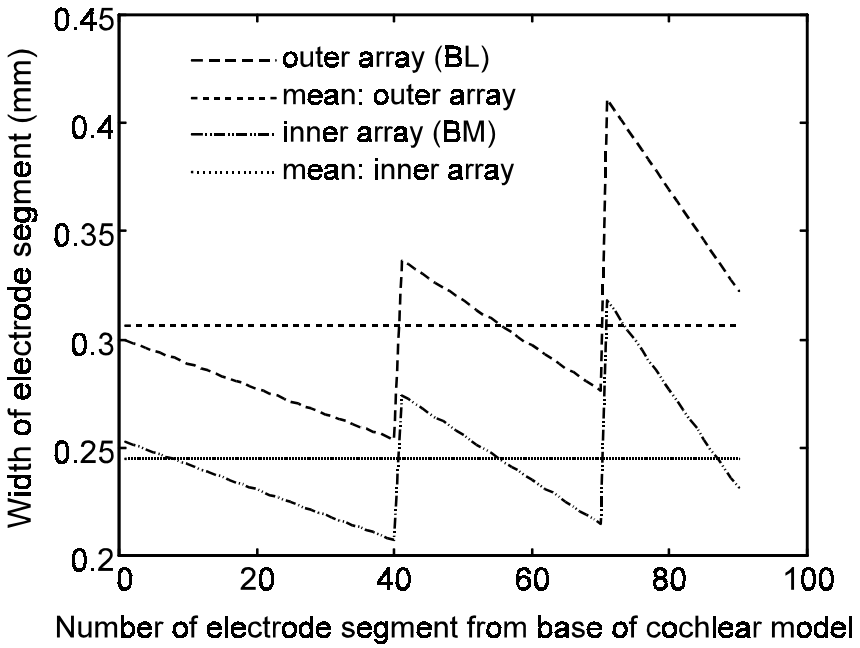

Figure 2.6. Electrode length as a function of position (and thus segment number) along the length of the scala tympani of the modelled cochlea.

The lengths of the electrode contacts varied because of the constant angles of extrusion over each half turn (Figure 2.6). For the inner array the length varied between 0.21 mm and 0.32 mm (approximately 35% relative to the widest section) and for the outer array between 0.25 mm and 0.41 mm (approximately 39% relative to the widest section). However, the variation within one half-turn over the first two half-turns did not exceed 17% for the medial electrode and 15% for the lateral electrode relative to the widest section in each half-turn. The expected effect of this variation is slightly unbalanced current densities on the two electrodes in an electrode pair, resulting in slightly elevated threshold currents for the electrode possessing the larger surface area. No compensation for this effect was made during the calculation of results.

The model was completed by "embedding" the cochlear spiral into a cylinder of bone with a radius of 5.5 mm and depth of 10 mm. Figure 2.7 shows the outlines of the

cochlear spiral embedded into the bone cylinder. The bone cylinder was automatically meshed by the software package. In total, 64 019 elements were generated.

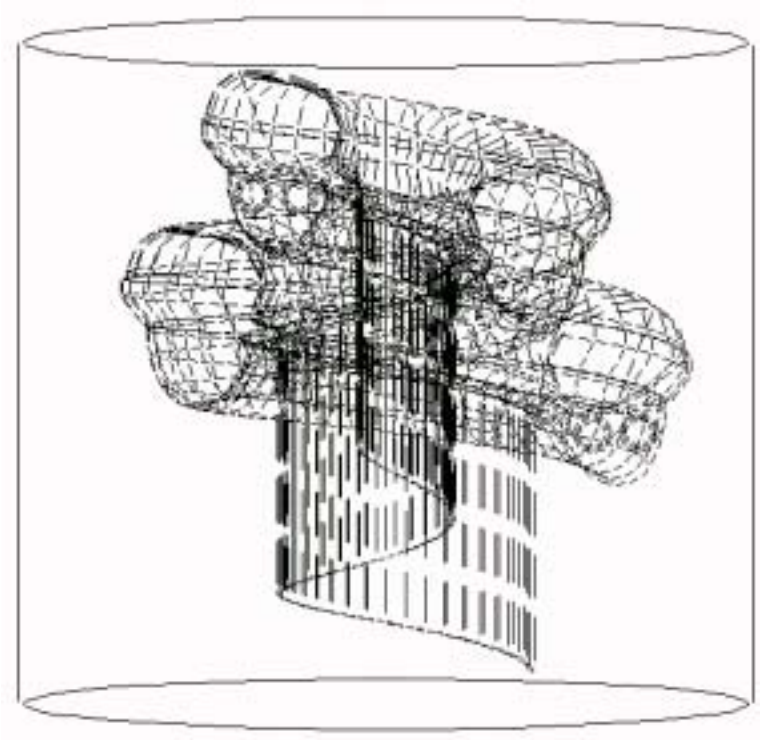

Figure 2.7. Location of cochlear model in bone cylinder.

2.2.5 Material properties

The materials in the model are, as a first approximation, purely resistive because it has been shown that the cochlear tissue impedances are well approximated by pure resistances (Black, Clark, & Patrick, 1981; Spelman et al., 1980; Spelman, Clopton, & Pfingst, 1982). Material properties (Table 2.2) are the same as those used by Finley, Wilson and White (1990), Frijns et al. (Frijns, de Snoo, & Schoonhoven, 1995), Strelioff (1973) and Grill and Mortimer (1994). Estimations of the *in vivo* thicknesses of the basilar membrane, Reissner's membrane and the stria vascularis are based on a mammalian (guinea-pig) cochlea and are 4 m, 1.7 m and 40 m respectively. To obtain well-shaped elements, the thicknesses of these membranes have been scaled up to 80 m, 50 m and 60 m respectively and therefore the

membrane resistivities were scaled down with factors 20, 30 and 1.5.

Table 2.2. Material properties of components in the cochlear model. The resistivity-values for the basilar membrane, Reissner's membrane and the stria vascularis are scaled down by factors 20, 30 and 1.5 respectively from the real values to correct for the increased thicknesses of the membranes in the model. All values are given in -mm.

Model Component	Resistivity (-mm)
Silicone rubber	1 010
Electrode metal	1
Perilymph (scalae tympani and vestibuli)	700
Endolymph (scala media)	600
Bone	6 410
Spiral ganglion	3 000
Peripheral axonal process (anisotropic)	3 000 axial 15 000 transverse
Reissner's membrane	340 130
Basilar membrane	4 000
Stria vascularis	125 790
Organ of Corti	83 333
Fibrous scar tissue	6 270

2.2.6 Source definition and boundary conditions

Electrical stimulation is performed with current stimuli. Since the material properties are purely resistive and the potential distributions could thus be scaled proportional to the source to create biphasic stimuli, a dc current was used as source. To create a uniform current density on the electrode contacts, the nodes of the elements constituting the contacts had to be coupled in the volt DOF. This defined the surface of the electrode contact as an equipotential surface. The full current was then applied onto the primary node in the coupled set. Boundary conditions were in the

form of DOF constraints, i.e. specific voltage values (e.g. 0 V) or voltage constraints (e.g. the continuity constraint between ohmic conductors in equation 2.6) on selected nodes.

2.2.7 Solution

To obtain a solution, the static solution option of the software package was selected. The default frontal solver of the FE software package was used. The solution of one simulation took approximately one hour on a Pentium II 300 MHz personal computer with 500 MB RAM.

2.3 Postprocessing

The FE software's postprocessing module was used to access the calculated scalar electric potential. Potential values at the nodes shown in Figure 2.4 on each segment of the FE model were written to a file. The data went through a number of processing steps before it was ready to serve as input to a nerve fibre model (section 3 in this chapter). Programs written in C were mostly used to process data while Matlab scripts were mostly used to plot results. A schematic representation of the data flow is shown in Figure 2.8.

First, a custom C-program was used to sort the nodal data into 12 sets of data corresponding to the 12 nodes shown in Figure 2.4. Each set of nodal data contained 91 values corresponding to the nodal locations on the intersections of the 90 segments of the model and the two outside planes at the most basal and most apical sections. Next the data were processed by a Matlab script to plot the potential distributions and activating functions (Rattay, 1999) as a function of distance along the basilar membrane and distance along the length of the nerve fibres. The data were also linearly interpolated to obtain potential values at the node locations in the model of a specific nerve fibre (section 3 in this chapter). The final output from this Matlab program was a text file containing the potential values along the length of each nerve fibre. This text file served as input to the C program containing the nerve fibre model.

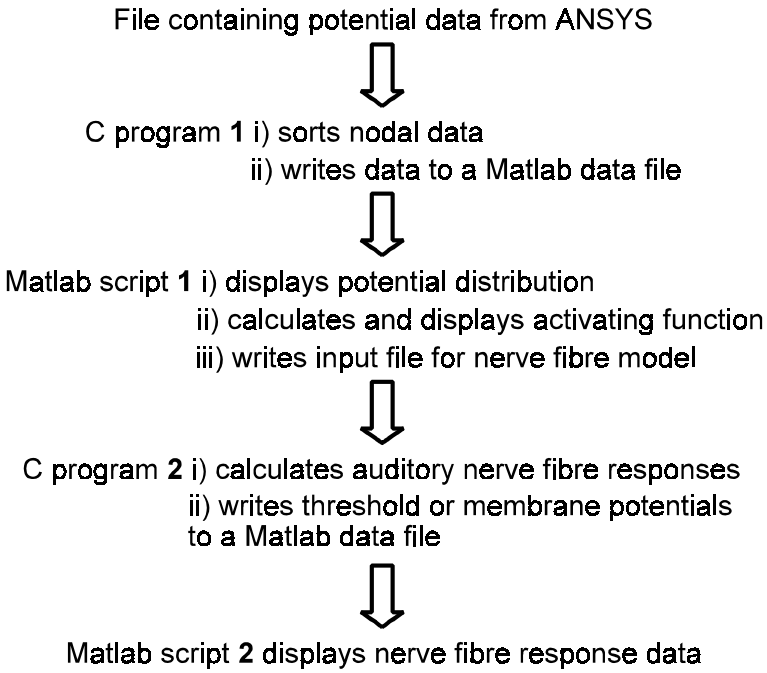

Figure 2.8. Schematic representation of data flow in the simulation of the implanted cochlea

2.4 Integrity and verification of the FE model

The integrity of the FE model was determined by (1) an assessment of the accuracy of the FE method for calculation of the electric potential and the effect of poorly shaped elements on model results, (2) a qualitative assessment of potential distributions as a result of a specific source current distribution that can be compared to results obtained with the FE model. The first aspect was addressed with an FE test problem, while the latter was addressed with analytical and LP models.

2.4.1 FE test problem

The generated mesh is one of the most important parts of the analysis since it affects the accuracy and economy of the analysis (ANSYS, 1997). The error made is a function of the equation solved over the element, the shape of the element, i.e. aspect ratio and angle between adjacent edges, and the type of element, e.g. linear or higher order. 3-D linear conduction elements were used to create the model.

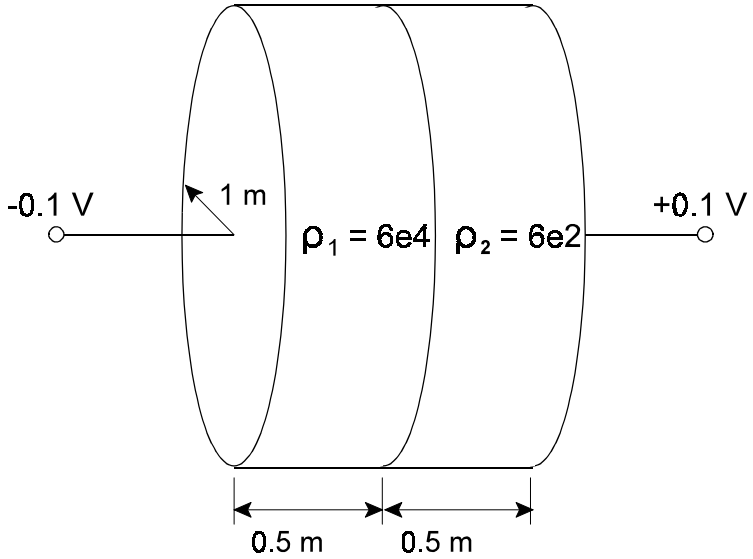

Figure 2.9. Geometry of test problem to verify the results obtained with the FE analysis.

Since the cochlear model has a complicated geometry, only a qualitative verification of the results obtained with the FE model could be done by comparison with analytically calculated values. A first step toward the verification of results obtained from a model with a complex geometry is the modelling of a simple sample problem of which the analysis results are compared with a hand-calculated solution of the same problem.

The test problem consists of two material disks having 1 m radii and 0.5 m thicknesses that were connected as shown in Figure 2.9. On the one end of the composite disk a potential of -0.1 V was applied and on the other side a potential of +0.1 V. The circular surfaces onto which the potentials were applied were assumed to be equipotential surfaces, i.e. perfectly conducting. The resistivities of the two materials were $6x10^4$ -m and $6x10^2$ -m respectively. The materials were assumed to be linear and isotropic and fringing effects were neglected. The hand calculated value for the voltage at the interface of the two materials is 0.09802 V and the worst value calculated by the FE software is 0.09801 V, which differs by 0.01% from the

calculated value. All the elements were well shaped. Since this is more accurate than the dimensional accuracy of the model, the accuracy of the analysis results with well-shaped elements was judged to be adequate.

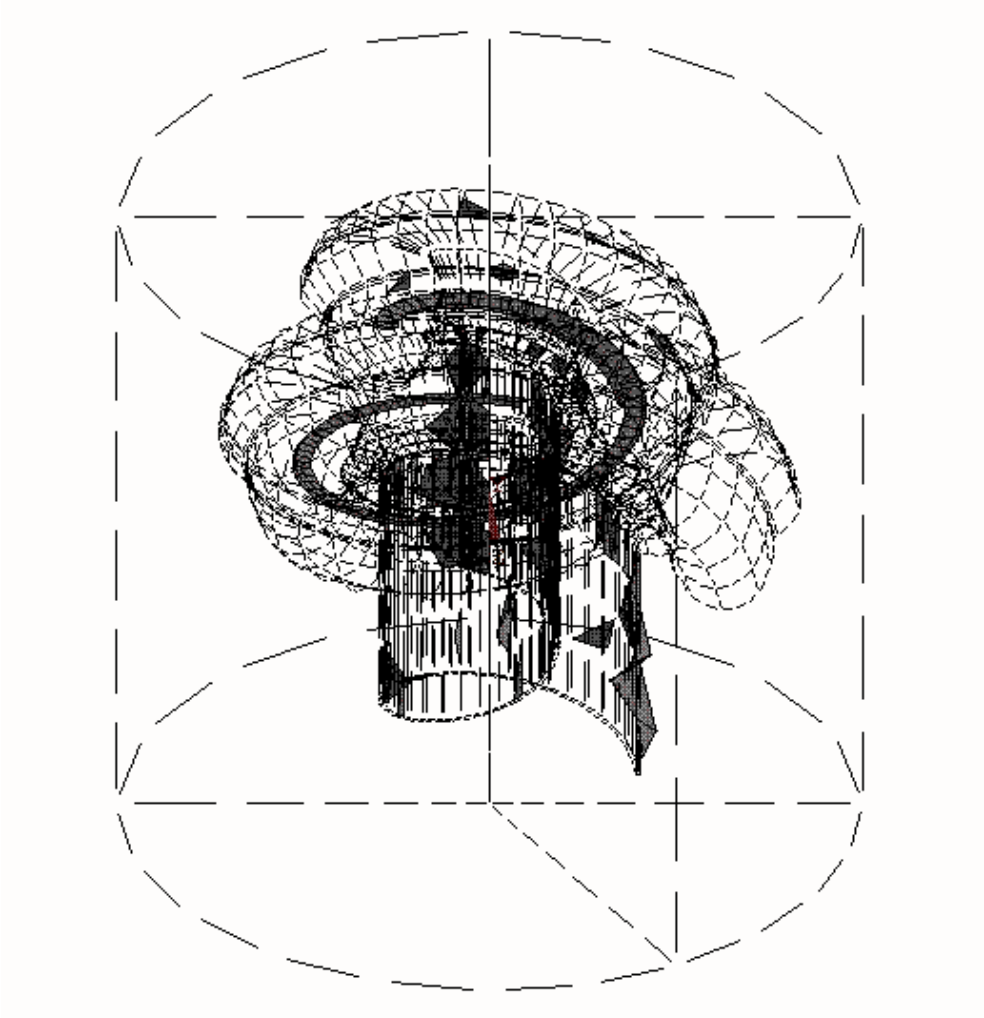

Figure 2.10. Location of poorly shaped elements in the FE model. Poorly shaped elements are shaded while well shaped elements are not shown.

To compensate for the potential loss in accuracy by using linear elements and some poorly shaped elements, a fine mesh with many elements was used to build the cochlear model. Out of the 64 019 elements, 245 tetrahedron elements in the bone cylinder were poorly shaped with the maximum aspect ratio warning issued at 42.73, which exceeds the software's default warning limit of 20, and the maximum angle

between adjacent edges was 172.5 degrees, which exceeds the warning limit of 165 degrees (Figure 2.10). In the cochlear part of the model there are a further 108 poorly shaped elements of which the maximum aspect ratio is 25.66 and the maximum angle between adjacent edges is 172.8 degrees. However, the limits of 20 for aspect ratio and 165 degrees for the angle between adjacent edges are only default guidelines provided by the software program and are also suitable for restrictive types of analyses, e.g. mechanical stress analyses.

Magnetic or electrical analyses typically do not suffer severe effects from poorly shaped elements (ANSYS, 1997). The analyses performed in this study were electrical conduction analyses which are less sensitive to element shape than, for example, structural analyses. The effect of poorly shaped elements located in a critical region is also more likely to be detrimental. Elements that produced shape warnings were mostly located along the centre of the modiolus part of the model, in the bone segment (spiral lamina) between the spiral ganglion and peripheral axonal process and the scala tympani and in the scala tympani between the inner electrode and the bone segment described above. The poorly shaped elements in the bone segment have aspect ratios not exceeding 25.66 and the poorly shaped elements in the scala tympani have aspect ratios not exceeding 22.55. Both these extreme aspect ratios are approaching the limit of 20.

To test the effect of poorly shaped elements, the test problem described above was used again and the elements were narrowed by a factor 100 so that all the elements were poorly shaped. The best shaped elements had an aspect ratio of 30.75 and the worst shaped elements an aspect ratio of 60.12. The maximum error in the analysis differed by 0.03% from the hand-calculated values. From this comparison it is obvious that the element distortion that occurs in the cochlear model is not detrimental to the results of the analyses.

2.4.2 Analytical model

An analytical model (Jolly, Spelman, & Clopton, 1996) of the implanted cochlea was

used to evaluate the potential distributions generated with the FE model (Figure 2.11) qualitatively. In the analytical model the electrical potential V at a location (x,y,z) is a simple superposition of the potential fields of different point current sources evaluated at the location (x,y,z) in a homogeneous isotropic conductive medium, i.e.

$$V(x,y,z) = \sum_{k=1}^{n} V_k , \tag{2.8}$$

where V_k is the potential field as a result of point current source k. The equation can be rewritten in terms of each current source as

$$V(x,y,z) = \sum_{k=1}^{n} \frac{I_k \rho}{4\pi} \frac{1}{R_k} , \tag{2.9}$$

where I_k is the value of the kth current source, is the resistivity of the medium and R_k is the distance from the point where the potential is being evaluated to the location of the kth current source.

The analytical model is used to evaluate the shape of potential distributions as a result of specific electrode configurations and array locations. A normalized value of the potential was therefore calculated by setting $\frac{\rho}{4\pi}$ equal to one. The normalized potential was thus given by

$$V_N(x,y,z) = \sum_{k=1}^{n} \frac{I_k}{R_k} \tag{2.10}$$

For the analytical model the location of the lateral array was defined as on the x-axis (y=z=0) while the location of the medial array was defined as parallel to the x-axis at y=0.5 and z=0. Potential distributions were calculated at a distance of 0.5 mm above the electrode array, i.e. on the plane z=0.5. The z=0.5 plane represented the surface containing the nerve fibres in the FE model (Figure 2.4). Values for the potential field were calculated at the same coordinates along the basilar membrane and along the

nerve fibres as for the FE model to facilitate calculation of electrical tuning curves[4] for both solutions.

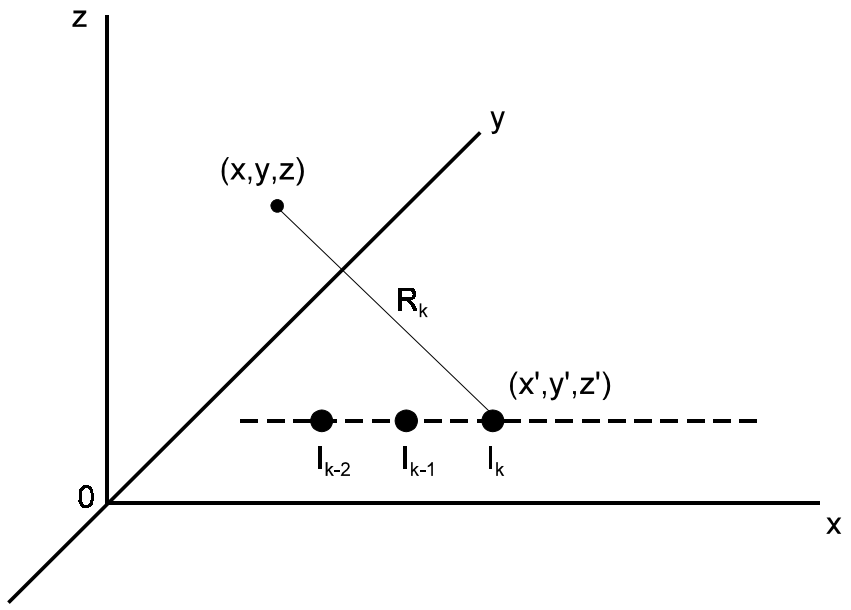

Figure 2.11. Diagram to illustrate the variables in the analytical model of the implanted cochlea. The potential at the field point (x,y,z) is the sum of the potential fields from the current sources I_{k-2}, I_{k-1} and I_k. The source point at I_k is given by (x',y',z'). The distance R_k is given by $R_k = \sqrt{(x-x')^2 + (y-y')^2 + (z-z')^2}$. The dashed line indicates the location of the electrode array; the x-axis is parallel to the basilar membrane; the y-axis is parallel to the nerve fibres and the z-axis represents the radial distance from the nerve fibres.

This formulation of the problem does not take electrode geometries other than point sources, i.e. banded electrode geometries (Chapter 3) and pseudo-continuous

[4] Electrical tuning curves give an indication of the spread of activation by showing the threshold for activation for modelled nerve fibres as a function of distance along the length of the basilar membrane. Electrical tuning curves are calculated by determining the threshold currents of an array of nerve fibres as a result of stimulation with a fixed electrode pair.

electrode geometries (Chapter 5), into account. The model also does not take the 3-D orientation of the electrodes relative to one another as a result of the cochlear geometry into account.

2.4.3 Lumped parameter models

LP models describe the structure of the cochlea with a network of resistive and capacitive components. The most well-known LP model is the transmission line model of the cochlea created by Strelioff (1973). Although LP models mostly do not take the 3-D orientation of the cochlear turns relative to one another into consideration, they are helpful to provide (1) an estimate of the potential distributions of the implanted cochlea for verification purposes and (2) a qualitative insight into some aspects of the volume conduction problem. An LP model is used in Chapter 3 to exemplify the effect of encapsulation tissue around implanted electrodes. The structure and parameters of the model are presented in Chapter 3.

3 THE NERVE FIBRE MODEL

3.1 Interfacing the FE and nerve fibre models

Since the FE model is spiralling, it is not possible to select a plane through it that will intersect all the neural elements in the same position. Consequently, and to compare model results with results and data in literature, a curved surface following the curve of the nerve fibres and spiralling along the length of the basilar membrane was defined (superior and medial surfaces of the structures shown in Figure 2.12). A simplified representation of this surface is shown in Figure 2.13a. Equipotential lines on this curved surface are displayed as contours along the length of the basilar membrane and along the length of the neural elements (Figure 2.13b). The abscissa represents the length of the basilar membrane from the round window (0 mm) to the end of the third half-turn of the cochlea (approximately 22 mm). The nerve fibre terminals are located at 0 mm (near the organ of Corti) and the medial axonal processes end at approximately 3.5 mm (inside the auditory nerve) on the ordinate.

The activating function was used to obtain a first impression of excitation patterns. The activating function is the direct stimulating influence of an extracellular potential on the n^{th} compartment (or node as used in this thesis) of the nerve fibre model (Rattay, 1999). The formulation of the activating function for a bipolar unmyelinated neuron with constant diameter but varying internodal length is given by

$$f_n = \left[\frac{V_{e,n-1} - V_{e,n}}{R_{n-1}} + \frac{V_{e,n+1} - V_{e,n}}{R_n} \right] / C_{m,n} \qquad (2.11)$$

where $V_{e,n}$ is the extracellular potential at the n^{th} node, R_n is the axoplasmic resistance to the next node and $C_{m,n}$ is the nodal membrane capacitance. The activating function was calculated for a fibre with internodal segment lengths corresponding to those of the GSEF model (Table 2.4). Since the first and last nodes do not have neighbouring fibre sections, a reduced form of (2.11) was used to calculate the activating function at these nodes.

The activating function is normally used to indicate the location along the length of a nerve fibre where activation is likely to occur. However, the exact site of activation of a nerve fibre was not relevant in this study. Excitation profiles[5] were calculated by detecting propagating action potentials at the 16th node of the modelled nerve fibres. Activating functions were thus used to determine the regions along the basilar membrane where excitation is most likely to occur, i.e. the selection of nerve fibres that are most likely to exibit propagating action potentials under specific stimulation conditions.

Contour plots of the activating function (hereafter called AF contours) over the curved surface defined above were used to calculate possible regions of excitation. A comparison between the AF contours generated for different electrode configurations

[5] Excitation profiles are the same as electrical tuning curves or spatial tuning curves, as used by some authors. In this thesis the terms "excitation profile" and "electrical tuning curve" is used interchangeably.

using the same stimulus intensities can also provide an indication of the effectiveness of stimulation since the intensity of the activating function gives an indication of the relative threshold that can be expected, i.e. a lower value of the activating function corresponds to a higher threshold current and a higher value of the activating function corresponds to a lower threshold current. Also, it it important to realize that when biphasic stimuli are used, maxima and minima in AF contours both indicate possible regions of excitation.

3.2 Modelling of auditory nerve excitation

The FE model of the cochlea consisted of 90 segments. Electrical potentials were calculated on the boundaries of the segments producing 91 sets of potential values. Consequently 91 nerve fibres were modelled. If a uniform nerve fibre density of 13 600 nerve fibres per cochlear turn[6] is assumed throughout the modelled cochlea, each modelled nerve fibre represents approximately 224 real nerve fibres.

Neural excitation patterns in the spiralling model were determined using the generalized SEF (GSEF) auditory nerve fibre model described by Frijns, de Snoo and Schoonhoven (1995). The GSEF model, an active model of an auditory nerve fibre, describes a myelinated nerve fibre with 15 segments (16 nodes) and is an active cable model of a guinea pig high spontaneous rate fibre. Potential values at the location of the 16 nodes in the GSEF nerve fibre model were calculated by interpolation of the potential values at the 12 nodes in the FE model. The first node in the GSEF model corresponds to node n_3 in the FE model. The potential values calculated with the FE model were thus applied as external excitation potentials on the nodes of 91 modelled nerve fibres.

[6] Calculated from Spoendlin and Schrott (1989) based on a cochlear length of 30 mm.

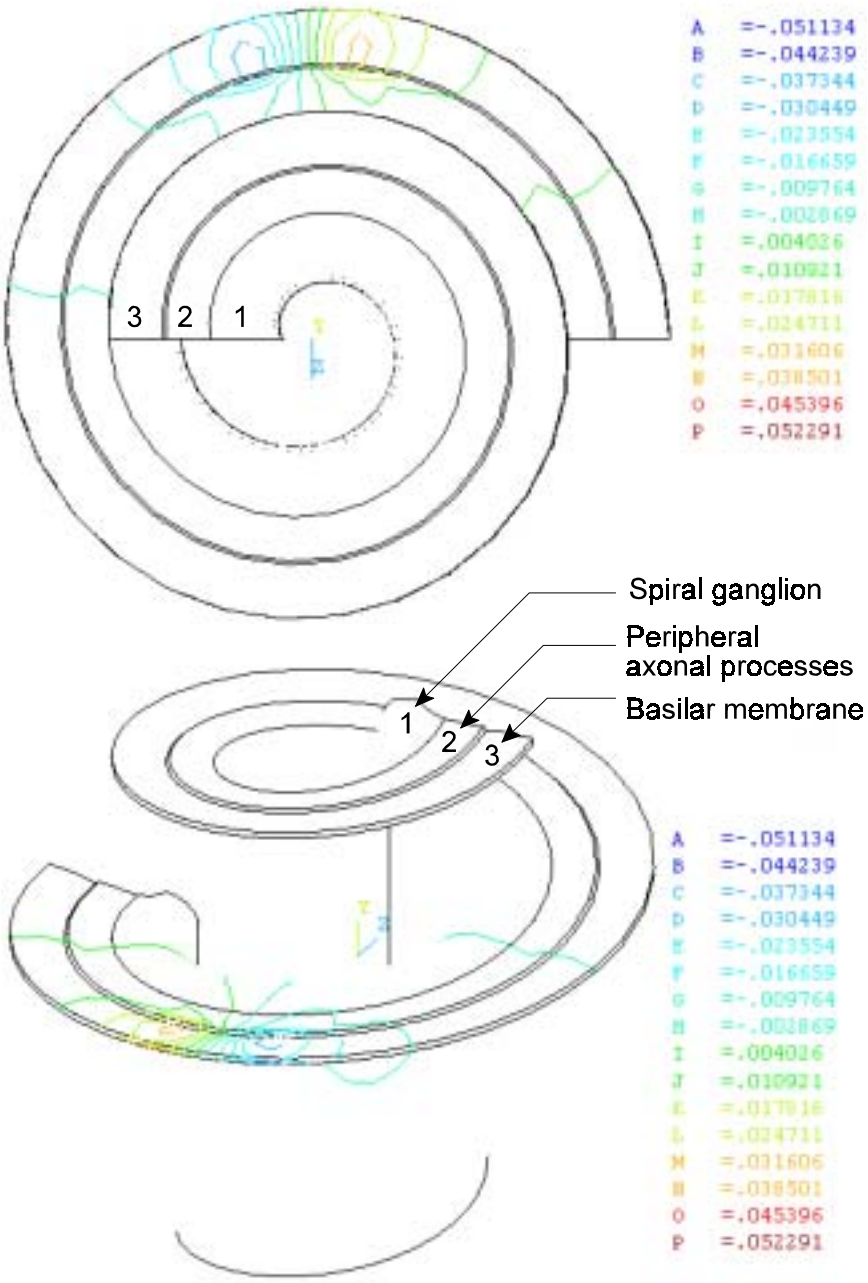

Figure 2.12. Top view (upper figure) and oblique view (lower figure) of spiral ganglion, peripheral axonal processes and basilar membrane of the FE model over which potential distributions were calculated. Equipotential lines are shown for a BP electrode configuration for the BM array.

The GSEF model is based on the original Frankenhaeuser-Huxley (FH) model (Frankenhaeuser & Huxley, 1964) which describes the membrane kinetics of the myelinated nerve fibre of the frog. Schwartz and Eikhof (1987) adjusted the FH model to represent mammalian nerve fibres which resulted in the Schwartz-Eikhof (SE) model for myelinated nerve fibres of the rat. Frijns (1995) adapted this model to represent a high spontaneous rate auditory nerve fibre based on measurements made on the guinea pig.

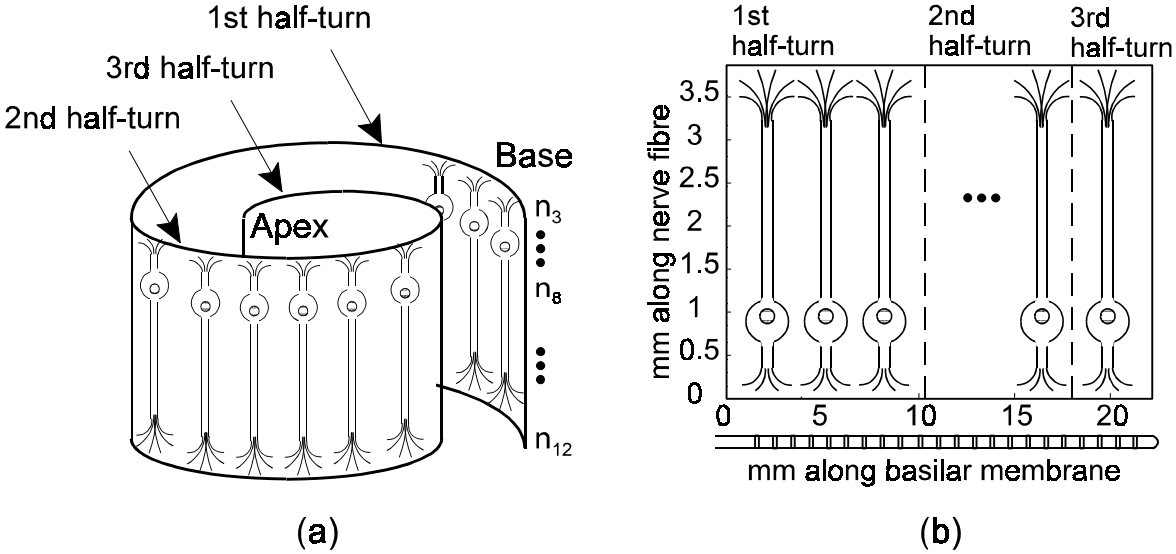

Figure 2.13. (a) A simplified diagram to illustrate the location of the plane in the FE model where the potential distributions are displayed. Nodes n_3 to n_{12} at the right of the figure correspond with the nodes in the FE model Figure 2.4. (b) The orientation of the nerve fibres and the basilar membrane on the potential distribution plots.

Although there are differences between human and guinea-pig nerve fibres, e.g., the myelinated cell body of the guinea-pig nerve fibre versus the unmyelinated cell body of the human nerve fibre, the model is used to make a *relative* assessment of the excitation properties of various electrode locations, configurations and geometries. Threshold currents vary considerably among implant users as a result of a number of inter-person variations such as variations in cochlear geometry, nerve fibre survival

patterns and electrode location, geometry and configuration. Variations in threshold currents that occur as a result of the use of a guinea-pig fibre are, as a first-order approximation, considered to be comparable to inter-person variations. Because of the use of a guinea-pig fibre, the exact site of excitation along the length of the nerve fibre is not considered in this study. To determine threshold currents, the presence or absence of a propagating action potential is used as measure.

Three nodes (k-1, k, k+1) of the GSEF cable model are shown schematically in Figure 2.14. The membrane potential is a function of the membrane's permeability to ions (P_{Na} and P_K in Figure 2.14), membrane capacitance C_m, nonspecific nodal leak current as a result of the leak conductance $G_{L,k}$, axial conduction through the axoplasmic conductance $G_{a,k}$ and externally applied electric fields $V_{e,k}$.

A uniform, finite length, active cable model of a nerve fibre with N nodes is described by the following coupled differential equations (Frijns, de Snoo, & Schoonhoven, 1995):

$$\frac{dV_1}{dt} = \frac{1}{C_m}\ [-(G_{a,1} + G_{L,1})\cdot V_1 + G_{a,k}\cdot V_2 + -(G_{a,1})\cdot V_{e,1} + G_{a,1}\cdot V_{e,2} + I_{act,1} + I_{L,1}] \quad (2.12)$$

for node 1,

$$\frac{dV_k}{dt} = \frac{1}{C_m}\ [G_{a,k-1}\cdot V_{k-1} - (G_{a,k-1} + G_{a,k} + G_{L,k})\cdot V_k + G_{a,k}\cdot V_{k+1} + G_{a,k-1}\cdot V_{e,k-1} - (G_{a,k-1} + G_{a,k})\cdot V_{e,k} + G_{a,k}\cdot V_{e,k+1} + I_{act,k} + I_{L,k}] \quad (2.13)$$

for nodes 2 to N-1, and

$$\frac{dV_N}{dt} = \frac{1}{C_m}\ [G_{a,N-1}\cdot V_{N-1} - (G_{a,N-1} + G_{L,N})\cdot V_N + G_{a,N-1}\cdot V_{e,N-1} - (G_{a,N-1})\cdot V_{e,N} + I_{act,N} + I_{L,N}] \tag{2.14}$$

for node N. V_k is the deviation of the membrane potential from the resting membrane potential, V_r.

The active current per node, I_{act}, is the sum of the active sodium and potassium currents per node

$$I_{act,k} = I_{Na,k} + I_{K,k} \tag{2.15}$$

where

$$I_{Na,k} = P_{Na,k} h_k m_k^3 \cdot \frac{E_k F^2}{RT} \cdot \frac{[Na^+]_o - [Na^+]_i \cdot \exp(\frac{E_k F}{RT})}{1 - \exp(\frac{E_k F}{RT})} \tag{2.16}$$

and P_{Na} is the nodal sodium permeability, h and m are the probabilities for opening the Na^+ ionic channels, $E_k = V_k + V_r$ is the transmembrane potential, $[Na^+]_o$ is the extracellular sodium concentration, $[Na^+]_i$ is the intracellular sodium concentration, T is the absolute temperature, F is Faraday's constant and R is the gas constant.

The equation for $I_{K,k}$ is similar to the equation for $I_{Na,k}$ and is given by

$$I_{K,k} = P_{K,k} n_k^2 \cdot \frac{E_k F^2}{RT} \cdot \frac{[K^+]_o - [K^+]_i \cdot \exp(\frac{E_k F}{RT})}{1 - \exp(\frac{E_k F}{RT})} \tag{2.17}$$

where P_K is the nodal potassium permeability, n is the probability for opening the K^+ ionic channels, $[K^+]_o$ is the extracellular potassium concentration and $[K^+]_i$ is the

intracellular potassium concentration.

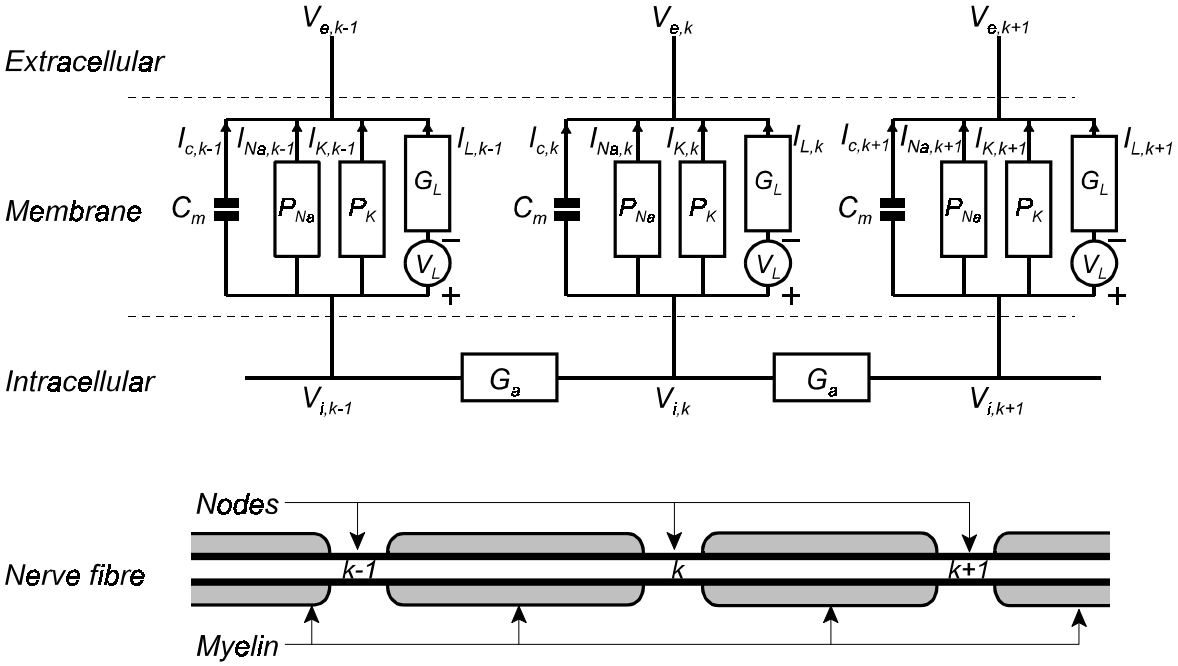

Figure 2.14. Schematic representation of three nodes in the GSEF model of a myelinated auditory nerve fibre. The lower part of the figure shows the physical structure of the section of myelinated nerve fibre of which the circuit representation is shown in the upper part of the figure. The reader is referred to the text for a description of the parameters.

The resting membrane potential V_r is calculated with the Goldman equation

$$V_r = \frac{RT}{F} \cdot \ln\left(\frac{P_K n_0^2 [K^+]_o + P_{Na} h_0 m_0^3 [Na^+]_o}{P_K n_0^2 [K^+]_i + P_{Na} h_0 m_0^3 [Na^+]_i} \right) \tag{2.18}$$

m, n and h are calculated by the following set of differential equations:

$$\frac{dm_k}{dt} = [-(\alpha_{m,k} + \beta_{m,k}) \cdot m_k + \alpha_{m,k}]$$
$$\frac{dn_k}{dt} = [-(\alpha_{n,k} + \beta_{n,k}) \cdot n_k + \alpha_{n,k}] \quad (2.19)$$
$$\frac{dh_k}{dt} = [-(\alpha_{h,k} + \beta_{h,k}) \cdot h_k + \alpha_{h,k}]$$

where

$$\alpha_{m,k} = \frac{A_{\alpha_m}(V_k - B_{\alpha_m})}{1 - \exp\left[\frac{B_{\alpha_m} - V_k}{C_{\alpha_m}}\right]} \cdot Q_{10,\alpha_m}^{\frac{T-T0}{10}} \quad (2.20)$$

$$\beta_{m,k} = \frac{A_{\beta_m}(B_{\beta_m} - V_k)}{1 - \exp\left[\frac{V_k - B_{\beta_m}}{C_{\beta_m}}\right]} \cdot Q_{10,\beta_m}^{\frac{T-T0}{10}} \quad (2.21)$$

$$\alpha_{h,k} = \frac{A_{\alpha_h}(B_{\alpha_h} - V_k)}{1 - \exp\left[\frac{V_k - B_{\alpha_h}}{C_{\alpha_h}}\right]} \cdot Q_{10,\alpha_h}^{\frac{T-T0}{10}} \quad (2.22)$$

$$\beta_{k,k} = \frac{A_{\beta_h}}{1 + \exp\left[\frac{B_{\beta_h} - V_k}{C_{\beta_h}}\right]} \cdot Q_{10,\beta_h}^{\frac{T-T0}{10}} \quad (2.23)$$

$$\alpha_{n,k} = \frac{A_{\alpha_n}(V_k - B_{\alpha_n})}{1 - \exp\left[\frac{B_{\alpha_n} - V_k}{C_{\alpha_n}}\right]} \cdot Q_{10,\alpha_n}^{\frac{T-T0}{10}} \quad (2.24)$$

$$\beta_{n,k} = \frac{A_{\beta_n}(B_{\beta_n} - V_k)}{1 - \exp\left[\frac{V_k - B_{\beta_n}}{C_{\beta_n}}\right]} \cdot Q_{10,\beta_n}^{\frac{T-T0}{10}} \quad (2.25)$$

Table 2.3. Values of A, B and C used to calculate the activation of a modelled nerve fibre

	m	m	h	h	n	n
A	0.49	1.04	0.09	3.7	0.02	0.05
B	25.41	21	-27.74	56	35	10
C	6.06	9.41	9.06	12.5	10	10

Table 2.4. Parameters for computation of action potentials

Parameter	Unit	Symbol	Value
Length of nodal membrane	cm	l	0.00001
Axonal diameter	cm	d	0.00003
Resistivity of axoplasm	k -cm		0.07
Leak conductance per unit area	k $^{-1}$/cm^2	g_L	25.78
Nodal potassium permeability	cm/s	P_K	0.000067
Nodal sodium permeability	cm/s	P_{na}	0.00172
Intracellular potassium concentration	mmol/cm^3	$[K^+]_i$	141
Extracellular potassium concentration	mmol/cm^3	$[K^+]_o$	4.2
Intracellular sodium concentration	mmol/cm^3	$[Na^+]_i$	10
Extracellular sodium concentration	mmol/cm^3	$[Na^+]_o$	142
Temperature	K	T	310.15
Faraday's constant	F	C/mol	96485
Gas constant	R	mJ/mol/K	8314.41
Internodal lengths First three internodal segments Soma Four segments after soma Last seven segments	m	L_k	 150,150,150 50 150,200, 250,300 350

The values of the parameters A, B and C were taken from the SE model and are given in Table 2.3. The values of other constants which occur in the GSEF equations are listed in Table 2.4.

3.3 Modelling of nerve fibres with degenerated peripheral processes

A recent study has shown that dendritic counts were consistently lower near the organ of Corti than at a location near the spiral ganglion in mice with sensorineural loss similar to humans (White et al., 2000). To determine the effect of degeneration

of the peripheral processes of nerve fibres, simulations were also performed with a truncated version of the GSEF model. The first four internodal sections were truncated, thus representing a nerve fibre with 12 nodes and 11 internodal segments having its terminal in the modiolus close to node n_5 in Figure 2.4.

4 CONCLUSION

The model of the cochlea presented here is a 3-D spiralling model of the implanted cochlea containing much anatomical detail. Except for the location of the spiral ganglion, the model is based on the anatomy of a human cochlea. Similar spiralling models are either for the guinea pig cochlea (much anatomical detail included) (Frijns, Briaire, & Schoonhoven, 2000) or for a simplified human cochlea (Rattay, Leao, & Felix, 2000). A novel technique is used to incorporate various electrode geometries at two electrode array locations (medial and lateral in the scala tympani relative to the modiolus). Activation of a specific array, electrode geometry and electrode configuration is effected by simply changing the appropriate elements' material properties, i.e. remeshing of model entities is not required. The model can thus be used to investigate electrode configurations and geometries currently used in cochlear implants, as well as experimental electrode configurations and geometries. A layer of scar tissue is also incorporated in the FE model and can be activated or deactivated by changing its elements' material properties. The electrical potential distributions at the target auditory nerve fibres as a result of stimulation current injection is the output from the FE model. The FE model is coupled to an auditory nerve fibre model to facilitate the calculation of neural responses from potential distributions. A truncated version of the nerve fibre model is defined to calculate the response of auditory nerve fibres of which the peripheral processes have degenerated.

Chapter 3
MODELLING OF THE ELECTRICALLY STIMULATED COCHLEA

Some of the results in this chapter have been accepted for publication in *Ear and Hearing* under the title "Three-dimensional spiraling finite element model of the electrically stimulated cochlea".

1 INTRODUCTION

The pitch sensation created during intracochlear stimulation is a function of place of stimulation and frequency of stimulation (Clark, 1996), but could also be a function of the physical placement of individual electrode contacts relative to the surviving nerve fibres, the geometry of the electrode contacts and the anatomy of the cochlea (Fu & Shannon, 1999a, 1999b; Rebscher et al., 1996; Shannon, 1983). In this chapter the effect of the placement and geometry of electrode contacts on excitation patterns for a specific cochlear geometry is considered. The shape of potential distributions around intracochlear electrodes could determine the characteristics of the place pitch information that can be provided with a specific implant system. More localized potential distributions and thus excitation patterns provide more degrees of freedom to shape the excitation pattern of the auditory nerve (Liang, Lusted, & White, 1999). An analysis of information supplied by stimulation with various electrode configurations is presented. In addition, the effect of the anatomical detail of the model is investigated to provide a qualitative indication of the degree of detail that is required in volume conduction models of the implanted cochlea.

2 MODEL AND METHODS

The combined FE-nerve fibre model described in Chapter 2 was used to investigate the effect of the electrode configuration, including electrode geometry and array location and parameter variations in the FE model, on the potential distributions and neural excitation patterns around intracochlear electrodes.

The most important output from the FE model is the shape (and not the absolute value) of the potential distribution (Rodenhiser & Spelman, 1995), as long as the intensity of the potential distribution is adequate to elicit a response. This is mainly because nerve fibre activation patterns are directly related to the shape and size (i.e. the spread) of the potential distributions. This relationship is described by the activating function (Rattay, 1999) that expresses the excitability of a nerve fibre as a function of the second spatial derivative of the electrical potential field along the length of the nerve fibre.

2.1 Electrode configuration and geometry

In this section variations in electrode configuration and geometry, and array location (hereafter collectively called "array variations") are discussed.

2.1.1 Longitudinal electrode configurations

Eight different longitudinal electrode configurations were modelled: narrow bipolar (NBP)[1], bipolar (BP), BP+1, BP+2, BP+3, two pseudo-monopolar or apical reference (AR1 and AR2)[2] configurations (Fig 3.1a) and one true monopolar configuration (MONO). For the true monopolar configuration the outer boundaries of the FE model

[1]NBP mode refers to an electrode spacing approximately half of the spacing between adjacent electrodes in the Nucleus cochlear implant (Clark, 1996).

[2]Pseudo-monopolar mode is not a true monopolar mode, as the reference is not located remotely, but inside the scala. This mode will be called "apical reference" (AR) mode.

(i.e. the external surfaces of the bone cylinder) were defined as an equipotential surface serving as the return electrode.

Table 3.1. Electrode dimension details of longitudinal electrode configurations.

[a] The interelectrode spacing is dependent on the exact location in the model. At this specific location in the model the interelectrode spacing is 828 m.

[b] The interelectrode spacing is taken as the length of the straight line crossing through the modiolus and connecting the centre of the electrode carrier between segments 19 and 55.

[c] The interelectrode spacing is taken as the length of the straight line connecting the centre of the electrode carrier between segments 19 and 80.

Electrode configuration	**Model segment number used as electrode**		**Inter-electrode spacing m**		
	basal	**apical**	**Nucleus**	**Lateral**	**Medial**
near BP	19	21	n.a.	277	277
BP	19	23	700	828[a]	688
BP + 1	19	26	1 700	1 646	1 365
BP + 2	19	30	2 700	2 719	2 252
BP + 3	19	34	3 700	3 775	3 121
AR1[b]	19	55	n.a.	7 944	6 685
AR2[c]	19	80	n.a.	1 665	1 468

AR1 electrode configurations were modelled because many subjects using the Nucleus implant have not been fitted with an extracochlear return electrode. However, pshychoacoustic data are available for AR1 electrode configuration for subjects wearing the Nucleus implant (Hanekom & Shannon, 1998). Also, since the electrode separation in AR1 electrode configuration is large, the effect of one electrode on the potential field at the nerve fibers close to the other electrode is small (less than 1% if a medium with uniform resistivity is assumed and potential field decay is assumed to be inversely proportional to distance). Each electrode in the

AR1 pair could thus be viewed as approximating a monopole, i.e., an AR1 electrode configuration approximates a "double" monopolar electrode configuration. The neural excitation pattern around any one of the electrodes in an AR1 configuration could thus be expected to be similar to that around a true monopolar electrode.

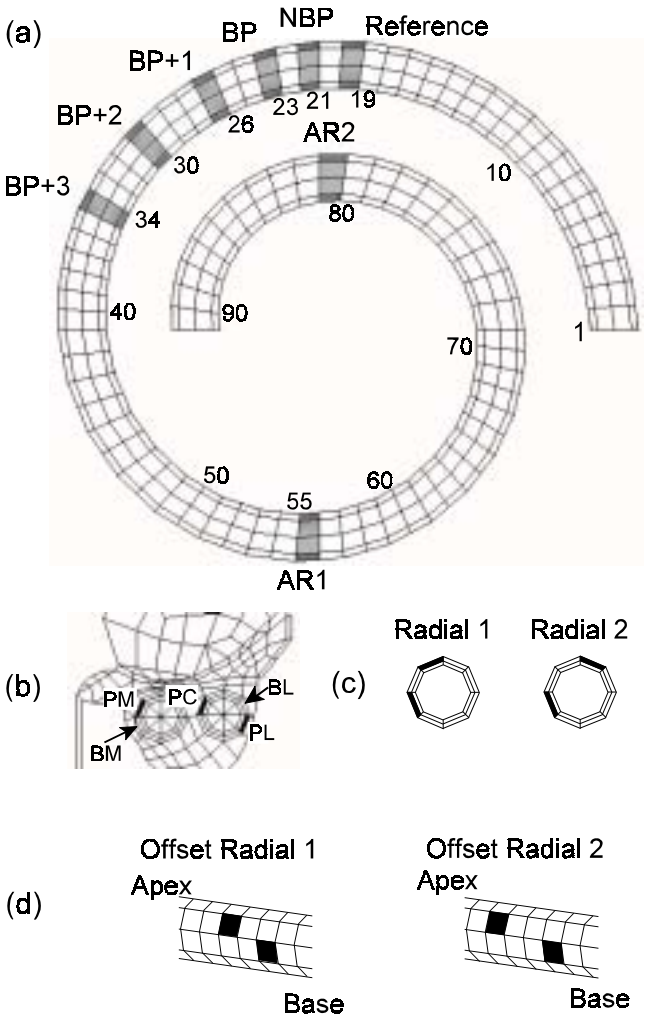

Figure 3.1. (a) Locations of electrode contacts along the length of the electrode carrier for longitudinal banded and longitudinal point configurations. Locations of electrode contacts on the perimeter of the electrode carrier for (b) longitudinal point (PM, PC and PL), (c) radial and (d) offset radial configurations. The locations of the BM and BL arrays can also be seen on (b).

AR2 electrode configurations were modelled to study the effect of electrodes that are placed in neighbouring canals.

Two banded array locations are modelled: one in a medial location in the scala tympani close to the modiolus (called "banded medial" or "BM") and one in a location lateral to the close to the outer wall of the scala tympani (called "banded lateral" or "BL"). Figure 3.1 shows the location of the two array locations. Point electrodes were modelled at three locations, medial, central and lateral in the scala tympani (called "PM", "PC" and "PL" respectively) and are shown in Figure 3.1b. Table 3.1 summarizes the details of the longitudinal electrode configurations. Electrode carrier diameters are 0.5 mm for banded electrode configurations and 0.6 mm for point electrode configurations.

2.1.2 Radial electrode configurations

Radial or offset radial electrode configurations are used in some implants, for example the Clarion implant from Advanced Bionics Corporation (Kessler, 1999). Narrowly spaced and widely spaced radial (Figure 3.1c) and offset radial configurations (Figure 3.1d) were modelled. The basal electrode in the offset radial configurations is inferior relative to the apical electrode. Dimensional details of the radial electrode configurations are given in Table 3.2. The carrier diameter is 0.6 mm.

Table 3.2. Electrode dimension details of radial electrode configurations.

Electrode configuration	**Model segment number used as electrode**		**Inter-electrode spacing (m)**
	return	**active**	
R1	19	19	392
R2	19	19	589
OR1	19	20	688
OR2	19	21	1 000

2.1.3 Hifocus-like[3] electrode geometry

The Hifocus electrode (Advanced Bionics Corporation, 2000) was designed to deliver highly selective electrical stimulation to the auditory nerve fibres and to limit channel interaction by limiting longitudinal current flow. The array is designed to assume a perimodiolar position and thus target the spiral ganglion cells for stimulation. This electrode is suitable for simultaneous stimulation on more than one electrode pair (or channel) because of the inhibition of lateral current flow.

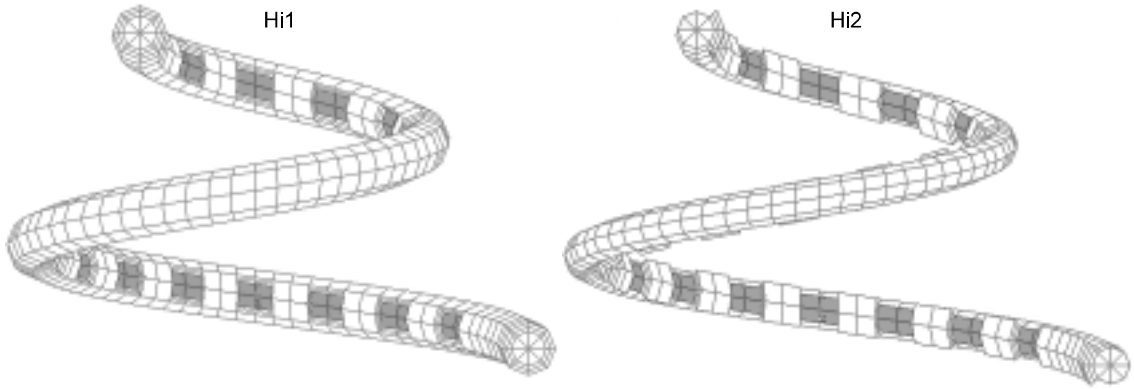

Figure 3.2. Two modelled Hifocus-like electrode arrays. The left array (Hi1) has its contacts recessed into the electrode carrier, while the right array (Hi2) has pillows of insulating material between the contacts.

Table 3.3. Electrode dimension details of Hifocus-like electrode array.

Electrode configuration	**Model segment numbers used as electrode**		**Approximate inter-electrode spacing in mm (centre to centre)**
	basal	**apical**	
BP	8-9	12-13	1.0
BP+1	8-9	16-17	1.9
AR1	12-13	55-56	6.9

[3]The Hifocus electrode is a new electrode design that creates highly focussed electrical stimulation (Advanced Bionics Corporation, 2000).

Two approximations of the Hifocus electrode were modelled. The first model (called Hi1 hereafter) was constructed by recessing the electrode contacts into the insulating electrode carrier. This configuration is shown in the left part of Figure 3.2. The second model (called Hi2 hereafter) was constructed by placing pillows of an insulating material (the same material as the electrode carrier for these simulations) between the contacts. The Hi2 FE model is shown in the right part of Figure 3.2. The surface area of the contacts was approximately 0.25 mm^2 but varied slightly as a function of location in the model (Figure 2.7). Recess depth (Hi1) and the height of the interelectrode pillows (Hi2) were 100 m.

2.2 Model parameter variations

2.2.1 Tapering of the scala tympani

To simulate tapering of the cochlea towards the apex, the resistivity of the perilymph was scaled to render lower resistivity in the basal region of the cochlea and higher resistivity towards the apex. Lower resistivity simulates a wider canal while higher resistivity simulates a narrower canal. The upper graph in Figure 3.3 shows the width of the scala tympani as a function of position along the length of the scala tympani. The percentage error between the width in the modelled scala tympani and the measured widths is also shown.

To determine a scaling function for the resistivity, a second order polynomial was fitted to the error function. Scaled resistivities $_{new}$ were determined by the equation

$$\rho_{new} = \frac{\rho_{model}}{1 + e} \tag{3.1}$$

where $_{model}$ = 700 -mm and is the error expressed as a fraction.

The resistivities were averaged over six FE model sections to render the discretized resistivity function shown in the lower part of Figure 3.3. The primary objective of the discretization was to reduce the number of sections for which the resistivities had to be changed from 90 sections to 15 sections. The polynomial fit was preferred above

a fit to the measured data because it produced smaller discontinuities between neighbouring model sections.

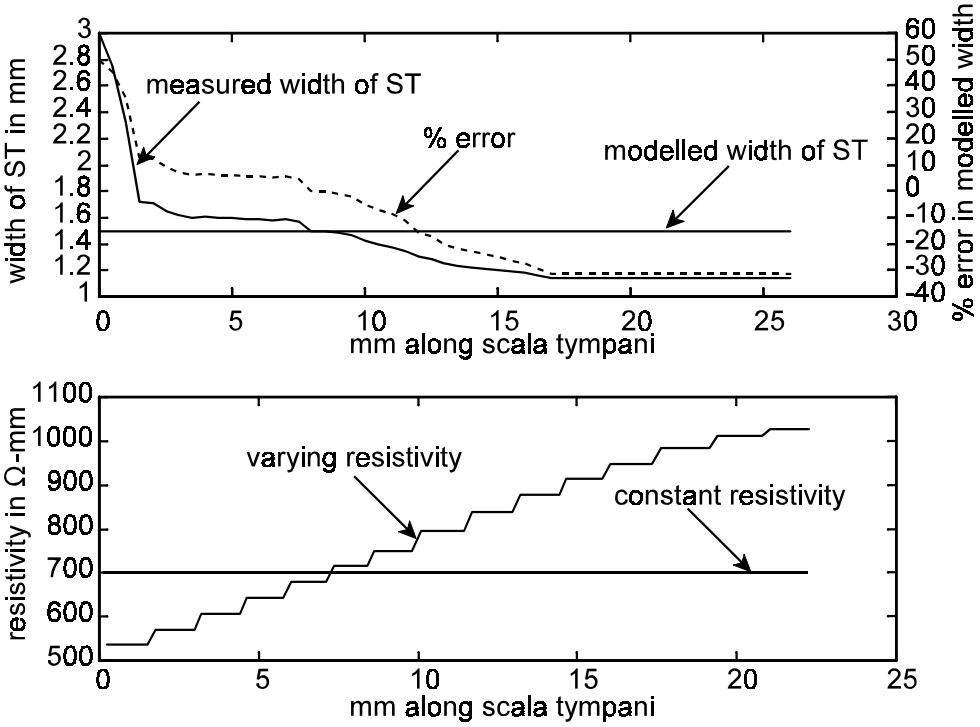

Figure 3.3. The upper graph shows the measured width of the human scala tympani (Hatsushika et al., 1990), the (constant) modelled width and the percentage error between the real and modelled widths as a function of distance along the scala tympani. The lower graph shows the varying perilymphatic resistivity that was used to simulate tapering of the cochlea and also the constant resistivity when no tapering was simulated.

2.2.2 Helicotrema

The effect of the connection between the scala tympani and the scala vestibuli on excitation patterns was investigated by changing the material properties of the last section of the scala media and surrounding membranes in the FE model to that of perilymph. This simulates a conductive pathway from the scala tympani to the scala vestibuli. Neural excitation patterns were determined for electrode locations close to the "helicotrema" and also for electrode locations in the first half-turn of the model (corresponding to the locations in Figure 3.1).

2.2.3 Other modelled structures

The effect of the fine structure of the cochlea on potential distributions and a qualitative indication of the sensitivity of model results to these structures were determined by merging the structure under investigation into the structure in contact with it. Details of structures that were investigated are given in Table 3.4.

Table 3.4. Details of structural changes to the FE model. The resistivity of the applicable structure is changed to that of the surrounding tissues.

Structure	Description	Correct -mm	New -mm
Organ of Corti	Organ of Corti is merged into scala media.	83 333	600
Stria vascularis	Stria vascularis is merged into bone.	125 790	6 410
Reissner's membrane	Reissner's membrane is merged into scala vestibuli.	340 130	700
Spiral lamina	Spiral lamina is merged into scalae tympani and vestibuli.	6 410	700
Basilar membrane	Basilar membrane is merged into scalae tympani and vestibuli.	4 000	700

2.3 Modelling of auditory nerve excitation

In this study the focus was not on the exact location of the site of excitation along the length of a nerve fibre, but rather on whether a particular nerve fibre is activated or not. A propagating action potential was assumed to signify neural excitation (Reilly, Freeman, & Larkin, 1985). Threshold currents were determined by examining the 16^{th} node of each nerve fibre for the occurrence of an action potential. The occurrence of an action potential was detected by an iterative process. An interval was defined in which the threshold current was expected to occur. The current level was then stepped down or up by halving the interval with each iteration depending

on whether the current level caused an action potential or not. The final resolution of the iterative process was 1 A.

The stimulation waveform used was a single balanced phase square pulse with cathodic and anodic phases equal to 0.2 ms. The more apical electrode was used to deliver the cathodic-first stimulus, unless otherwise noted. Neural responses were calculated over a period of 1 ms.

3 RESULTS

3.1 Potential distributions and AF contours

Potential distributions and AF contours are presented in this section. The activating function is calculated along the length of a single nerve fibre and gives an indication of the exciting ability (a positive value for the activating function indicates possible excitation) of the extracelluler potential distribution (i.e. the potential distribution as a result of stimulation). An AF contour plot is a two-dimensional graph showing the intensity of the activating function over all modelled nerve fibres. Maxima and minima in this AF contour plot give a relative indication of the spread of neural excitation without calculating the neural response with a nerve fibre model. Potential distributions and AF contours are discussed in three categories. First, an overview is given of occurrences that are common to all array locations, electrode configurations and electrode geometries. Secondly, potential distributions as a result of specific model structure and parameter variations are discussed. Only selected variations in model structure and parameters are discussed since not all variations render clearly visible differences in the potential distributions. Lastly, potential distributions and AF contours generated with Hifocus-like electrode geometries are presented.

3.1.1 Overview

A 200 A dc stimulation current was used to calculate potential distributions.

Although potential distributions were calculated with a dc stimulus, biphasic stimuli could be generated by scaling because of the resistive nature of the FE model. Potential distributions were calculated on the nerve fibres in the FE model.

Figure 3.4 shows potential distributions (left) and AF contours (right) for BP and BP+3 configurations for the PM (upper four graphs) and BL (lower four graphs) arrays calculated with the FE model. Figure 3.5 shows potential distributions for similar electrode configurations for medial (upper four graphs) and lateral (lower four graphs) array locations calculated with the analytical model. In Figure 3.4 equipotential lines are for 20 mV increments for the PM array and for 10 mV increments for the BL array. Equipotential lines are alternately labelled (except for the additional 0 V label on the plots for the PM array). No absolute values for potentials or activating function intensity are given for the analytically calculated contours (Figure 3.5) since only qualitative comparison between FE calculated and analytically calculated potential distributions is possible, i.e. the shapes and relative intensities of the potentials and AF contours calculated with the analytical model are compared to results obtained with the FE model. Vertical dashed lines indicate boundaries between the half-turns of the modelled cochlea while vertical solid lines indicate the location of the electrodes along the length of the basilar membrane.

Potential distributions for different electrode locations and geometries are similar for different electrode separations, i.e. maxima and minima are located at approximately the same distance along the nerve fibres relative to the fibre terminals, but at different locations along the basilar membrane, depending on the location of the electrode contacts. The intensity of the potential field is, however, higher for widely spaced electrode configurations than for narrowly spaced configurations (compare potential maxima and minima for BP and BP+3 electrode configurations). This is because the impedance between the electrode contacts (and thus over the tissues between the electrode contacts) increases, causing an increase in the voltage drop between the electrode contacts.

Since the BL array is more distally located from the nerve terminals than the PM array, the location of the maximum potential along the length of the nerve fibres is displaced. This is also visible in results from the analytical model. Maxima and minima in the potential distribution on the nerve fibres occur at the point where the nerve fibres are closest to the electrode contacts.

Potential maxima and minima differ substantially between banded electrode geometries (lower part of Figure 3.4) and point electrode geometries (upper part of Figure 3.4) using the same stimulus intensity. Furthermore, potential fields are narrowest for closely spaced electrode configurations and increase with increasing interelectrode separation. This can be seen both in results from the FE model and from the analytical model when potential distributions for BP and BP+3 electrode configurations are compared. The spread of excitation is also expected to increase for more widely spaced electrode configurations because of the wider spread of the maxima and minima in the AF contours relative to maxima and minima in the same plots for narrowly spaced electrode configurations.

Contrary to the analytical model, potential distributions generated with the FE model (Figure 3.4) are not symmetrical because of the spiralling nature of the cochlea. A toroidal model generated from the same 2-D geometry from which the spiralling model was created (Figure 2.4) produced symmetric potential distributions. The results of the toroidal model are not shown. The width[4] of potential distributions is a function of both array location and electrode configuration. NBP electrode configurations create wider potential distributions in the region of the more *apical* electrode for all array locations, while wider electrode separations usually create

[4]The width of the potential field refers to distance from the electrode where a specific magnitude of potential occurs, i.e. a 10 mV potential magnitude will occur further away from the electrode for a wide potential distribution than for a narrow potential distribution. The width is qualitatively evaluated on a line parallel to the basilar membrane on the neural plane at the location of the electrodes, i.e., the "0 mm along nerve fiber" line for lateral electrode arrays and approximately the "0.5 mm along nerve fiber"-line for medial electrodes.

wider potential distributions around the more *basal* electrode. The electrode separation where the transition occurs from wider distributions around the more apical electrode to wider distributions around the more basal electrode is a function of the array location. Array locations closer to the nerve fibres often create wider potential distributions around the *basal* electrode than array locations further away from the nerve fibres.

For array locations close to the nerve fibres and the fibre terminals (i.e. BM, BL, PM and PC) the transition occurs at BP+1 electrode configuration and at BP+2 electrode configuration for the PL array. This could, however, partly be a result of the slightly larger surface area of the model segments toward the basal end of each half-turn. The effect of variation in electrode surface area is expected to be greater for electrode arrays close to the nerve fibres.

AF contours for potential distributions generated with the FE model show locations of possible ectopic stimulation (i.e. stimulation of nerve fibres other than the target nerve fibres) in the third half-turn of the modelled cochlea. Since the intensity of the AF contour plot at this location in the model is low compared to its intensity in the first half-turn, excitation thresholds can be expected to be higher. The intensity of the AF contours at the ectopic location shows that ectopic excitation can be expected to occur at lower stimulation currents for array locations close to the nerve fibres (i.e. the BM array) and for widely spaced electrode configurations (BP+3 in the case shown). The analytical model does not show this ectopic region of excitation.

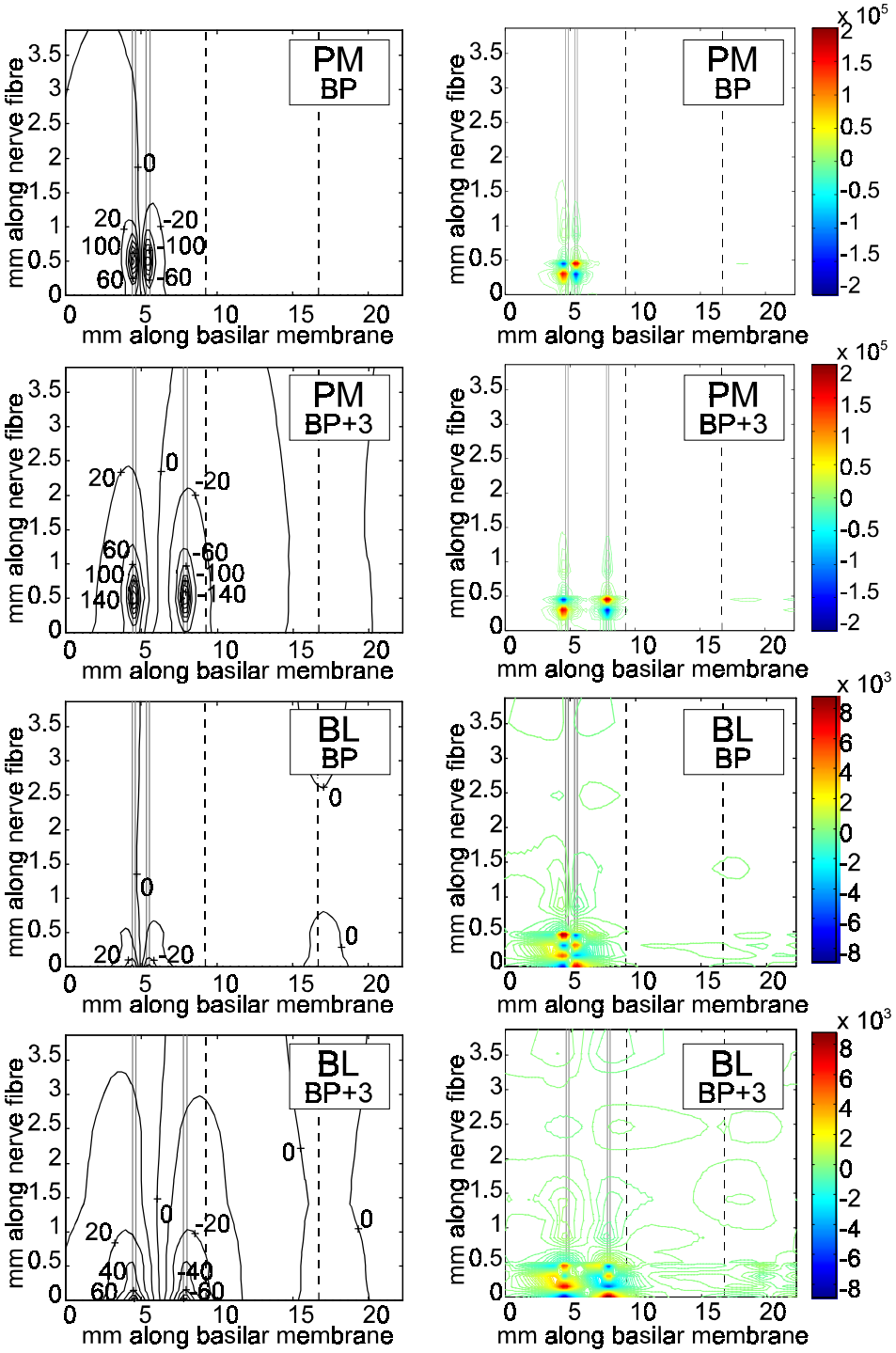

Figure 3.4. Potential distributions (left) and AF contours (right) for the BP and BP+3 electrode configurations for the PM array (upper four graphs) and the BL array (lower four graphs) calculated with the FE model described in Chapter 2. Equipotential lines are for 10 mV intervals and are alternately labelled. Units of AF contours: mV/ms.

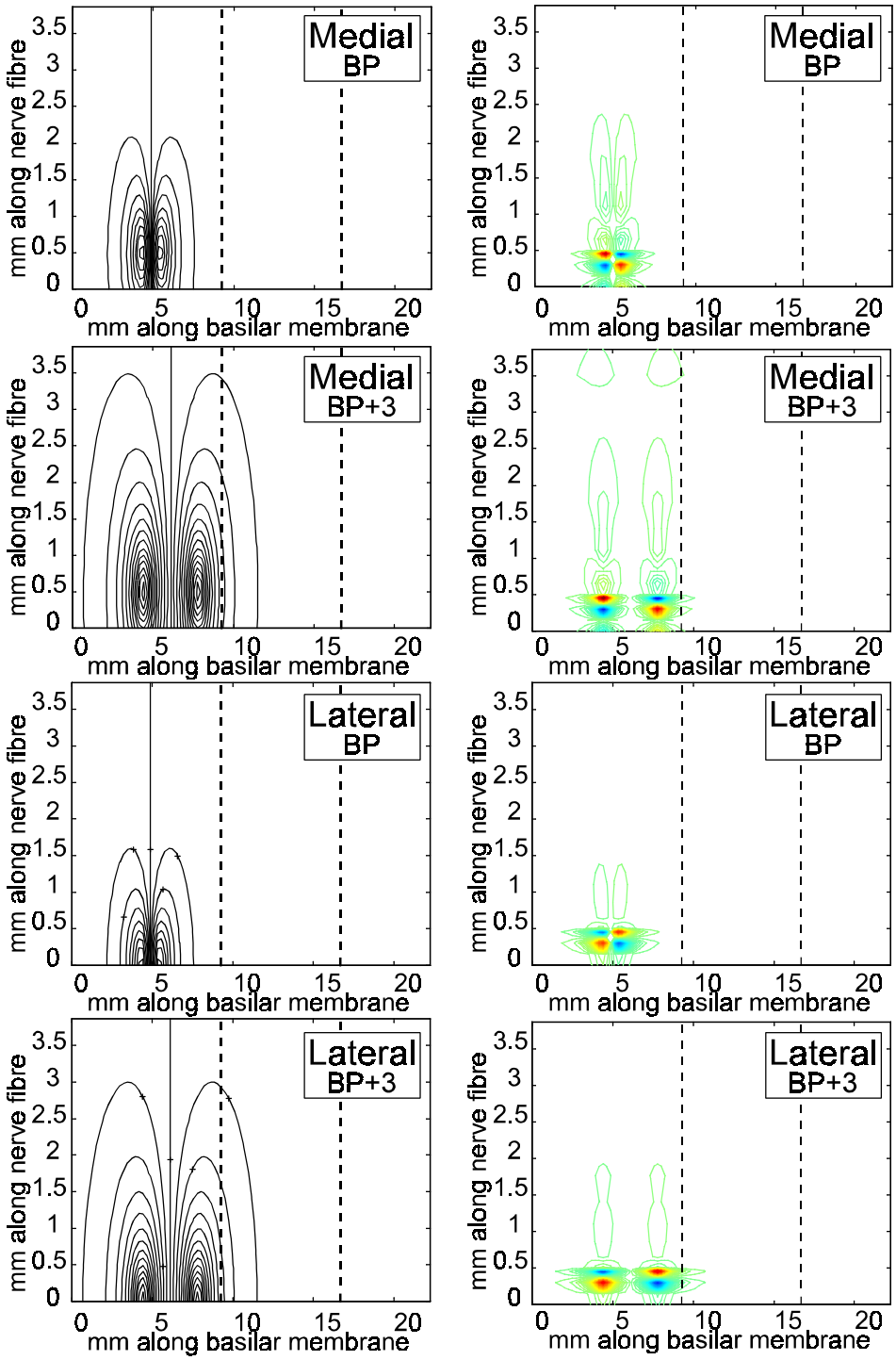

Figure 3.5. Potential distributions (left) and AF contours (right) for the BP and BP+3 electrode configurations for a medial array (upper four graphs) and a lateral array (lower four graphs) calculated with the analytical model described in Chapter 2.

3.1.2 Effect of model variations on potential distributions

3.1.2.1 Potential distributions with varying perilymphatic resistivity

Potential distributions increase in width from base to apex when the resistivity of the perilymphatic spaces is scaled to simulate tapering of the cochlea (left graphs in Figure 3.6). At the base, potential distributions are somewhat narrower for the scaled resistivity compared to the constant resistivity (upper two graphs in Figure 3.6). At the apex the situation is reversed (lower two graphs in Figure 3.6). Halfway through the first half-turn of the modelled cochlea the resistivities in the scaled and constant versions of the model were approximately equal. Consequently, potential distributions for the scaled and constant resistivities are approximately the same at this location (middle two graphs in Figure 3.6).

3.1.3 Hifocus-like electrode arrays

Figure 3.7 shows potential distributions (left graphs) and AF contours (right graphs) for the two Hifocus-like electrode geometries and a control geometry. The intensity of the potential field is higher for Hi1 (upper left) than for Hi2 (middle left) and the control geometry (lower left). Hi1 can be expected to have lower threshold currents because activating function intensity is higher than for Hi2 and the control electrode geometry. Potential distributions are similar for Hi2 and the control geometry except that distributions appear slightly elongated toward the medial processes of the nerve fibres for Hi2.

3.2 Auditory Nerve Excitation Patterns

Auditory nerve excitation patterns are characterized by calculating minimum threshold current (i.e. the current required to activate a single nerve fibre in the model) and by electrical tuning curves. The minimum threshold current gives an indication of the effectiveness of stimulation while electrical tuning curves show the localization of neural excitation.

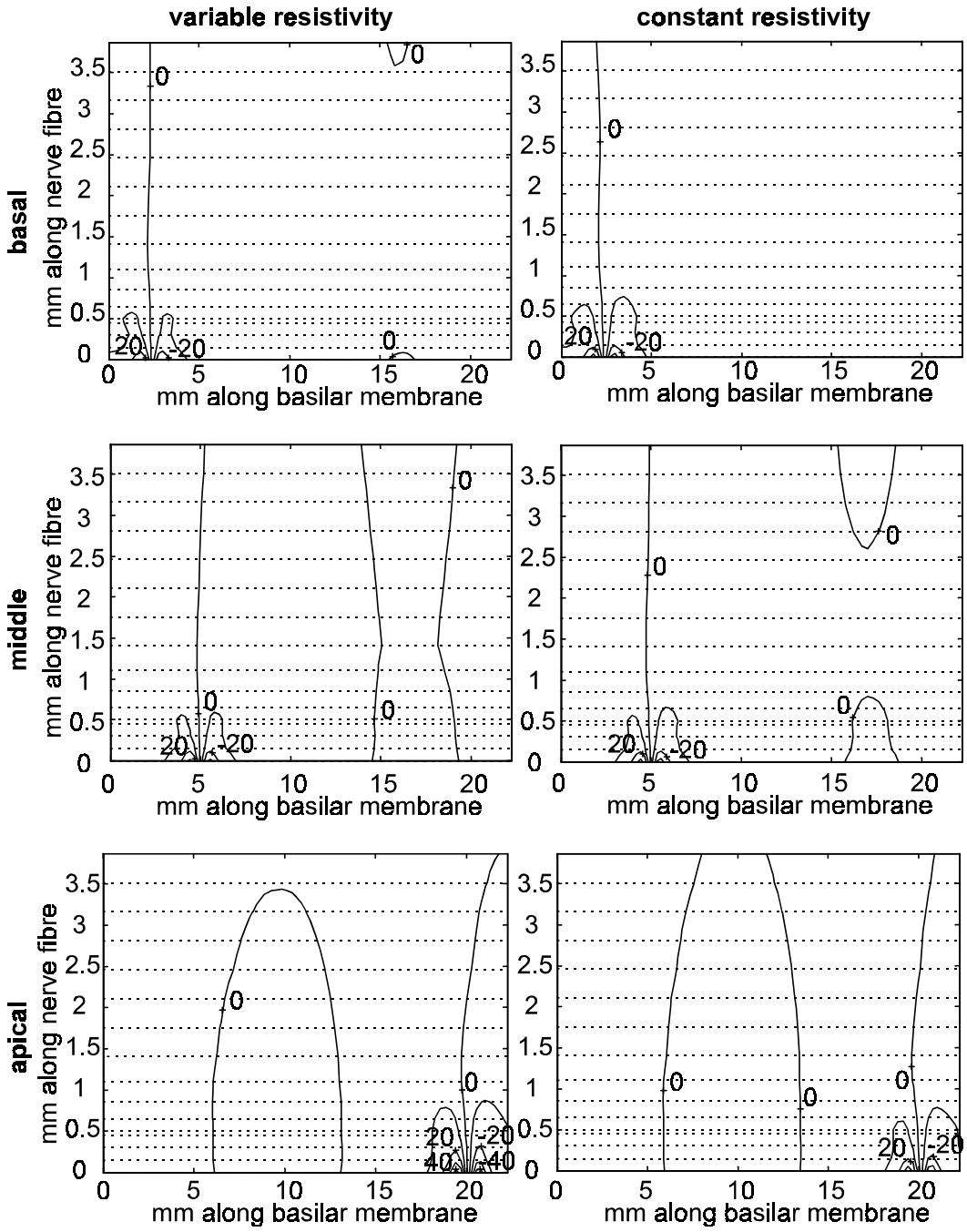

Figure 3.6. Potential distributions as a result of stimulation at different locations along the length of the basilar membrane. The graphs on the left are for an increase in the resistivity of the perilymph toward the apex, while the graphs on the right are for constant perilymphatic resistivity. Results are for the BL array. Equipotential lines are for 10 mV intervals and are alternately labelled.

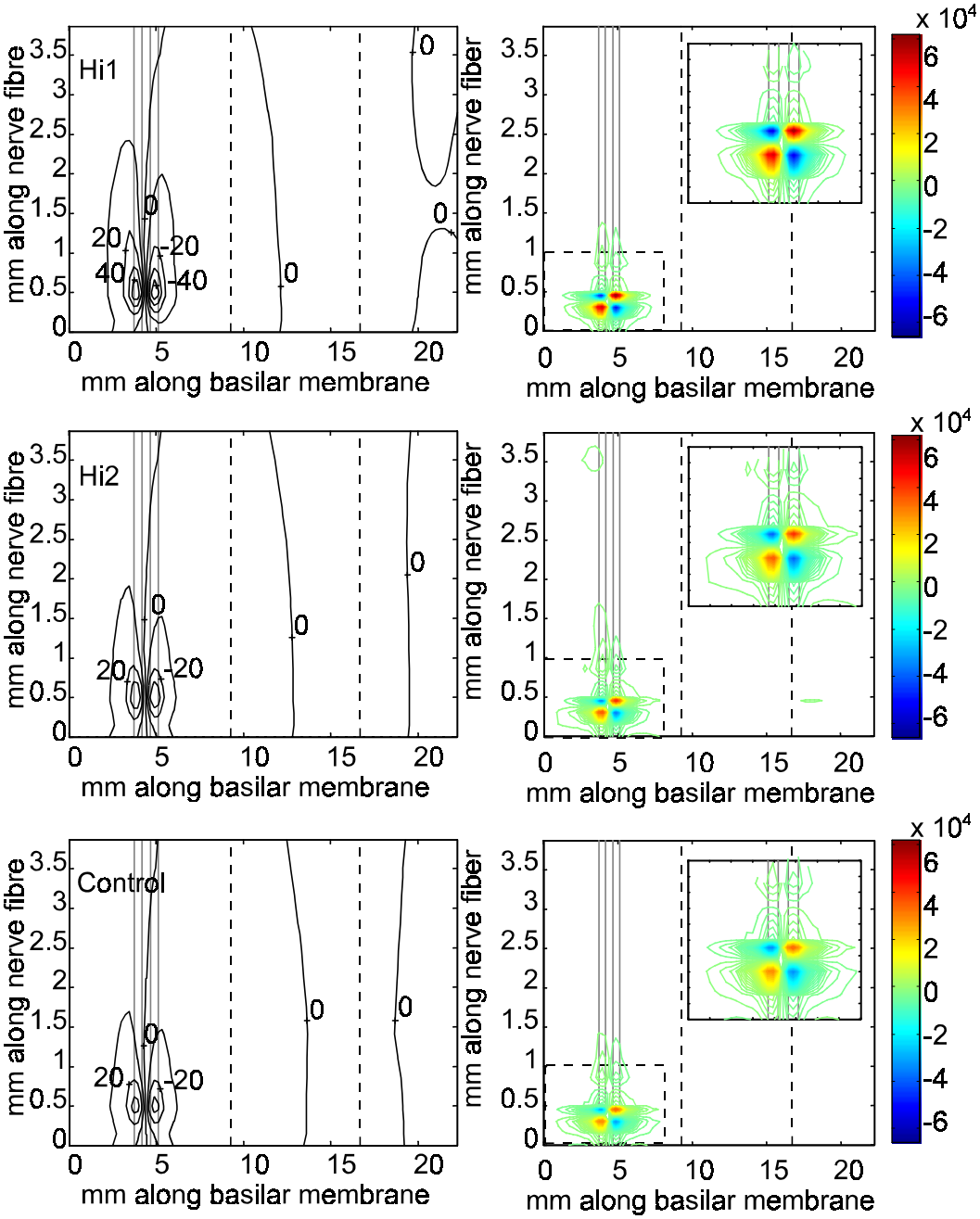

Figure 3.7. The graphs on the left show the potential distributions for BP electrode configuration created with Hi1 (upper), Hi2 (middle) and an unfocussed control geometry (lower), while the graphs on the right show AF contours for the same geometries (insets show an enlargement of the regions in dashed blocks). Equipotential lines (left graphs) are shown for 10 mV intervals and are alternately labelled. Units of AF contours: mV/ms.

3.2.1 Minimum threshold current

3.2.1.1 General trends

Figure 3.8 shows minimum threshold current versus electrode separation curves for both electrodes in a bipolar electrode pair. Minimum threshold current for anodic-first stimulation is defined as the lowest threshold for any nerve fibre close to the electrode delivering the anodic-first stimulus, while the opposite is true for cathodic-first minimum threshold current. Threshold currents were determined for full (intact) nerve fibres (16 nodes) as well as for truncated nerve fibres of which the peripheral axonal processes were degenerated (12 nodes). Results discussed are for the full nerve fibre model unless stated otherwise. Minimum threshold currents for cathodic-first stimulation are shown for monopolar stimulation for the full and truncated nerve fibre models (stars in Figure 3.8).

For longitudinal electrode configurations the model does not always predict the lowest threshold currents for nerve fibres close to the electrode delivering the cathodic-first stimulus (Figure 3.8). Threshold currents are always lower for nerve fibres around the *basal* electrode for closely spaced electrode configurations (NBP and BP). For more widely spaced configurations (BP+1 and wider), threshold currents are lower for nerve fibres around the cathodic-first electrode if the array overlaps with the nerve fibres. However, excitation also occurs on nerve fibres close to the cathodic-first electrode for array locations far from the fibres and widely spaced electrode configurations (AR1 and AR2) when a truncated nerve fibre model is used. Figure 3.9 show that anodic-first to cathodic-first threshold ratios are very close to unity. The greatest deviations from unity generally occur for closely spaced electrode configurations close to the nerve fibres. The dotted lines in Figure 3.8 show threshold currents for reversed stimulus polarity.

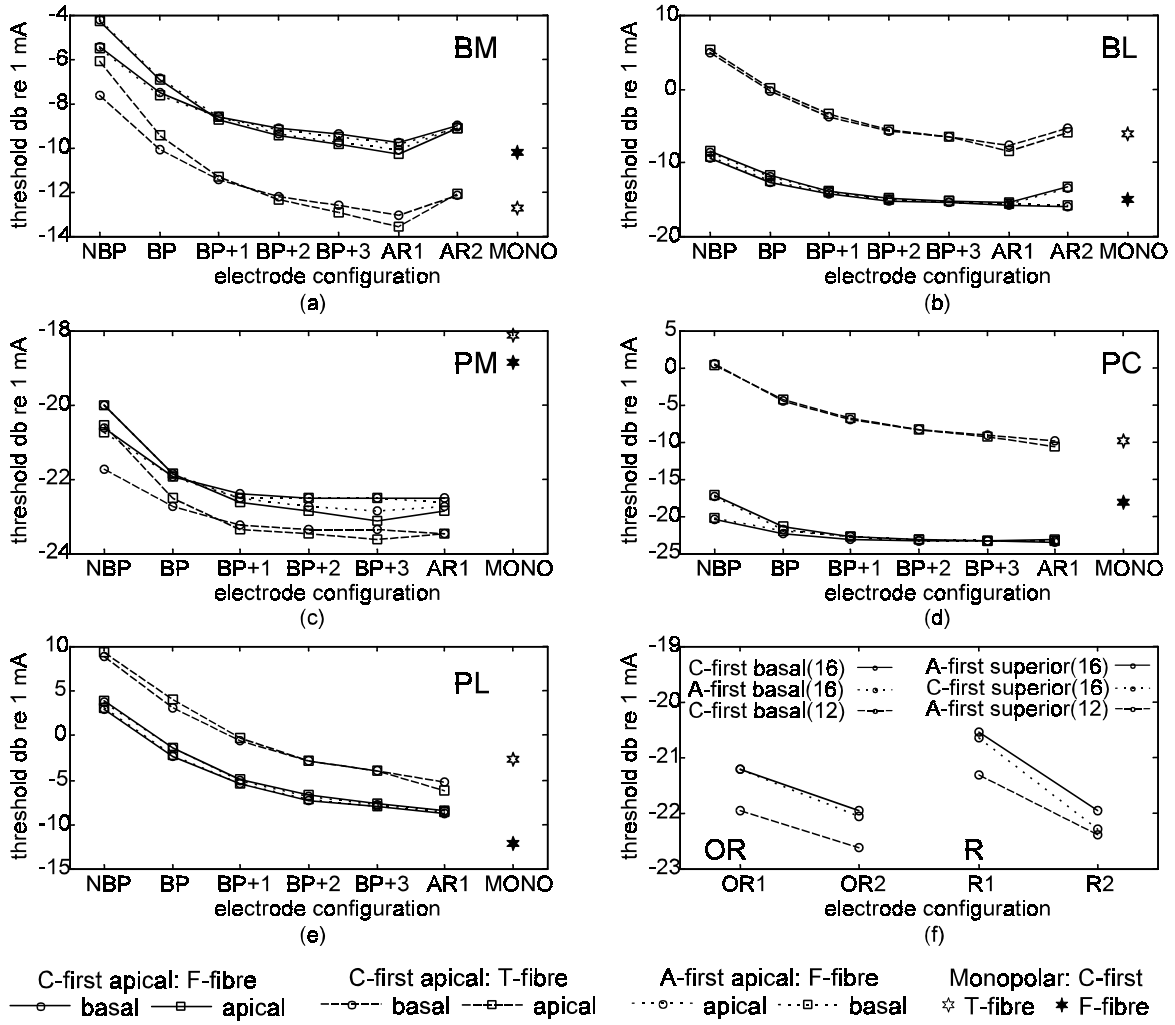

Figure 3.8. Threshold currents for nerve fibres activated by the electrode delivering the cathodic-first (Q) (C-first) and anodic-first (") (A-first) stimuli. Results are presented for both cathodic-first on the apical electrode (solid lines) and cathodic-first on the basal electrode (dotted lines) when a full nerve model is used, and for cathodic-first stimulation on the apical electrode when a truncated nerve model is used (dashed lines). (a) to (e) are results for longitudinal electrode configurations for the BM, BL, PM, PC, and PL arrays respectively, while (f) shows results for radial and offset radial electrode configurations. Threshold currents for cathodic-first monopolar stimulation are indicated with stars. The legend for figures (a) to (e) is at the lower edge of the figure. "F-fibre" is used to indicate the full nerve fibre model with 16 nodes and "T-fibre" to indicate the truncated nerve fibre model with 12 nodes.

When the polarity of the stimulation current is reversed, the model usually predicts minimum threshold currents to occur for the same nerve fibre. Thus, stimulus polarity does not influence the location of excitation along the basilar membrane. Also, the threshold current versus electrode separation curve for a specific electrode remains almost unchanged irrespective of stimulus polarity. Threshold currents are usually the lowest when the apical electrode in a bipolar pair delivers the cathodic-first stimulation, although this minimum current might excite nerve fibres close to the basal electrode. Typically, the model predicts lower threshold currents for nerve fibres near the basal electrode irrespective of stimulus polarity.

Similar to bipolar stimulation, threshold currents for monopolar stimulation are a function of array to surviving nerve fibre proximity and of electrode geometry. Generally, threshold currents are approximately the same as those for widely spaced bipolar electrode configurations. The exception is the PM and PC arrays where thresholds are substantially elevated from those of widely spaced bipolar configurations. This elevation in threshold current is most likely as a result of the configuration of the remote electrode. For monopolar stimulation the remote electrode is configured as an equipotential surface carrying a uniform current density over the outer boundaries of the bone cylinder. This causes current to be dispersed radially from the electrode contact, whereas current is directed mostly between the two electrodes in an AR configuration. Because of elevated threshold currents for the PM array, less variation exists between threshold currents for different electrode geometries and array locations for monopolar electrode configuration than for AR1 stimulation.

Truncation of the nerve fibre model causes minimum threshold currents to decrease for medial array locations (BM and PM) and to increase for lateral array locations (BL, PC and PL). The largest differences in threshold current are seen for the BL and PC arrays (approximately 7 dB to 15 dB) while the PM and BM arrays show the smallest differences (approximately 1 dB to 3 dB). The PL array is moderately influenced by nerve truncation with a threshold increase from the full to the truncated model of

approximately 6 dB. Figure 3.8f shows that threshold currents for pure radial and offset radial electrode configurations are comparable to threshold currents for bipolar stimulation with the PM array. Similar to longitudinal electrode configurations, threshold currents for radial and offset radial configurations are lower for widely spaced electrode pairs than for closely spaced electrode pairs. Lower threshold currents are achieved when the superior electrode is used to deliver the cathodic-first stimulus.

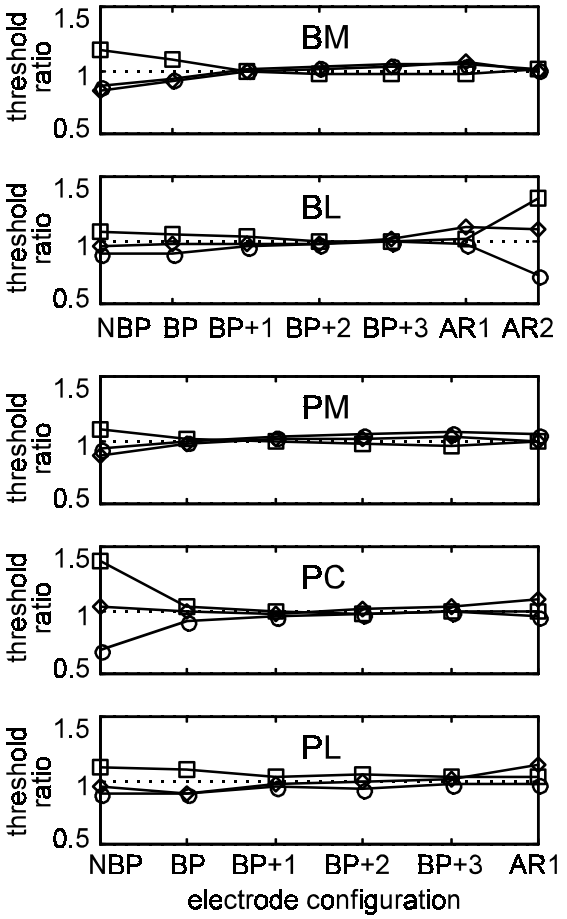

Figure 3.9. Anodic-first to cathodic-first threshold ratios for the BM, BL, PM, PC, and PL arrays as a function of electrode separation.

3.2.1.2 Threshold currents in a model with varying perilymphatic resistivity

The effect of varying the resistivity of the perilymphatic spaces in the modelled cochlea is to elevate threshold currents in the basal region while lowering these currents in the apical region of the model (Figure 3.10). Threshold currents for constant perilymphatic resistivity are relatively constant over the entire length of the modelled cochlea.

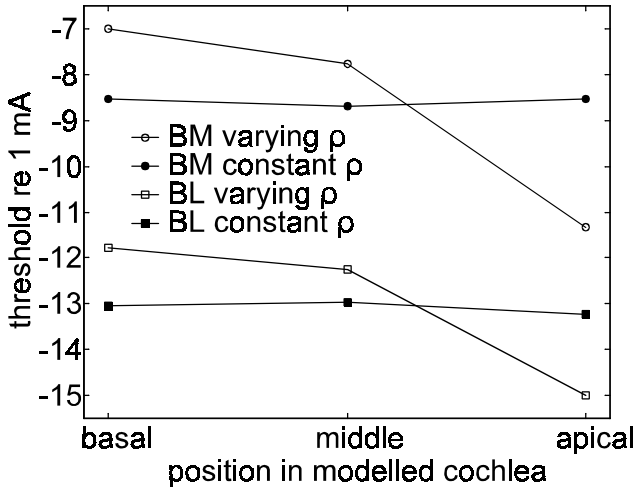

Figure 3.10. Threshold currents as a function of location in the modelled cochlea for constant and varying perilymphatic resistivities.

3.2.1.3 *Threshold currents for a Hifocus-like electrode geometry*

Minimum threshold current is lowest for the Hi1 geometry while the control geometry exhibits the highest minimum threshold current (Figure 3.11). Similar to banded and point electrode geometries, minimum threshold current is lower for widely spaced electrode configurations (AR1) than for narrowly spaced configurations (BP). Note that threshold currents are higher than those for the PM array because the surface area of the electrodes used for the Hifocus-like electrode geometries are approximately four times larger than the surface area of the electrodes used for the PM array.

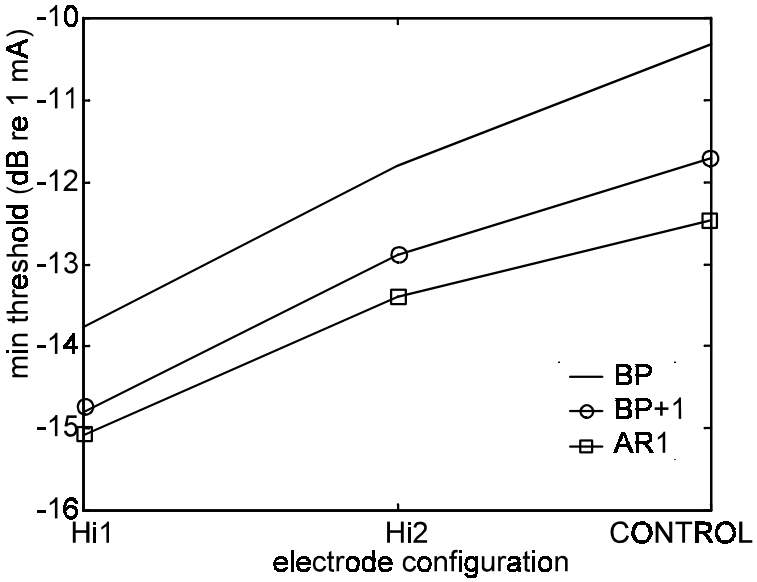

Figure 3.11. Minimum threshold current as a function of electrode geometry for BP, BP+1 and AR1 electrode configurations.

3.2.1.4 Influence of cochlear structures on minimum threshold currents

No discernable changes in threshold currents are observed when the helicotrema is simulated at the apical end of the FE model (results are thus not graphically presented). The cochlear structures that have the largest effect on threshold currents predicted with the model compared to other structures, are Reissner's membrane and the spiral lamina (Figure 3.12). The basilar membrane is the third most important structure, while the effects of the Organ of Corti and the stria vascularis are almost negligible. The influence of the basilar membrane might be more pronounced for array locations distal from the nerve fibres, i.e. the BL array, where the array is located directly next to the basilar membrane.

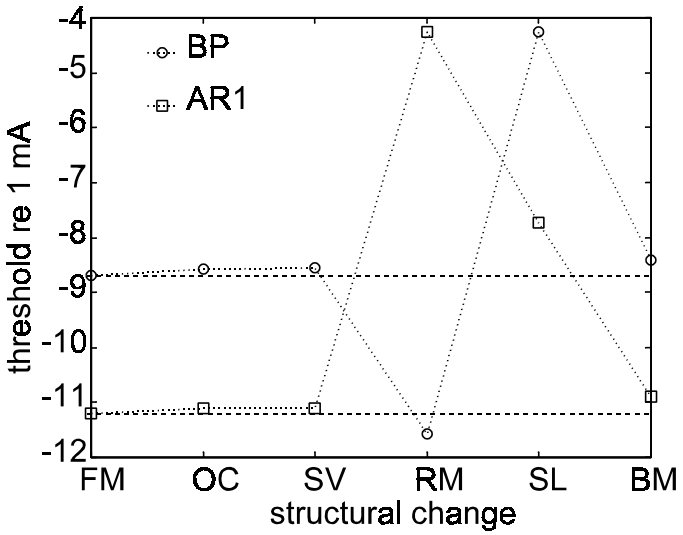

Figure 3.12. Minimum threshold currents as a function of model structure for BP and AR1 electrode configurations for the BM array. FM = full model (no structural changes); OC = Organ of Corti; SV = stria vascularis; RM = Reissner's membrane; SL = spiral lamina; BM = basilar membrane. Dotted lines are added between data points to accentuate differences between threshold currents for the various structural variations.

3.2.2 Electrical tuning curves

Figures 3.13 and 3.14 display spread of excitation as electrical tuning curves. The upper graph in each set shows electrical tuning curves for banded electrode geometries while the lower graph shows electrical tuning curves for point electrode geometries. To enable comparison of electrical tuning curves among different electrode locations and geometries, the minimum threshold current (i.e. the lowest threshold current for any nerve fibre in the model irrespective of stimulus polarity) for each configuration was used as reference (0 dB). Results are again presented for both a full nerve fibre model (solid lines) and a truncated nerve fibre model (dotted lines). Results discussed are for the full nerve fibre model unless stated otherwise. Since electrical tuning curves generated with opposite stimulus polarities differ only marginally, only electrical tuning curves for cathodic-first stimulation on the apical

electrode are presented.

Electrical tuning curves reach minimum levels on nerve fibres directly opposite the stimulating electrodes for array locations close to the target nerve fibres. Similar to the findings of Frijns (1995) longitudinal displacement of the minima toward the apex relative to the stimulating electrodes often occurs for array locations further away from the nerve fibres. Excitation spread for stimulus intensities below 10 to 30 dB, depending on the electrode configuration, is confined to fibres close to the stimulating electrodes.

3.2.2.1 Bimodal versus unimodal excitation

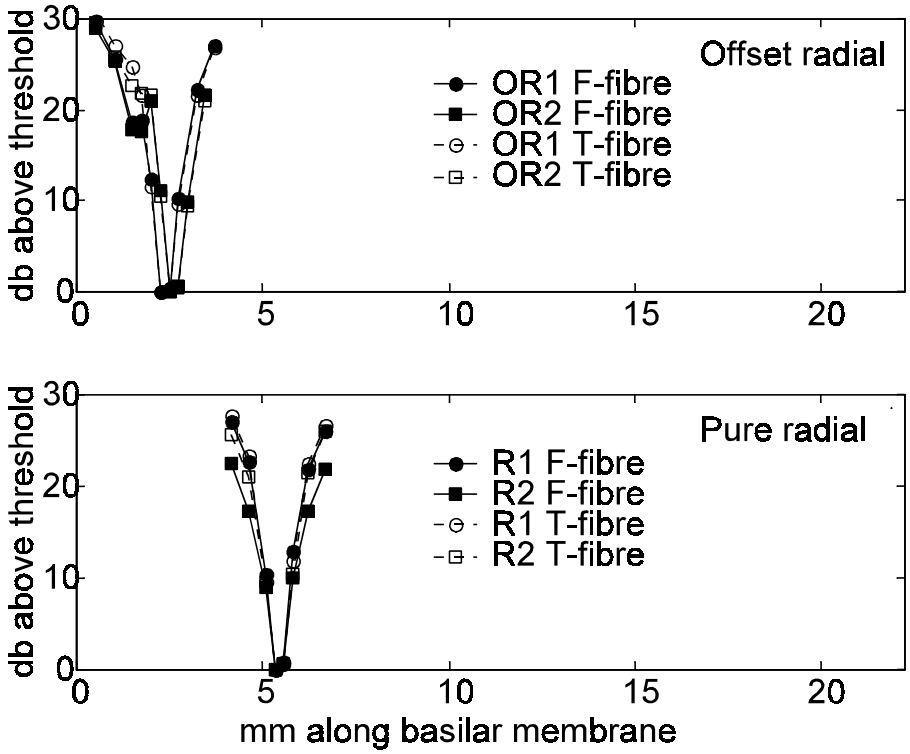

Figure 3.13. Offset radial (upper graph) and pure radial (lower graph) electrode configurations. Electrode locations are not shown.

For bipolar stimulation two regions of excitation, one at each electrode, exist during one stimulus cycle. The magnitude of the central maximum is a function of electrode

separation. For closely spaced electrode configurations (NBP and BP) the maximum is usually lower than the maximum between more widely spaced electrode configurations. Also, the magnitude of the maximum tends to level off toward wider electrode configurations.

With monopolar (Figure 3.14f) and also with radial and closely spaced offset radial electrode configurations (Figure 3.13) only one threshold minimum occurs, contrary to the two minima created with bipolar longitudinal electrode configurations (Figures 3.14a to 3.14e). For the wider offset radial configuration (OR2), a second region of excitation emerges at approximately 17 dB above threshold. Similar to bipolar configurations, the location of the threshold minimum is independent of polarity. Threshold minima are generally the lowest for radial electrode configurations when the electrode closest to the fibre terminals, i.e. the superior electrode, is used to deliver the cathodic-first stimulus.

3.2.2.2 Spatial selectivity

Most electrical tuning curves for arrays close to the nerve fibres display discontinuities in slope at approximately three model segments (approximately 700 to 820 m along the length of the basilar membrane) from their respective minima. These discontinuities indicate high spatial selectivity close to the electrodes up to stimulus intensities where the discontinuity occurs and less selectivity at stimulus intensities above the discontinuity. The critical focussing intensity (CFI) is defined as the lowest stimulus intensity relative to the minimum threshold at which this discontinuity occurs. The definition specifies the minimum intensity because some variation exists in the exact stimulus intensity where the discontinuity occurs on different sides of the location of a minimum in the electrical tuning curve and also for different electrodes in the array. The CFI gives an indication of the range of relative stimulus intensities over which focussing of neural excitation occurs.

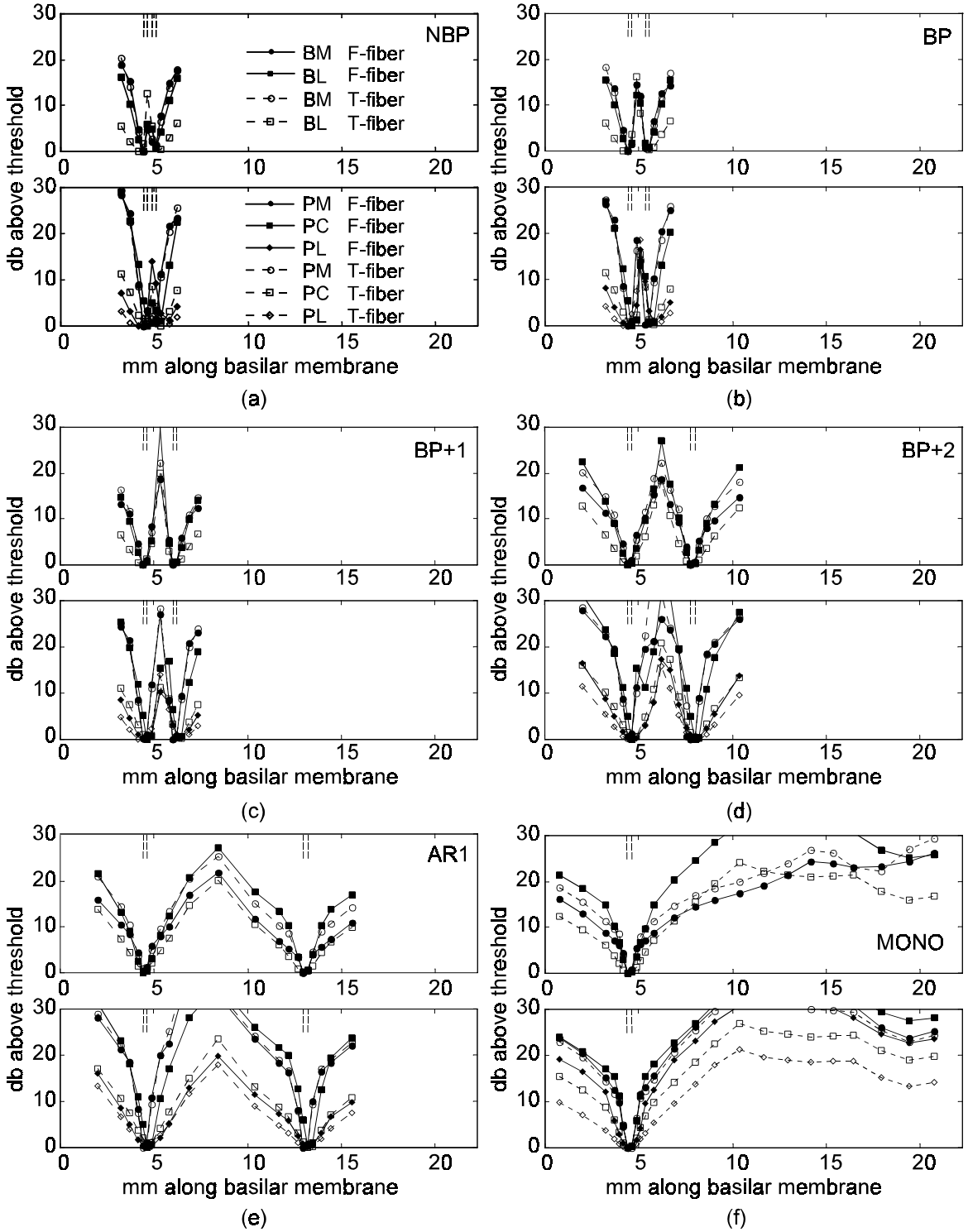

Figure 3.14. Electrical tuning curves for (a) NBP (b) BP, (c) BP+1, (d) BP+3, (e) AR1 and (f) MONO electrode configurations. The legend is shown in (a). "F-fibre" refers to a full nerve model with 16 nodes and "T-fibre" refers to a truncated nerve model with 12 nodes. The location of the electrodes is indicated by the dashed lines in the upper part of each graph.

The CFI decreases with increasing interelectrode separation (Figure 3.15). For the BM array with a full fibre model relatively localized excitation is achieved up to approximately 15 dB above threshold for NBP electrode configuration, while localized excitation is only achieved up to approximately 4 dB for AR1 electrode configuration. Localized activation is achieved up to approximately 4.4 dB for monopolar stimulation, which is comparable to the localization ability of widely spaced electrode configurations.

The CFI is either not visible or only faintly visible for array locations distal to the nerve fibres, indicating that spread of excitation is more or less directly proportional to interelectrode separation. This is also true for monopolar stimulation if the electrode is located far from the nerve fibres. The CFI is also not very pronounced for radially oriented electrode configurations when compared to those of longitudinal electrode configurations (compare R1 in Figure 3.13 with BM in Figures 3.14a to 3.14e).

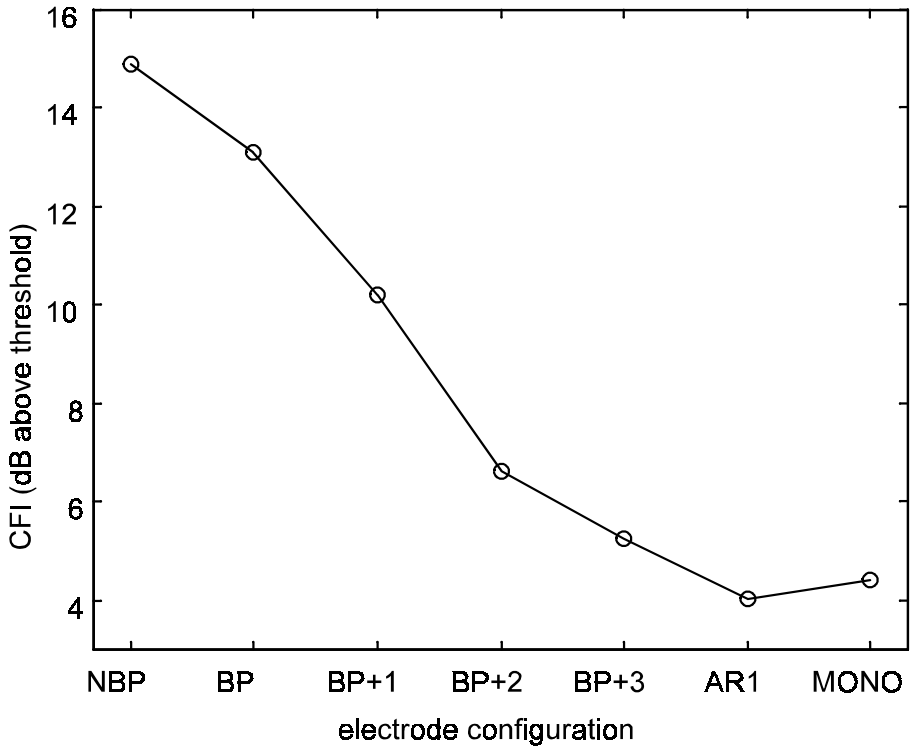

Figure 3.15. CFI as a function of electrode configuration for the BM array for a full nerve fibre model.

3.2.2.3 Symmetry

The symmetry of excitation around the two electrodes in a longitudinal electrode pair is evaluated by folding electrical tuning curves back onto themselves through a point halfway between the electrodes (Figure 3.16). The effect of unequal model segment lengths is partly compensated for by the mapping of tuning curves onto the same section of the basilar membrane. These plots display a fair amount of symmetry[5] between electrical tuning curves around basal and apical electrodes for closely spaced electrodes. For BP electrode configuration (upper set of graphs in Figure 3.16) substantial deviations from symmetry exist in electrical tuning curves of the PC and PL arrays. Asymmetry is more pronounced for AR1 electrode configuration, shown in the lower set of graphs in Figure 3.16. Though the initial location of excitation along the basilar membrane (i.e. the locations of the minima in the curves) remains unchanged for all array locations except for the PC array (for the full nerve fibre model), excitation is more localized around the basal electrode than around the apical electrode.

3.2.2.4 Spread of excitation

The upper graph in Figure 3.17 shows the spread of excitation close to *one* electrode in an electrode pair along the basilar membrane at 10 dB above threshold for a full nerve fibre model while the lower graph in Figure 3.17 shows the same for a truncated nerve fibre model. Excitation spread for NBP electrode configuration is not included since the regions of excitation for the two electrodes are not separate at 10 dB above threshold. Likewise, results for the PL array for the truncated nerve fibre model are not included above BP+1 electrode configuration since the 10 dB spread exceeds the length of the basilar membrane over which electrical tuning curves were calculated.

---

[5]The term "symmetry" is used to decribe the situation where initial excitation, i.e. minimum threshold current, for both electrodes occur on the same nerve fibre(s), e.g. the BP electrode configuration for the BM array and a full nerve fibre model in the upper set of graphs in Figure 3.16 where the minima occur on the nerve fibres directly opposite the boundaries of the electrodes. Asymmetry is also defined as noticeable differences in the amplitude of the tuning curves.

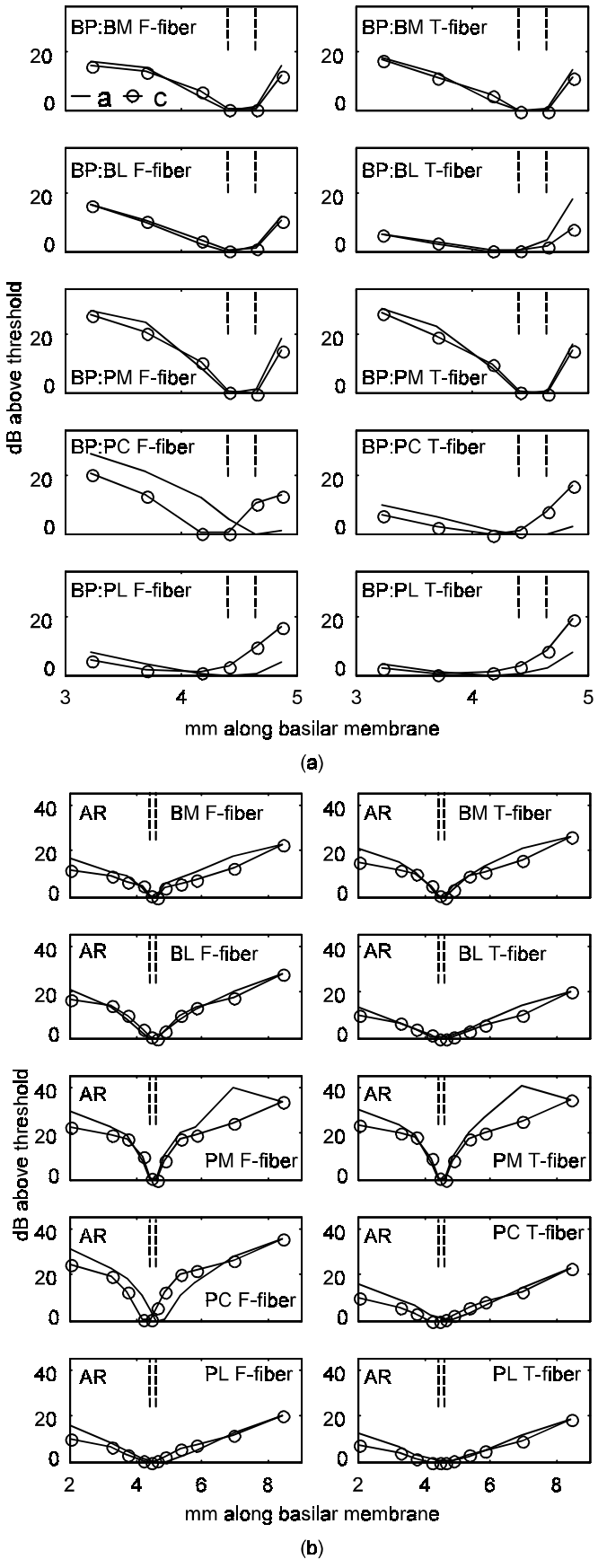

Figure 3.16. Electrical tuning curves of BP (upper set of graphs) and AR1(lower set of graphs) electrode configurations folded back around a point halfway between the electrode contacts to demonstrate the degree of symmetry between excitation pattern generated with the cathodic-first (solid line marked with circles) and the anodic-first (clean solid line) stimuli. Cathodic-first stimuli were applied to the apical electrode, which implies that the left side of the graph would be toward the apex for the cathodic-first curve and toward the base for the anodic-first curve.

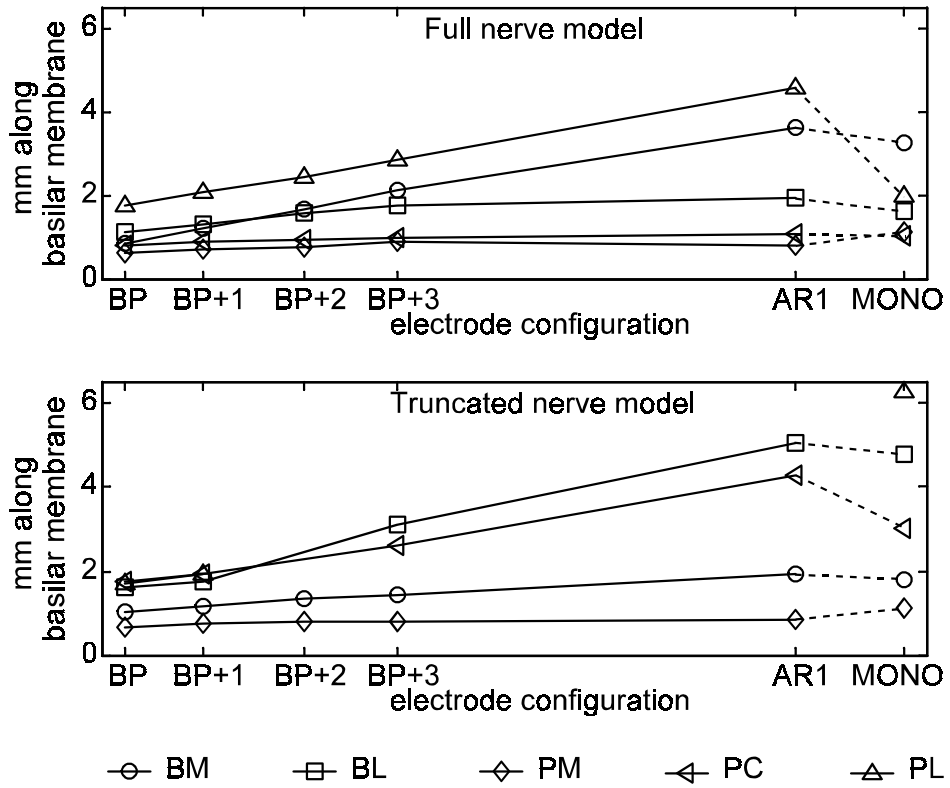

Figure 3.17. Excitation spread along the length of the basilar membrane as a function of electrode separation for a full nerve fibre model (upper graph) and a truncated nerve fibre model (lower graph) at 10 dB above threshold. Note that spread of activation is calculated around *one* electrode only. For bipolar electrode configurations the total spread is approximately twice the values indicated in the figure. Electrode separation for each configuration is indicated to scale relative to BP configuration on the abscissa except for monopolar electrode configuration.

The 10 dB spread levels off for array locations close to the target nerve fibres (except the BM array in the upper graph in Figure 3.17), e.g. for arrays BL, PM and PC when a full nerve fibre model is used and for arrays PM and BM when a truncated nerve fibre model is used. 10 dB spread increases almost linearly with electrode separation for array locations distal to the nerve fibres (and for the BM array when a full nerve fibre model is used). Narrower electrode separations and array locations close to the target nerve fibres usually cause narrower 10 dB spread than widely spaced

electrode configurations far from the target nerve fibres. For the bipolar electrode configurations the narrowest spread is produced by the PM array under all conditions while the widest spread is produced by the PL array.

For monopolar electrode configuration, spread of excitation is generally lower than for AR1 electrode configuration. It is approximately the same as around one electrode for BP+3 electrode configuration. However, it is interesting to observe that the decrease in spread of excitation relative to that for AR1 is much larger for the PL array using monopolar electrode configuration when a full nerve fibre model is used than for any other electrode geometry or array location. In this case monopolar stimulation yields spread of excitation similar to BP+1 electrode configuration. Like minimum threshold currents, spread of excitation is less sensitive for electrode geometry and array location for monopolar stimulation compared to that for AR1 stimulation.

3.2.2.5 *Ectopic excitation*

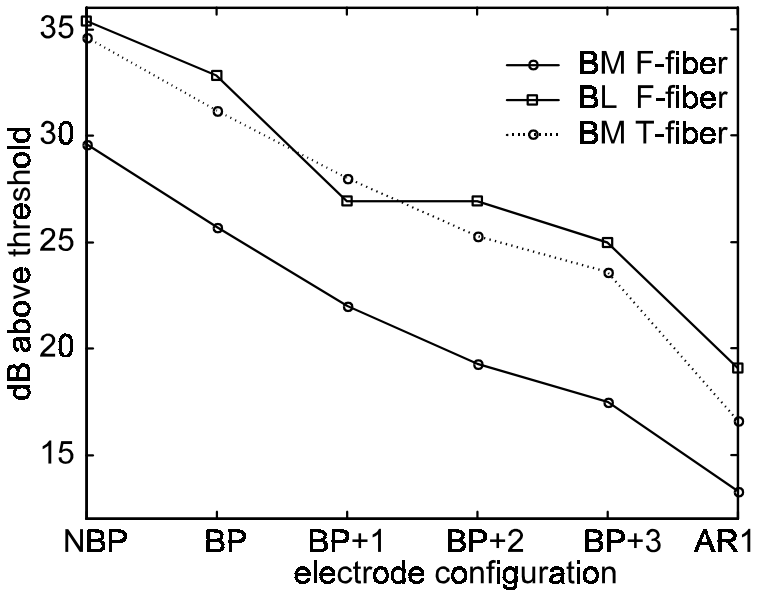

Figure 3.18. Stimulation intensities where ectopic stimulation occurs as a function of electrode separation for different array locations. Legend is explained in the caption of Figure 3.14.

Ectopic excitation was evaluated by determining threshold currents for nerve fibres originating from the superior cochlear turn. Figure 3.18 shows ectopic stimulation threshold currents for different electrode configurations for the BM and BL arrays using the full nerve fibre model, and also for the BM array using the truncated nerve fibre model. Results show that ectopic stimulation can be expected to occur more readily for widely spaced electrode configurations and that ectopic stimulation for the BM array decreases when the peripheral processes of the nerve fibres have degenerated.

Figure 3.14f shows that for monopolar stimulation, the stimulation current intensity where ectopic stimulation occurs depends on the nerve fibre model used (full or truncated) and the array location. For this case, ectopic stimulation tends to occur at lower stimulation currents when the truncated nerve fibre model is used. The only exception is the BM array for which ectopic excitation occurs at higher stimulus intensities because of the displacement of the fibre terminals relative to the location of the array. The same effect is expected for bipolar electrode configurations.

3.2.2.6 *Resolution of electrode arrays*

Two neighbouring pairs[6] of NBP electrodes (Figure 3.19) have similar excitation patterns with a high degree of overlap. However, an offset (approximately equal to the offset between the electrode pairs along the basilar membrane) exists between the regions of excitation of the two electrode pairs even at high stimulus intensities (10 to 20 dB above threshold).

[6]Two neighbouring pairs in this case are made up of three neigbouring electrodes, i.e. the first pair comprises electrodes *n-1* and *n* and the second pair electrodes *n* and *n+1*.

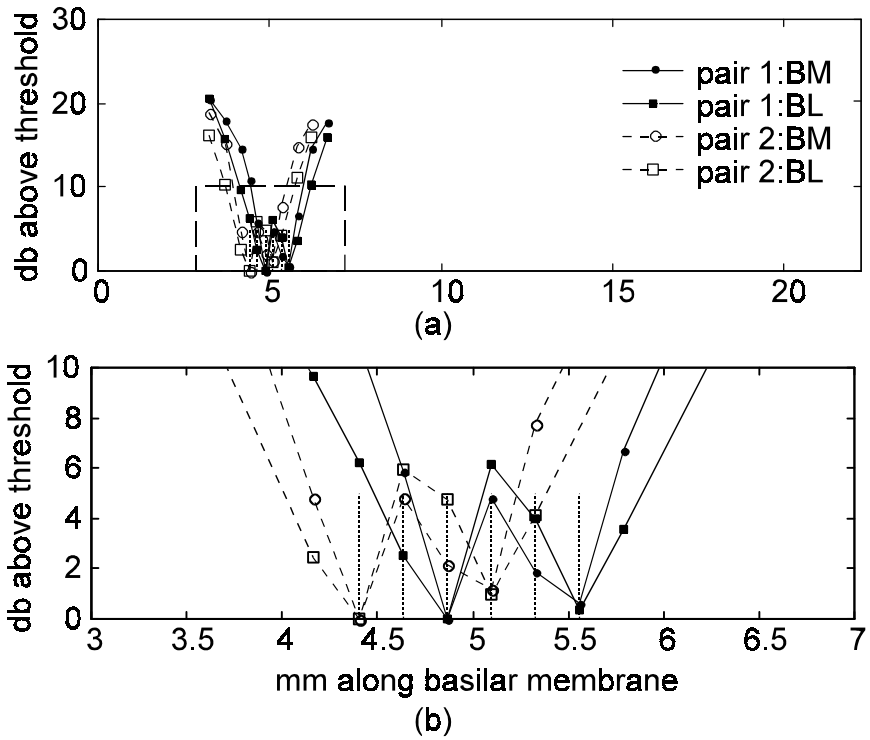

Figure 3.19. Electrical tuning curves generated with two sets of neighbouring NBP electrode pairs (upper graphs). The vertical dotted lines indicate the boundaries of the three electrodes that are used to define the two neighboring electrode pairs (i.e., pair one comprises the left and middle electrodes and pair two the middle and right electrodes). The lower graph shows an enlarged view of the dashed block in the upper graph to present a clear view of the offset between the regions of excitation. Results are for the BM and BL arrays respectively for a full nerve fibre model.

3.2.2.7 Simulated tapering of the scala tympani and scala vestibuli

Scaling of the resistivity of the scalae tympani and vestibuli to simulate tapering of the cochlea does not have a pronounced effect on the spread of excitation at low stimulus intensities (Figure 3.20). However, consistent with what is expected, an increase in spead of excitation at high stimulus intensities can be observed in the tuning curve calculated for the scaled resistivity relative to the tuning curve for constant resistivity closer to the base of the modelled cochlea (upper graph in Figure 3.20) especially for the BM array. The opposite takes place near the apex (lower

graph in Figure 3.20). Tuning curves calculated at a location halfway through the first half-turn of the cochlea are less affected because the resistivities in this region are approximately equal in both the model with constant resistivity and the model with scaled resistivity.

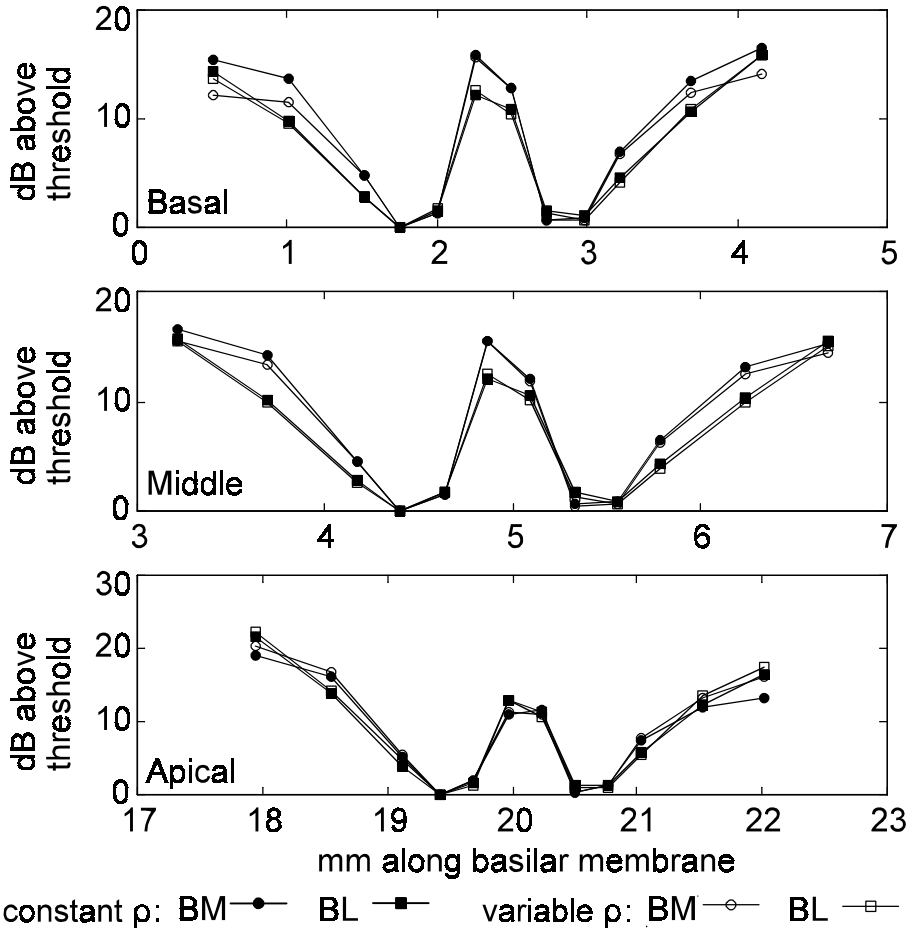

Figure 3.20. Electrical tuning curves at different locations in the modelled cochlea for constant and scaled perilymphatic resistivities. BP electrode configuration was used.

3.2.2.8 Hifocus-like electrode geometries

Electrical tuning curves for the Hifocus-type electrode geometries and for the control electrode geometry are shown in Figure 3.21. Excitation is more localized for the Hifocus-like electrode configurations than for the control geometry for all electrode configurations. The CFI is higher for Hi1 and Hi2 than for the control geometry

(Figure 3.22). The CFI also tends to be lower for Hi1 than for Hi2, indicating a lower range of stimulus intensities over which focussing occurs.

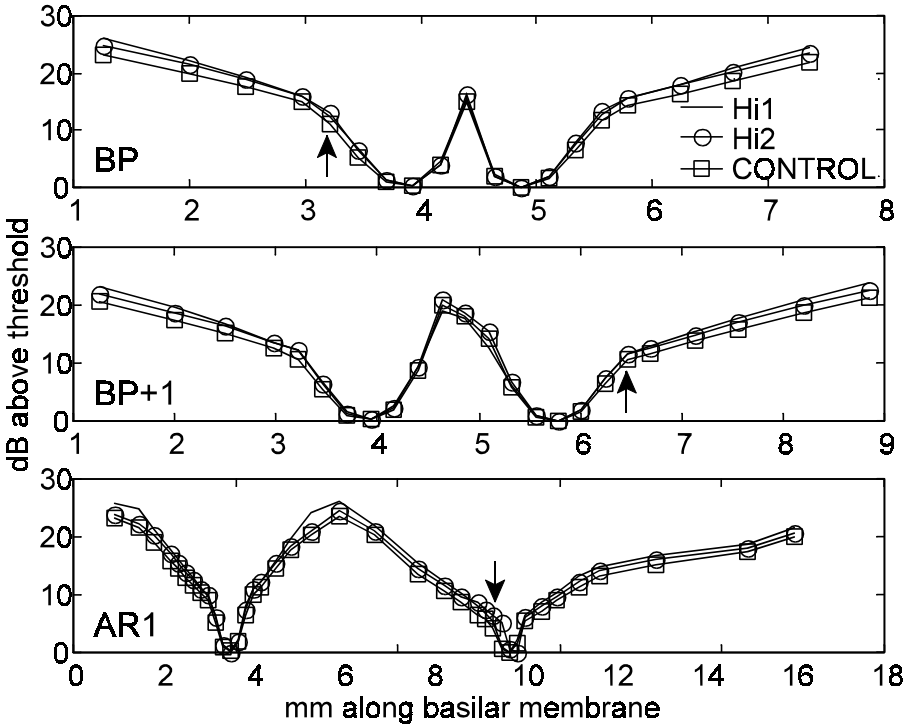

Figure 3.21. Electrical tuning curves for different electrode geometries for BP (upper graph), BP+1 (middle graph) and AR1 (lower graph) electrode configurations. The arrows indicate the location of the CFI in the curves (see Figure 3.23). The legend is the same for the three graphs.

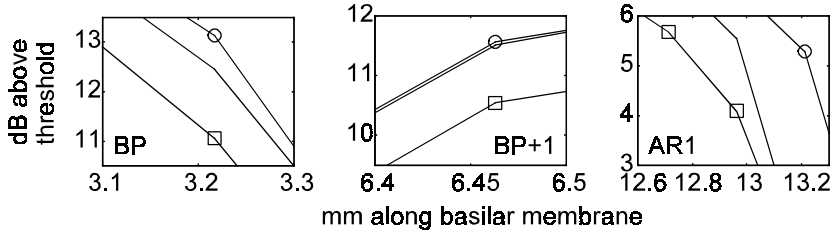

Figure 3.22. An enlarged view of the position of the CFI in Figure 3.21 (arrows) for the electrode geometries Hi1 (no marker), Hi2 (marked with ") and the control geometry (marked with Q).

The focussing ability of the electrode geometries is calculated as the percentage decrease in spread of excitation along the basilar membrane relative to the control electrode geometry. Both Hi1 and Hi2 exhibits better focussing than the control electrode geometry at all stimulus intensities. For narrowly spaced electrode configurations the focussing ability tends to increase as a function of stimulus intensity. However, there is a limit above which the focussing ability starts to decrease. This limit is clearly visible in the 20 dB curve for AR1 electrode

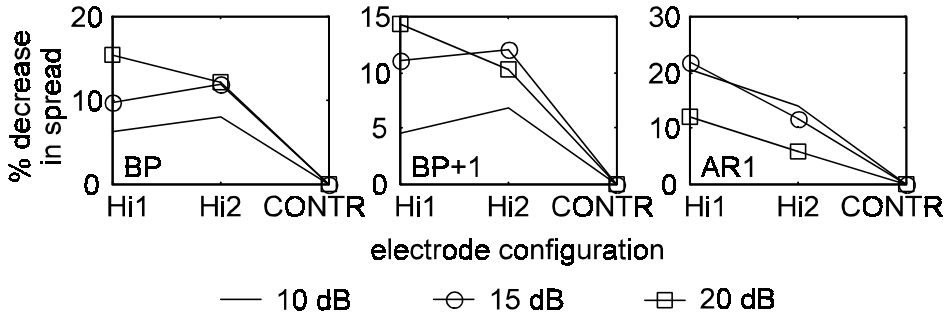

Figure 3.23. Percentage decrease in spread as a function of electrode geometry for BP (left), BP+1 (middle) and AR1 (right) electrode configurations. The legend is the same for the three graphs.

configuration (rightmost graph in Figure 3.23). A decrease in the focussing ability of a test electrode pair relative to a reference electrode pair indicates that the test electrode pair is operating above its CFI or that its focussing ability is less than that of the reference electrode pair. Above their respective CFIs, electrical tuning curves for Hi1 and Hi2 display a constant difference with respect to the tuning curve of the control electrode (i.e. the tuning curves are approximately parallel to one another for AR1 electrode configuration in Figure 3.21). The focussing ability therefore decreases because focussing as a fraction of spread of excitation decreases. For narrowly spaced electrode configurations the focussing ability of Hi1 and Hi2 geometries are similar for 10 and 15 dB relative stimulus intensities. However, at 20 dB relative stimulus intensity Hi1 has better focussing ability than Hi2.

3.2.2.9 *Influence of cochlear structures on neural excitation*

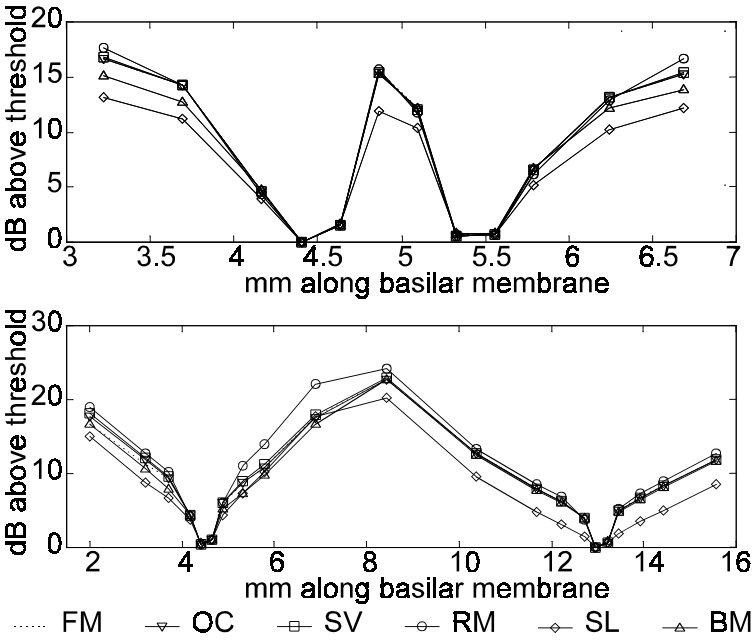

Figure 3.24. Electrical tuning curves showing the effect of omission of the Organ of Corti (OC), stria vascularis (SV), Reissner's membrane (RM), spiral lamina (SL) and the basilar membrane (BM) for BP (upper graph) and AR1 (lower graph) electrode configurations. Results for the full FE model (FM) are also shown.

Inclusion of a helicotrema in the FE model did not have a noticeable effect on neural excitation patterns. Figure 3.24 shows electrical tuning curves as a result of potential distributions generated with structural variations in the FE model for the BM array and BP and AR1 electrode configurations. The basilar membrane and the spiral lamina have the most pronounced influence on excitation patterns. The CFI is lowered in the absence of these structures. This effect is also present, but less obvious for Reissner's membrane. When Reissner's membrane is omitted, spread of excitation is in fact limited relative to spread of excitation in the full FE model for AR1 electrode configuration at stimulus intensities above the CFI. Neither the Organ of Corti nor the stria vascularis has a marked influence on electrical tuning curves.

4 DISCUSSION

Spread of excitation and minimum threshold currents are both important parameters for the effectiveness and functioning of cochlear implants. Results are thus discussed in terms of these two parameters. Spread of excitation determines the number of independent information channels that can be used to transfer auditory information to the brain. This is because spread of excitation as a result of stimulation with one electrode pair, places a limitation on how close to this electrode pair another pair can be placed to excite a sufficiently different set of nerve fibers so that a sound produced by the first set is discriminable from a sound created by the second set. Spread of excitation therefore has an influence on the number of electrodes that can effectively be used to transfer auditory information (Hanekom & Shannon, 1998).

Threshold currents should be as low as possible for three primary reasons: (1) lower currents are safer for both the electrodes (Rose & Robblee, 1990) and the nerve fibers (Shannon, 1992), (2) consistent use of lower currents prolongs the life of the energy source (Roland et al., 2000; Spelman et al., 1982; Tykocinski et al., 2000) and (3) lower threshold currents could provide an increase in dynamic range (Shepherd et al., 1993).

4.1 Potential distributions and AF contours

The model predicts an increase in the size and intensity of potential distributions for wider electrode separations, consistent with the experimental findings of Suesserman & Spelman (1993), Pfingst et al. (1995) and also with results obtained with the analytical model. Potential distributions generated with the spiralling model are not symmetric for longitudinal electrode configurations. The greatest deviation from symmetry is seen with array locations close to the nerve fibres (e.g. PM in Figure 3.4) and also for widely spaced electrode configurations. Deviations from symmetry for widely spaced electrodes could occur as a result of variation in the length of model segments. However, asymmetry was also observed in some cases for closely

spaced electrode configurations (e.g. BP electrode configuration for the PC and PL arrays in Figure 3.16a). Asymmetry is thus not only a function of the tapering of the cochlea but also of the spiralling geometry of the cochlea and thus the position of the electrode contacts along the length of the basilar membrane. Asymmetry for BP electrode configuration did not increase noticeably with simulated tapering in the model, probably because the electrode pair was located within segments of constant resistivity (refer to section 2.2.1 of this chapter), e.g. the electrode pairs located at the base and halfway through the first turn of the model, or the electrode pair was situated over a boundary between two resistivities, but the change in resistivity was low, e.g. the electrode pair at the apex of the modelled cochlea. However, in a real cochlea greater asymmetry is expected as a result of tapering of the cochlear canals, especially in the basal region of the cochlea where the diameter of the scala tympani changes rapidly (Hatsushika et al., 1990).

Neural excitation can be evaluated through the activating function (Rattay, 1990; Rattay, 1999) which is proportional to the second spatial derivative of the potential along a long homogeneous nerve fibre. The width of the potential distribution around an electrode gives an indication of the magnitude of the activating function. If the maximum potential is fixed, a wider potential distribution will result in a lower activating function than a narrower potential distribution. Since the activating function at a node is proportional to the nett current flow through the membrane at the node (Finley, Wilson, & White, 1990), the magnitude of the activating function gives an indication of the excitation ability of a potential distribution. A scaled-down version of an activating function (i.e. an activating function with a lower magnitude) will create a narrower region of activation than a scaled-up version of the same activating function. Although this effect is not very profound in the model, it is evident in, for example, the potential distribution for BP+3 electrode configuration for the PM array in Figure 3.4, where the potential distribution around the basal electrode is wider than the potential distribution around the apical electrode. The spread of excitation around the basal electrode at 10 dB above threshold is calculated as 0.72 mm, while the excitation spread around the apical electrode at the same stimulus intensity is

calculated as 0.92 mm. In the *in vivo* situation the cochlea widens toward the base, which leads to a decrease in the resistance of the volumes close to the electrode contacts (Spelman, Clopton, & Pfingst, 1982). At a specific stimulus intensity one would therefore expect even wider potential spread than predicted with the current model, resulting in narrower spread of excitation. This is consistent with data indicating more localized currents (and thus excitation) around basal electrodes than around apical electrodes (Black, Clark, & Patrick, 1981), as well as increased perceptual thresholds toward the base of the cochlea (Lim, Tong, & Clark, 1989).

Maxima and minima in the AF contours show the location along the basilar membrane (and along the nerve fibres) where excitation can be expected to occur first. The highest activating function intensities occur at the location of the electrodes on the basilar membrane-nerve fibre plane. Maxima and minima occur approximately 0.5 mm from the nerve fibre terminals for medial arrays and at close to the nerve fibre terminals for the lateral array.

AF contours also show that excitation can be expected to spread along the basilar membrane at higher stimulus intensities. This is because the activating function deviates from zero over extended areas along the basilar membrane (Figure 3.4). The intensity of the activating function, which gives an indication of the exciting ability of the stimulus, increases with stimulus intensity, indicating more widespread excitation along the length of the basilar membrane. AF contours also predict an increase in spread of excitation with increasing interelectrode separation. This can be seen in the spatial increase of regions where the intensity of the activating function deviates from zero for wider electrode separations relative to narrower electrode separations. The values of the activating function maxima and minima also increase with interelectrode separation indicating that lower minimum threshold currents are required for widely spaced electrode configurations than for narrowly spaced electrode configurations. This is consistent with the observations of Pfingst et al. (1995).

4.2 Effects of electrode configuration, electrode geometry and array location

4.2.1 Excitation thresholds

Neural excitation patterns predicted by the model are dependent on the exact location of the electrode contacts relative to the nerve fibre terminals (Kral et al., 1998). In pathological cochleas the distal nerve processes are frequently degenerated (Shepherd, Hatsushika, & Clark, 1993). If degeneration of the peripheral nerve processes is assumed up to the soma, threshold currents change markedly for the BL and PC arrays while remaining relatively unchanged for the PM and BM arrays compared to threshold currents for a full nerve fibre model. Consistent with experimental results from Shepherd, Hatsushika and Clark (1993), much lower threshold currents are predicted for array locations close to the nerve fibres and fibre terminals than for array locations further away. Electrode arrays should thus be placed in close proximity of the modiolus for two reasons: to achieve optimal (i.e. minimum) threshold levels and to reduce the effect of postsurgical neural degeneration (Leake et al., 1992) on threshold currents. Minimum threshold currents are more energy-efficient than high threshold currents and prolong the life of electrodes and the power source of the implant (Roland et al., 2000; Spelman, Clopton, & Pfingst, 1982; Tykocinski et al., 2000).

The use of point electrode geometries is recommended above banded electrode geometries if array location can be controlled. However, banded electrode geometries are superior to point electrode geometries for obtaining low threshold currents when the array location cannot be precisely controlled, as is evident from high threshold currents obtained with the PL array (Figure 3.8e) and also the PC array (Figure 3.8d) when a truncated nerve fibre model is used.

Minimum threshold currents determined for Hifocus-like electrode geometries are lowest when the electrodes are recessed into the electrode carrier on all sides (Hi1). Partly recessed electrodes (insulating pillows between the contacts) also lower minimum threshold currents relative to non-recessed electrodes, but not as much as totally recessed electrodes. The planar nature (Advanced Bionics Corporation, 8-21-

2000) of the electrodes of the Hifocus electrode, which could also limit current spread, was not modelled (the modelled electrode approximates a curved surface). However, based on model results for a curved electrode surface, the focussing ability of the Clarion Hifocus electrode could potentially be improved further by extending the electrode carrier over the superior and inferior sides of the contacts so that these sides are also recessed like the lateral sides.

Several researchers have presented data showing that initial excitation can be produced by either the anodic or cathodic phase of a stimulus waveform (Liang, Lusted, & White, 1999; van den Honert & Stypulkowski, 1987). Also, the polarity of the leading phase in a biphasic stimulus does not have a pronounced influence on the minimum current required to elicit a nerve fibre response. When the electrode contacts are close to the fibre terminals or distally toward the outer wall of the scala tympani, the nerve fibre model usually predicts lower threshold currents for nerve fibres close to the basal electrode than for nerve fibres close to the apical electrode in an electrode pair, irrespective of stimulus polarity. However, as a consequence of the manner in which the model was constructed (equal angle sections), lower thresholds would be expected for the apical electrode (smaller surface area and thus higher current density) if only the electrode surface area and its proximity to the nerve fibres were to determine minimum threshold currents. Model results therefore suggest that the location of the electrodes along the length of the basilar membrane has a stronger influence on the location of excitation along the basilar membrane than the polarity of the stimulus waveform. This observation cannot be fully tested with the current model since the equal angle model segments cause variation in the surface area of electrode contacts. The model does not allow continuous tapering of the cochlea either. Models incorporating tapering of the cochlea and constant electrode surface areas, and also measurement of neural excitation in the vicinity of both electrodes in an electrode pair in real cochleas, are required to verify the observation.

4.2.2 Spread of excitation

The CFI of a specific electrode pair gives an indication of the dynamic range over which relative focussed stimulation can be expected for that electrode pair. Variations in the CFI can be expected between different pairs of the same electrode configuration since it could be affected by electrode to nerve fibre proximity, the impedance pathway between the electrodes, electrode geometry and survival patterns of auditory nerve fibres. EABR input-output functions measured by Shepherd, Hatsushika and Clark (1993) on cats display a CFI in most cases. For electrodes placed near the spiral ganglion and the dendrites, the CFI is between 16 and 20 dB above threshold for BP electrode configuration and between 3.5 and 14 dB above threshold for BP+1 and BP+2 electrode configurations.

Five observations can be made from the CFI for different electrode configurations: 1) closely spaced bipolar electrode configurations have the best focussing ability, 2) if focussing is desired, an electrode pair should ideally operate at stimulus intensities below its CFI, 3) for electrode configurations that do not show a CFI, there is no critical range of operation, i.e. spread of excitation is proportional to stimulus intensity, 4) the focussing ability of monopolar electrode configurations is comparable to that of widely spaced bipolar electrode configurations, and 5) the focussing ability of recessed electrodes is higher than that of unrecessed electrodes.

Three observations regarding the effect of electrode configuration and array location on excitation patterns can be made from 10 dB excitation spread and will be explained below: 1) electrode separation cannot compensate for array location, 2) there is little difference between BP, BP+1, BP+2 and BP+3 electrode configurations, 3) excitation spread generated by array locations distal from the target nerve fibres increases significantly at wide electrode separations. Implications for cochlear implant subjects are the following: If threshold cannot be achieved with narrowly spaced electrode configurations, more widely spaced configurations (up to BP+3) can be used without a considerable increase in the 10 dB spread. This is also evident from

gap threshold data[7] (that give an indication of the amount of interaction between electrodes) that are similar for BP to BP+3 electrode configurations (Hanekom & Shannon, 1998) and from pitch ranking experiments where subjects' performances were similar for BP+1 and BP+3 electrode configurations (Hanekom & Shannon, 1996). The most effective way to control excitation spread is thus by controlling the location of the array relative to the target nerve fibres, i.e. arrays close to the target nerve fibres create more localized excitation spread. Electrode separation can to a limited extent be used to control excitation spread (i.e. closely spaced electrode configurations limit excitation spread) but not as effectively as correct placement of the array. When an array is located toward the outer wall of the scala tympani, as is often the case with the Nucleus implant (Shepherd, Hatsushika, & Clark, 1993), closely spaced electrode configurations should be used to limit spread of excitation. Again, a banded electrode geometry is superior to a point electrode geometry to limit excitation spread in this case (compare results for arrays BL and PL in Figure 3.17). Results for the AR1 configuration suggest that excitation (at comfortable stimulus intensities) is less localized with arrays located far from the target nerve fibres and is similarly not localized with true monopolar stimulation if the array is far from the target nerve fibres. However, localization is possible with AR1 and also with true monopolar stimulation when the array is close to the modiolus.

Based on the CFI and spread of excitation as functions of electrode configuration,

[7]Gap threshold is the minimum duration of a temporal gap between two sounds (i.e., sound, silence, sound) that is detectable by the auditory system. For cochlear implant wearers the experiment is performed by applying two stimuli to either the same electrode set or different electrode sets before and after a non-stimulation period. Hanekom and Shannon (1998) used two different sets of electrodes to deliver the stimuli. For this case, gap detection is presumably determined by a centrally located auditory integration mechanism. The more distinct the two excited neural populations, the longer the integration time constant and the higher the gap threshold. Similar gap thresholds for BP to BP+3 electrode configurations imply that the excited neural populations are similar and are therefore caused by similar spreads of excitation.

monopolar stimulation is recommended above widely spaced bipolar stimulation because of three reasons. Firstly, because focussing ability for the two configuration types is comparable, secondly because the unimodal excitation pattern of monopolar stimulation implies that only the intended neural population is activated and thirdly, because spread of excitation for monopolar stimulation is in actual fact approximately half that of widely spaced electrode configurations.

4.2.3 Banded versus point electrode geometries

A general overview of simulation results indicates that point electrode geometries and banded electrode geometries behave differently when they are located close to the fibre terminals. In general, a point electrode array close to the fibre terminals produces excitation paterns similar to those produced by an array overlapping with the nerve fibres, i.e. its behaviour is similar to that of the BM and PM arrays, while a banded electrode array at the same location produces excitation patterns similar to those produced by a laterally located array, i.e. its behaviour is similar to those of the BL and PL arrays.

4.3 Ectopic stimulation

Ectopic stimulation was evaluated by determining the stimulus intensity above threshold where *modelled* nerve fibres from the superior cochlear turn will be excited. Nerve fibres located in the region between the target nerve fibres and nerve fibres from superior cochlear turns will be excited at stimulus intensities between threshold currents for these two nerve populations. Also, the cochlea in the model is 25% higher than a real cochlea, which causes an underestimation of ectopic stimulation as a result of current spread to neighbouring cochlear canals. Figure 3.18 thus gives a relative indication of the occurrence of ectopic stimulation that can be expected with a specific electrode configuration and array location. Excitation spreads along the cochlear canal rather than across the modiolus or across neighbouring canals, i.e. excitation of nerves from superior cochlear turns occurs only at higher stimulus intensities. Ectopic stimulation occurs more readily for widely spaced electrode configurations than for closely spaced electrode configurations. Similarly, medial

array locations are more prone to ectopic excitation than arrays located more distally relative to the nerve fibres. There is thus a tradeoff between the extent of ectopic excitation and the proximity of the array to the target nerve fibres, especially at wider electrode configurations. The optimal arrangement to reduce ectopic excitation would thus be a *laterally* located array using a *closely spaced* electrode configuration. However, to reduce the spread of excitation along the length of the basilar membrane and to limit threshold currents, medial array locations are preferable, making the use of narrowly spaced electrode pairs even more important. Ectopic excitation can, however, also be defined as any unintentionally stimulated nerve fibres. According to this definition, one of the minima in the bimodal excitation pattern generated by bipolar electrode configurations is also an ectopic excitation region.

4.4 Bimodal versus unimodal excitation patterns

Anodic-first to cathodic-first threshold ratios for charge-balanced biphasic stimulation are close to unity in most cases, implying a very small difference in the excitation ability of the two electrodes in an electrode pair. At comfortable stimulus intensities[8] of 4.5 to 22.5 dB above threshold, bimodal excitation exists when a bipolar electrode configuration is used. These two excitation regions have been modelled (Frijns, 1995; Kral et al., 1998) and measured (Kral et al., 1998) for longitudinal bipolar stimulation. Eddington et al. (1988) also reported that subjects describe sound sensations generated with bipolar electrodes as "not as pure" as sensations generated with monopolar electrode configurations. To create a single region of excitation one of four electrode configurations can be used: NBP, offset radial, radial and monopolar electrode configurations. The two regions of excitation around the electrodes in an NBP electrode configuration overlap to a great extent if the array is located close to the nerve fibres, creating a single region of excitation above approximately 5 dB above threshold. However, excitation threshold currents for NBP are high compared to other electrode configurations (Figure 3.8).

[8]Comfortable stimulus intensities are assumed to be at 75% of dynamic range, which is 6 to 30 dB (Shannon, 1983).

Offset radial and pure radial electrode configurations are optimal for creating a single region of excitation at all stimulus intensities (Figure 3.13). Threshold currents are much lower for radially oriented configurations (up to 17 dB) than for NBP configurations and also (to a lesser extent) for monopolar electrode configurations. Threshold differences between NBP for the PM array and the radially oriented configurations are, however, not significant. However, NBP configuration creates a wider region of excitation under all circumstances than radially oriented configurations (compare Figures 3.13 and 3.14a). Thus, NBP configuration would only be advantageous if a banded electrode geometry is used. If a point electrode geometry is used, radially oriented electrode configurations are the configurations of choice because of their lower threshold currents and narrower regions of excitation. Offset radial electrodes should, however, not be separated by more than approximately 1 mm where a second region of excitation emerges at stimulus intensities in the order of 17 dB above threshold.

4.5 Resolution of intracochlear electrode arrays

Although excitation is not necessarily localized at higher stimulus intensities, model results indicate that excitation regions are different for different electrodes even when the electrodes in a bipolar pair are narrowly spaced (NBP). Based on this observation, the resolution of cochlear implant electrodes could potentially be improved, which could lead to improved speech recognition (Kral et al., 1998). The model firstly suggests that localized excitation is possible with NBP electrode configuration although threshold currents are 2 to 3 dB higher than threshold currents for BP electrode configuration (Figure 3.8). Secondly, results suggest that excitation profiles created with two bipolar pairs made up from three adjacent closely spaced electrodes are *different* since the regions of excitation do not overlap completely. It is possible that cochlear implant subjects can discriminate between overlapping though different excited nerve populations (Liang, Lusted, & White, 1999; Pfingst et al., 1999). Evidence of this is found in electrode discrimination data where subjects could rank pitch consistently for a number of neighbouring, overlapping electrode pairs using BP+1 and BP+3 electrode configurations (Hanekom & Shannon, 1996).

NBP electrode configuration close to the surviving nerve fibres could limit threshold currents to values for which the full dynamic range of the nerve population can be included within the range of currents deliverable with the prosthesis. However, for arrays located toward the outer wall of the scala tympani threshold currents might exceed the stimulator's maximum current. Still, a greater number of electrodes could be beneficial if wider electrode separations are used. The current model contains 45 closely spaced electrode contacts that could provide 43 BP longitudinal electrode pairs which could potentially activate 43 different (but overlapping) sets of nerve fibres. Less overlap between excited nerve populations will occur if *radially* oriented electrode configurations are used. With well-placed arrays, e.g. the Clarion electrode array (Kessler, 1999), it might be possible to create at least two significantly different regions of excitation per mm along the length of the basilar membrane. An electrode array with a penetration depth of 25 mm could thus potentially create 50 different regions of excitation. This finding is supported by experimental data from Jolly et al. (1997) that show that a high contact density electrode array, i.e., an electrode array with center-to-center contact separation of 225 m, can effect excitation of nerve fibers if it is placed close to the spiral ganglion cells.

4.6 Variations in the cochlear model

Model results supplied a qualitative measure of the importance of different cochlear structures with respect to modelling. Inclusion of the helicotrema in the FE model did not have a significant effect on potential distributions and consequently on threshold currents and neural activation patterns. Exclusion of the Organ of Corti and the stria vascularis did not have an adverse effect on model results. The spiral lamina, Reissner's membrane and the basilar membrane do, however, play an important role during calculation of threshold currents and also spread of excitation. Future FE models could thus be constructed without the helicotrema, Organ of Corti and the stria vascularis, but have to include the spiral lamina, Reissner's membrane and the basilar membrane.

Tapering of the cochlea as simulated by scaling of the resistivity of the perilymphatic

spaces has a significant effect on primarily threshold currents for stimulation at different locations in the cochlea. Lower threshold currents at the base of the cochlea relative to threshold currents at a more apical location in the cochlea have been experimentally observed in implant users (Ulehlova, Voldrich, & Janisch, 1987). This is associated with a more proximal location of the array relative to the nerve fibres towards the apex because of tapering of the cochlea. In addition, model results suggest that an electrode at the same distance from the target nerve fibres will display different threshold currents at different locations in the cochlea because of the variation in resistance of the volume conductor that results from tapering of the cochlea. The effect of scaled resistivity on excitation patterns is less prominent, but present in the model. Spread of excitation tends to increase at the base of the cochlea where the resistance of the volume conductor is lower relative to the resistance towards the apex[9], especially at higher stimulus intensities. In this thesis most simulations were performed in a specific region of the cochlea. For these simulations the effect of tapering of the cochlea is thus negledible. However, it is concluded that tapering of the cochlea is an important model parameter when an extended region of the implanted cochlea is modelled.

5 CONCLUSIONS

The following observations were made from this study:

1) Asymmetry in potential distributions is not only a function of the tapering of the cochlea but also of the spiralling geometry of the cochlea. Also, the location of electrodes along the length of the basilar membrane has a stronger influence on the location of excitation along the length of the basilar membrane than the polarity of the leading phase of the stimulus waveform.

[9]Note, however, that at a specific stimulus intensity, spread of excitation is lower for electrodes located towards the base than for electrodes towards the apex because the minimum threshold current required to elicit a response is higher for basally located electrodes. Refer to page 83.

2) The helicotrema, stria vascularis and Organ of Corti do not have a significant effect on potential distributions, minimum threshold currents and neural excitation patterns in the model presented. Inclusion of the spiral lamina, Reissner's membrane and the basilar membrane in 3-D models of the implanted cochlea is required to obtain accurate estimates of potential distributions.

3) To limit threshold currents and to limit the effect of postsurgical neural degeneration on threshold currents, arrays should be placed close to the modiolus. Point electrode geometries are recommended above banded electrode geometries only when the array can be placed close to the modiolus.

4) When close to the fibre terminals, point electrode arrays produce excitation patterns similar to those produced by arrays close to the nerve fibres, while banded electrode arrays produce excitation patterns similar to those produced by arrays far from the target nerve fibres.

5) Array location is the primary parameter that controls excitation spread. A secondary but less effective parameter is electrode separation. Consequently, there is little difference in excitation spread generated with BP, BP+1, BP+2 and BP+3 electrode configurations. Excitation spread for array locations distal from the target nerve fibres increases notably for wide electrode separations.

6) There is a tradeoff between the proximity of the array to the target nerve fibres and the degree of ectopic excitation caused by the specific array location. Laterally located arrays using closely spaced electrode configurations limit ectopic excitation most efficiently. However, if an array is placed close to the nerve fibres to reduce threshold currents and spread of excitation, closely spaced electrode pairs should be used to limit ectopic excitation.

7) Bimodal excitation exists at comfortable stimulus intensities for longitudinal bipolar electrode configurations. Radial and monopolar electrode configurations are optimal to create unimodal excitation. NBP electodes can alternatively be used to create unimodal excitation for longitudinal electrode configurations, but have higher threshold currents and broader excitation

regions than radial electrode configurations.

8) The focussing ability of monopolar electrode configurations is comparable to that of widely spaced bipolar electrode configurations. In addition, spread of excitation is limited with monopolar stimulation relative to that of widely spaced bipolar stimulation. In contrast to bipolar electrode configurations, only the target nerve fibres are activated during monopolar stimulation because of the unimodal excitation pattern resulting from monopolar stimulation.

9) The resolution of cochlear implant electrode arrays can potentially be improved to at least two different locations of excitation per mm along the basilar membrane if arrays are placed close to the modiolus.

Chapter 4
MODELLING ENCAPSULATION TISSUE AROUND COCHLEAR IMPLANT ELECTRODES

1 INTRODUCTION

Cochlear implant subjects often experience changes in threshold current during the first few months after implantation. During one study Pfingst (1990) reported that in 88% of cases thresholds were highest during a period some time during the first month after implantation and then decreased by 8 to 37 dB during the following weeks. Eddington et al. (1988) and Miller, Morris and Pfingst (2000) also found threshold reduction over the first two to three months postsurgery. Pfingst (1990) suggested that threshold reduction results from either changes in conductivity between the electrodes and the neural elements or changes in the sensitivity of the neural elements themselves.

Fibrous scar tissue and new bone often grow around intracochlear electrode arrays in animals and humans (Leake et al., 1992; Linthicum et al., 1991; Webb et al., 1988; Zappia et al., 1991). Tissue reaction to implanted materials can vary from toxic reactions (where inflammation and infection occur as a result of degradation of the implant material and/or implant orientation or geometry), to vital reactions where the body detects the foreign object and incorporates it into the body by covering it in a vascularized fibrous scar tissue encapsulation (Nanas, 1988). Perfect biocompatibility does not exist in the true sense of the word (Bertoluzza et al., 1992) since tissue reactions always occur to a greater or lesser extent at the biomaterial-tissue interface. Vital tissue reaction to intracochlear electrode arrays is thus the

desired tissue response and also the most frequently observed response.

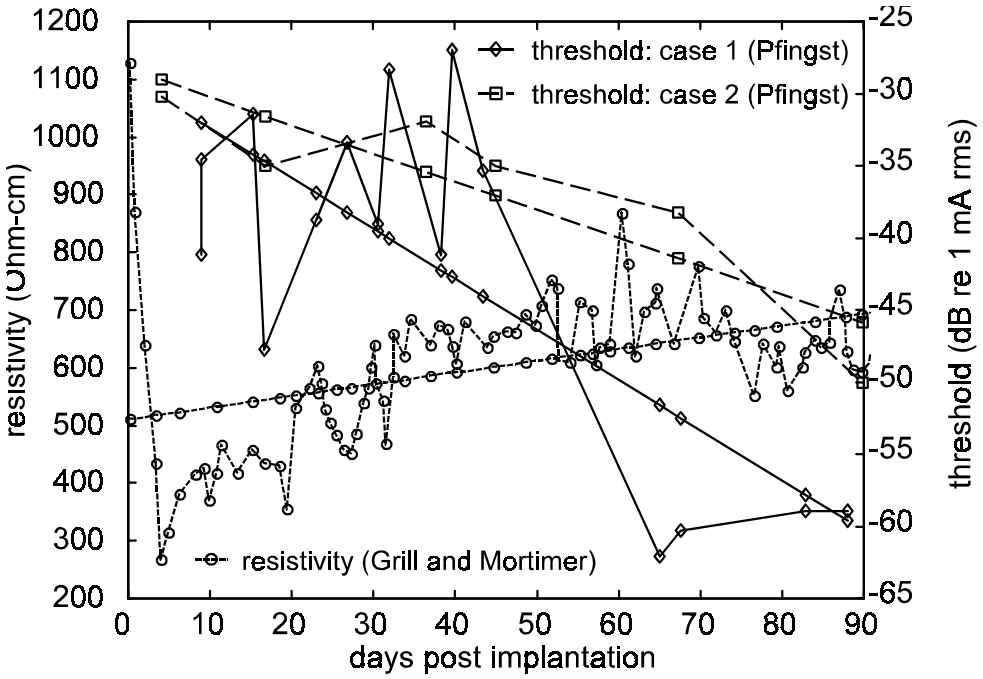

Figure 4.1. Impedance and threshold data as functions of time post-implantation after the data of Grill and Mortimer (1994) and Pfingst (1990). Impedance data are represented by resistivity in -cm while threshold currents are given in dB relative to 1 mA rms. Each set of data is represented by the original data (irregular lines) as well as a linear fit through the data (straight lines).

Tissue reactions to intracochlear electrodes range from very little fibrous tissue (Leake et al., 1992; Linthicum et al., 1991; Zappia et al., 1991), to a dense connective tissue cuff surrounded by loose, less-dense tissue (Zappia et al., 1991) around the implant inside the scala tympani. New bone sometimes envelops the electrode array in the scala tympani of the basal turn (Leake et al., 1992; Linthicum et al., 1991). Grill and Mortimer (1994) reported that the resistivity of encapsulation tissue is sufficient to alter the shape and magnitude of the electric field generated by chronically implanted electrodes. Clark et al. (1995) also suggested that bone and fibrous tissue formation in the cochlea could account for variations in patients' speech perception. Changes in the tissues surrounding cochlear implant electrodes can thus be

expected to affect the neural excitation patterns and therefore detection thresholds and dynamic ranges of electrical stimulation overall.

Pfingst (1990) found at most weak correlation between implant impedances and threshold changes during the first months after implantation, whereas De Sauvage et al. (1997) reported that compound action potential amplitudes and electrode impedance increased in correlation with each other. A comparison of the data of Grill and Mortimer (1994) and Pfingst (1990) suggests that while an increase in electrode impedance takes place, a decrease in threshold current occurs (Figure 4.1).

The objective of this chapter is to explain the effect of encapsulation tissue around cochlear implant electrodes on electrical potential distributions and auditory nerve excitation patterns during electrical stimulation.

2 MODEL AND METHODS

2.1 Combined finite element-nerve fibre model

The FE model of the first one-and-a-half turns of the electrically stimulated cochlea described in Chapter 2 was used to determine the effect of electrode encapsulation on the electrical potential distributions and thus neural excitation patterns during electrical stimulation. Two possible banded array locations were modelled: one at a medial location in the scala tympani (called banded medial or "BM") and one at a more lateral location in the scala tympani (called banded lateral or "BL"). Only one array existed during a specific simulation. An array was selected by changing the material properties of its elements to those of an insulator or a conductor, while changing the material properties of the other array to that of perylimph. Six electrode configurations were modelled corresponding to the first six configurations described in Table 3.1. The encapsulation tissue was modelled as a material layer with a resistivity of 627 -cm in direct contact with the electrode array. The resistivity of the encapsulation tissue is based on the measurements of Grill and Mortimer (1994) on

encapsulation tissue around electrodes implanted subcutaneously in cats. Grill and Mortimer (1994) reported an encapsulation tissue thickness of approximately 500 m. However, this fibrous tissue thickness was reported for subcutaneous implants and not intracochlear implants. In the FE model an encapsulation tissue thickness of 50 m was used based on observations of an average intracochlear fibrous tissue thickness around silastic electrode carriers of 48.5 m (Seldon et al., 1994) and to allow two electrodes surrounded by encapsulation tissue to fit within the scala tympani. Simulation results were generated for an electrode without encapsulation tissue (hereafter called "clean") and for an electrode surrounded by a 50 m layer of encapsulation tissue (hereafter called "encapsulated").

Electrical potential distributions generated by electrical stimulation with a 200 A dc current were calculated on a plane in the model (Chapter 2) containing the auditory nerve fibres.

2.2 Lumped-parameter model

A lumped-parameter (LP) model (Figure 4.2) of the implanted cochlea that incorporates the effect of fibrous tissue encapsulating an electrode array was created. The LP model illustrates the principle by which encapsulation tissue causes changes in the electrical potential and current at the target nerve fibres. The model is based on several LP models found in the literature (Kral et al., 1998; Strelioff, 1973; Suesserman & Spelman, 1993). Resistances included are for the perilymph in the scala tympani (R_p), the basilar membrane or bone separating the scala tympani from the scala media (R_b), the peripheral dendrites of the nerve fibres (R_n), an extracochlear current return pathway through the surrounding tissues (R_{e1} and R_{e2}) and radial and longitudinal components of the encapsulation tissue (R_r and R_l). The radial component of the encapsulation tissue represents the current pathway normal to the electrode surface and the longitudinal component represents the current pathway through the encapsulation tissue parallel to the electrode. Resistances of electrode contacts and the electrode carrier are not included since they are treated as perfect conductors and perfect insulators respectively. Each segment of the

model represents 200 m of the implanted cochlea. The model consists of 63 segments (12.6 mm) terminated with a 64th set of radial resistances equivalent to the radial resistances in the rest of the model.

Table 4.1. Description of circuit elements of LP model in Figure 4.2.

Circuit Element	Description	Value ( )	
		Clean	**Encapsulated**
R_p	Perilymph in scala tympani	700	700
R_b	Basilar membrane	8 000	8 000
R_n	Nerve fibres	3 000	3 000
R_{e1}	Extracochlear tissues	6 300	6 300
R_{e2}	Extracochlear current return pathway	6.3	6.3
R_r	Radial resistive component of encapsulation tissue	0	720
R_l	Longitudinal resistance component of encapsulation tissue	0	12 300

Resistance values are based on material properties used by Frijns et al. (1995), Grill and Mortimer (1994) and Kral et al. (1998). The resistivity of encapsulation tissue was approximated by application of the equation R = /A[1] in the radial and longitudinal directions and assuming that no current leaves the encapsulation tissue toward the electrode array except at the stimulating electrodes. Resistive values of

[1]R represents resistance, the resistivity of the encapsulation tissue, the length of the tissue in the direction of current flow and A the area of the annular region normal to the direction of current flow.

model components are given in Table 4.1.

2.3 Modelling of Auditory Nerve Excitation

Thresholds were determined with the generalized SEF auditory nerve fibre model (Frijns et al., 1995). Two types of nerve survival were modelled: one where the nerve fibres were intact and thus included the peripheral dendrites and another where the peripheral dendrites of the nerve fibres had degenerated. To simulate loss of peripheral dendrites, a truncated version of the generalized SEF model (Chapter 2) was used.

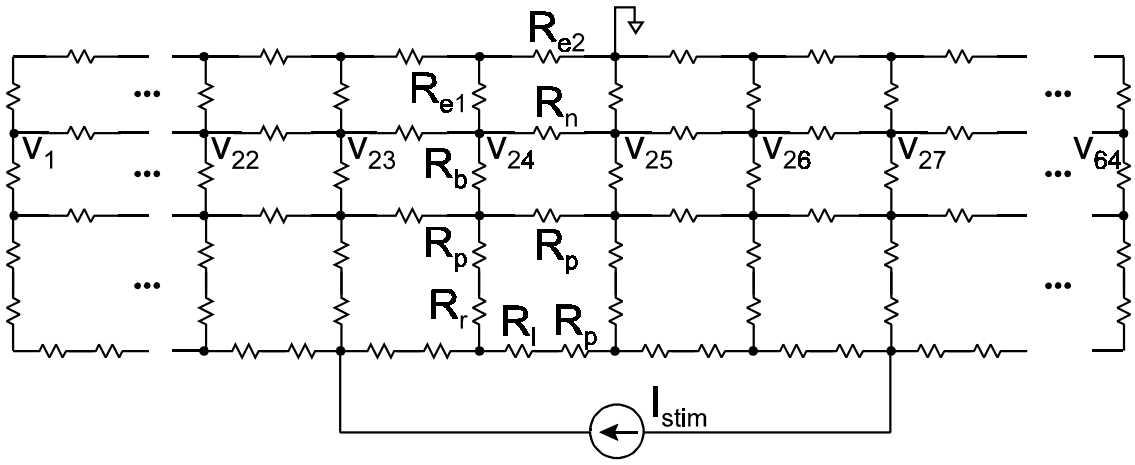

Figure 4.2. Schematic representation of LP model of intracochlear stimulation with radial and longitudinal resistances of encapsulation tissue included. Refer to Table 4.1 for component values.

The stimulus was a 200 s per phase charge balanced biphasic current pulse generated by scaling the electrical potentials predicted by the FE model. The threshold current for a nerve fibre was defined as the lowest current level that excited the nerve fibre during a single stimulation cycle. Nerve excitation was assumed when a propagating action potential occurred (Reilly et al., 1985).

3 RESULTS

3.1 Electrical potential distributions

The electrical potential amplitude and the spread of the electrical potential along the length of the basilar membrane are overestimated by the LP model. The slight differences in the prediction of the location of the maximum and minimum electrical potential amplitudes between the LP and FE models can be attributed to dimensional variations between the two models.

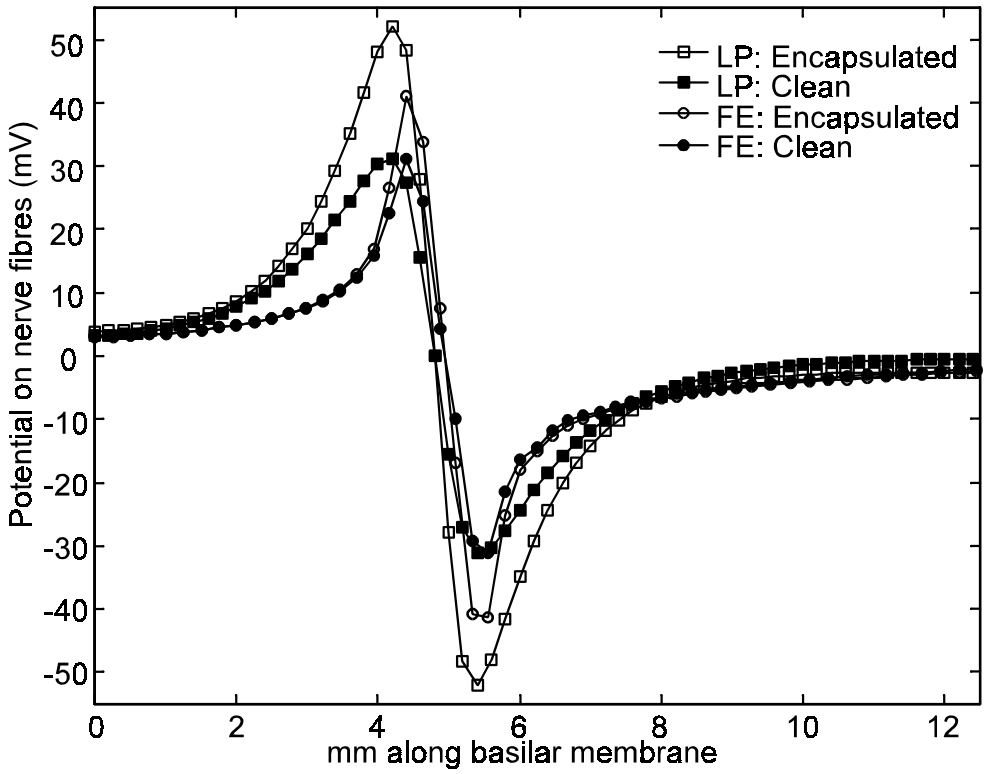

Figure 4.3. Comparison of electrical potential distributions along the basilar membrane predicted by the LP and FE models for BP electrode configuration.

Both models predict higher electrical potential amplitude deviations at the target nerve fibres in the presence of encapsulation tissue than in its absence. Figure 4.3 shows electrical potential distributions along the length of the basilar membrane calculated at the nerve fibres with the LP and FE models. At this location in the model, an increase of approximately 20 mV_{p-p} can be seen in the electrical potential

for the FE model and an increase of approximately 42 mV_{p-p} for the LP model. At the electrode contacts the FE model predicts an increase of approximately 90 mV_{p-p} while the LP model predicts an increase of 265 mV_{p-p} as a result of electrode encapsulation. If the radial resistive component of the encapsulation tissue in the LP model is increased, the potential at the target nerve fibres remains unchanged (Figure 4.3), but the potential at the electrode contacts increases substantially (to 478 mV_{p-p} if R_r is doubled).

3.2 Auditory nerve excitation

3.2.1 Minimum threshold current as a function of electrode encapsulation

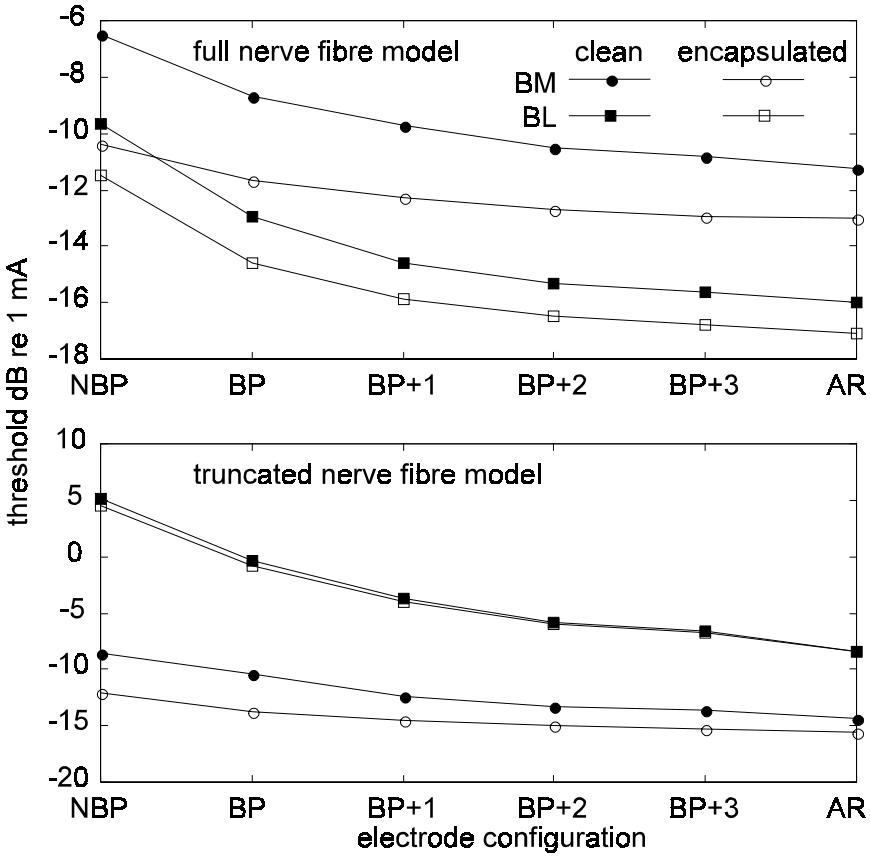

Figure 4.4. Threshold current as a function of electrode configuration in the presence and absence of electrode encapsulation for a full nerve model (upper graph) and a truncated nerve model (lower graph).

Figure 4.4 summarizes threshold currents determined with the combined FE-nerve model while Figure 4.5 shows the differences in threshold currents between clean and encapsulated electrodes. Threshold currents are generally reduced in the presence of encapsulation tissue. A maximum reduction in threshold current of 3.5 to 4 dB occurs for closely spaced (NBP) electrode configurations close to the modiolus (BM array). The smallest threshold current reduction is predicted for array locations far from the target nerve fibres using widely spaced (AR) electrode configurations, i.e., 0 to 1 dB for the BL array.

3.2.2 Spread of excitation

Spread of excitation was evaluated with electrical tuning curves (Figure 4.6) that show threshold current profiles for the nerve fibre array as a result of electrical stimulation. Electrical tuning curves for BP and AR1 electrode configurations for full (upper set of graphs) and truncated (lower set of graphs) nerve fibre models are shown.

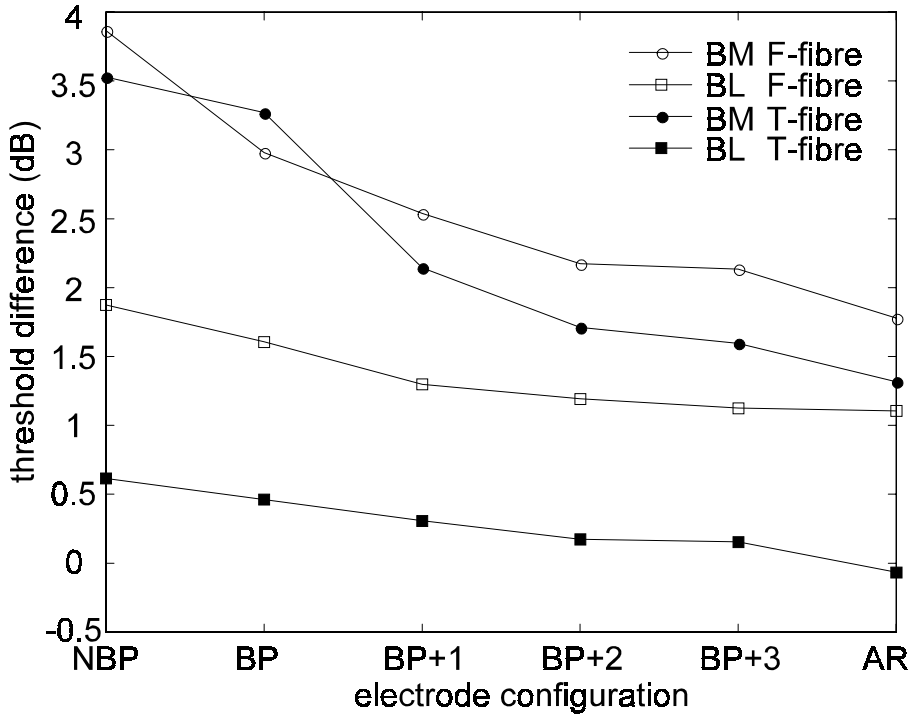

Figure 4.5. Threshold differences between clean and encapsulated electrode arrays as a function of electrode configuration.

Excitation patterns are different for clean electrodes and electrodes encapsulated with fibrous tissue. To evaluate this difference in excitation patterns, spread of excitation along the basilar membrane at 10 dB above threshold was plotted as a function of electrode separation (Figure 4.7). In general, the presence of encapsulation tissue around electrode arrays limits (narrows) the spread of excitation noticeably (up to 1 mm). The exception is where the array is located far from the target nerve fibres where virtually no difference in the spread of excitation occurs between clean and encapsulated arrays, e.g., the BL array for the truncated nerve model.

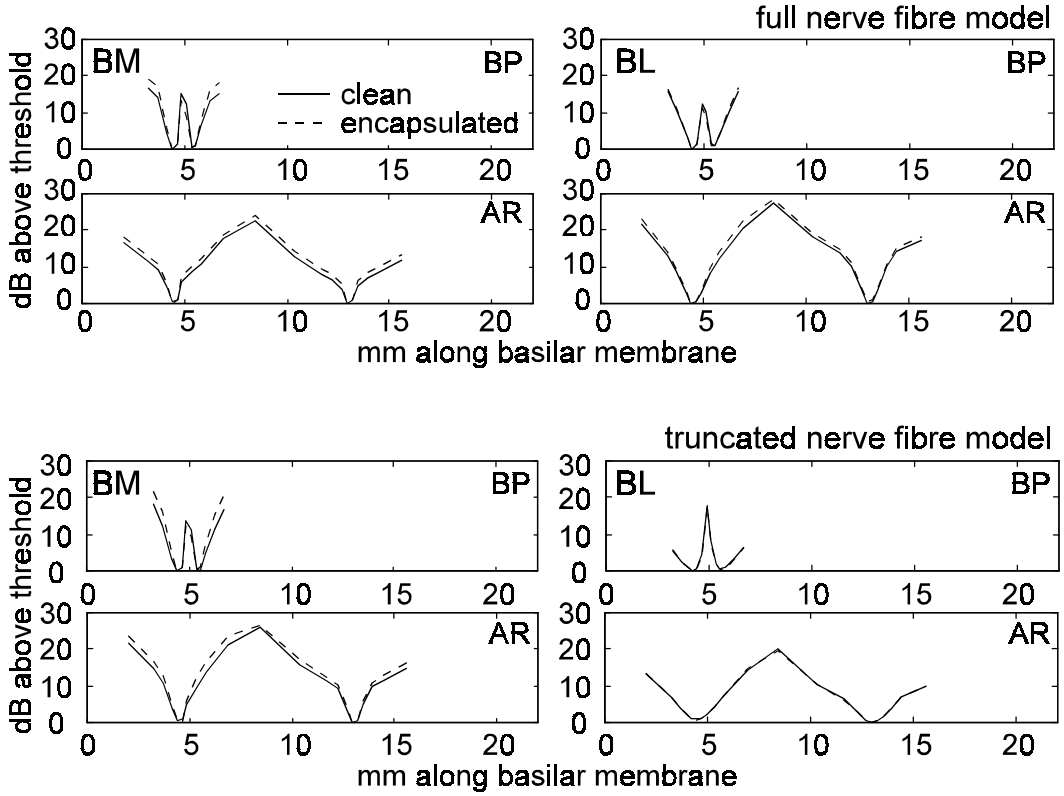

Figure 4.6. Electrical tuning curves for the P array for a full nerve fibre model (upper set of graphs) and a truncated nerve fibre model (lower set of graphs).

4 DISCUSSION

Both the FE and LP models predict an increase in the electrical potential amplitude at the target nerve fibres in the presence of encapsulation tissue. The mechanism responsible for the increase in electrical potential can be explained by the LP model.

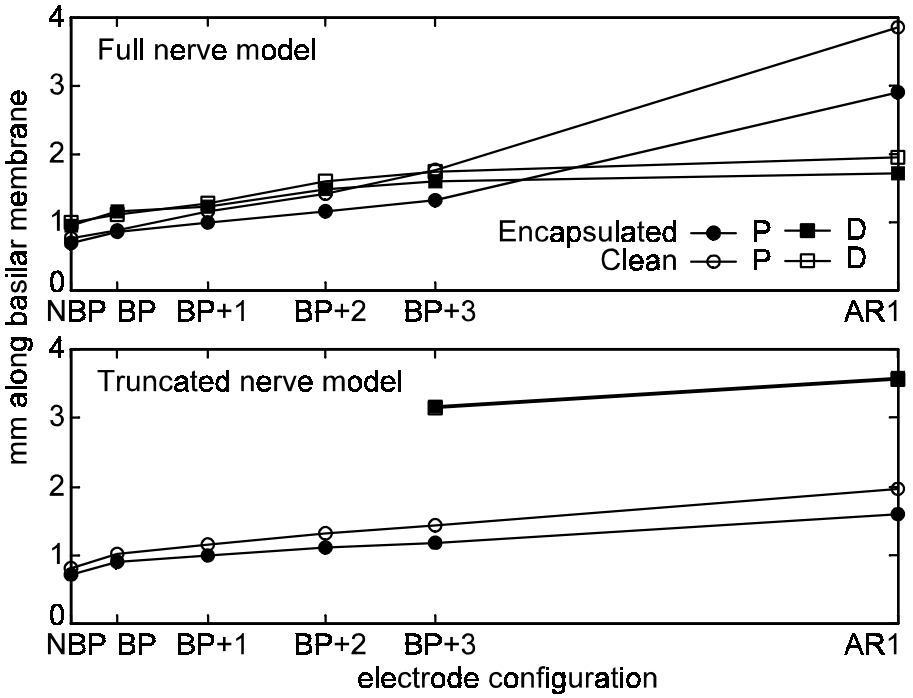

Figure 4.7. Spread of excitation along the length of the basilar membrane as a function of electrode separation at a stimulus intensity of 10 dB above threshold. The locations of electrode configurations on the abscissa have been scaled to represent their respective interelectrode spacings in the FE model. Spread of excitation has not been plotted for narrowly spaced electrode configurations for the BL array using the truncated nerve model (lower graph) since the spread of excitation exceeded the region over which thresholds were calculated.

The two resistances representing the encapsulation tissue in the LP model each has a specific effect. The longitudinal resistance R_l of the encapsulation tissue is responsible for the increase in electrical potential at the target nerve fibres, while the

radial resistance R_r is responsible for an increase in electrical potential at the electrode contacts. If R_r becomes very high, compliance problems may occur near the upper limits of dynamic range since the stimulator may not be able to drive the current into the increased load resistance. This might be especially true for narrowly spaced electrode pairs, e.g. the offset radial electrode pairs of the electrode of the Clarion implant (Kessler, 1999), where loudness growth problems frequently occur. The effect of R_l can be explained by observing that the network branch containing R_l carries a part of the current injected by the current source (I_{stim}) along the length of the model. If the resistance in this branch is increased, i.e., R_l increases, more current will be forced into the other parallel branches, causing the electrical potential across these branches to increase. Encapsulation tissue therefore increases the resistance of the current pathways close to the electrode carrier, thereby forcing the current through more remote pathways. Such remote pathways could include the nerve fibres, as is suggested by both the FE and LP models. The primary effect of R_l is thus to increase the electrical potential (and currents) that occur at the nerve fibres and consequently to lower the current levels at which nerve excitation will occur.

The effect of R_l can be seen in the decrease of minimum threshold currents in the presence of encapsulation tissue (Figures 4.4 and 4.5) and is a function of both array location and electrode separation. For array locations far from the target nerve fibres and widely spaced electrode configurations the effect of encapsulation tissue is limited by greater volumes of cochlear tissue between the electrodes and the target nerve fibres. One would therefore expect to see more pronounced threshold current reductions because of electrode encapsulation for implants with arrays close to the modiolus, e.g., the Clarion (Kessler, 1999) cochlear implant, than for implants with arrays far from the modiolus, e.g., the Nucleus (Clark, 1996) cochlear implant. Some evidence for this observation can be found in threshold current reductions over time reported by Pfingst (1990) (who used arrays that positioned electrode contacts in the region between the modiolus and the middle of the scala tympani) and Dorman et al. (1992) (for patients using the Ineraid cochlear implant), while unchanged EABR

thresholds over time were reported for Nucleus implant users (Brown et al., 1995) Threshold current reduction predicted by the combined FE-nerve model occurs at a maximum rate of 0.2 dB per day[2]. This is comparable to threshold current reductions of 0.2 to 1 dB per day reported by Pfingst (1990). More severe threshold reduction predictions as a result of electrode encapsulation can be modelled by increasing the thickness of the encapsulation tissue in the FE model. The weak correlation between implant impedance and threshold current changes observed by Pfingst (1990) could be because the relatively high electrode-body fluid interface impedance, i.e., 10 to 20 k (de Sauvage et al., 1997; Dorman et al., 1992), dominates resistance changes caused by encapsulation tissue in the neighbouring cochlear tissues. Brown et al. (1995) reported slight but significant reduction in EABR slope with time for subjects implanted with the Ineraid implant. EABR slope gives an indication of the increase or decrease in the number of excited nerve fibres. EABR slope can thus be interpreted as a measure of spread of excitation and dynamic range, i.e., a shallower EABR slope corresponds with a narrower region of excitation (a slow increase in the number of excited nerve fibres with increasing stimulation current) and a larger dynamic range (Frijns, de Snoo & Schoonhoven, 1995). Model results indicate that spread of excitation is reduced by the presence of encapsulation tissue (Figures 4.6 and 4.7). This suggests that dynamic range could be increased by the presence of encapsulation tissue. Similar to threshold current reduction, encapsulation of electrodes mainly influences spread of excitation for array locations close to the target nerve fibres.

Although reduction in spread of excitation as a result of electrode encapsulation appears to be small (less than 1 mm in most cases), it cannot be ignored. Since the neural resolution of the model is rough, i.e. each modelled nerve fibre represents approximately 224 real nerve fibres, noticeable but small reductions in spread of excitation amounts to at least 224 nerve fibres for which the threshold current of an

[2]Average threshold current reduction rate calculated over a period of 25 days using the reduction in threshold current as a result of electrode encapsulation and assuming that the encapsulation thickness reaches the modelled 50 m after 25 days.

electrode pair has changed.

Results presented in this chapter suggest that electrode encapsulation can alter the shape and magnitude of the electric fields produced by intracochlear electrode arrays. These changes are reflected in reduction in threshold currents and spread of excitation. Cochlear implant subjects also show improved speech recognition performance from one to nine months post implantation (Tye-Murray et al., 1992) which could indicate an increased sensitivity developed for electrical stimulation. Also, for array locations close to the modiolus an increase in sensitivity to electrical stimulation could be a result of the degeneration of the peripheral dendrites of the auditory nerve fibres (Chapter 3). The mechanism responsible for the decrease in threshold current could thus be a combination of electrode encapsulation, sensitization for electrical stimulation and in some cases degeneration of the peripheral dendrites of the auditory nerve fibres.

5 CONCLUSION

An LP model of the implanted cochlea was presented to explain the mechanism by which encapsulation tissue could induce changes in threshold currents. It was found that a longitudinal resistive component of encapsulation tissue around cochlear implant electrodes causes currents and thus electrical potentials at the target nerve fibres to increase, while a radial resistive component causes an increase in the electrical potential at the electrode contacts.

The effect of electrode encapsulation was described through changes in threshold currents and spread of excitation. A combined FE-auditory nerve fibre model was used to quantify this effect. The effect of electrode encapsulation on neural excitation is controlled by electrode separation and array location. Narrowly spaced electrode configurations and array locations close to the modiolus are most sensitive to the effects of electrode encapsulation. Electrode encapsulation could be beneficial

since its presence could (1) decrease thresholds with 0.5 to 4 dB according to model results and (2) limit spread of excitation with up to 1 mm for widely spaced medial arrays, and thus increase dynamic range. However, if the radial resistive component of the encapsulation tissue becomes very high, compliance problems may arise at the upper end of the dynamic range of an electrode pair.

Chapter 5
MULTIPOLAR ELECTRODE CONFIGURATIONS AND SIMULTANEOUS STIMULATION

1 INTRODUCTION

Electrode configuration influences aspects such as phoneme recognition in the speech recognition ability (Fu & Shannon, 1999a;1999b) and pitch perception (Busby et al., 1994) of implant users. This could be because dissimilar neural populations are activated by different electrode configurations (Busby et al., 1994; McKay, O'Brien, & James, 1999). Besides the potential distributions around cochlear implant electrodes, the stimulation strategy also has an influence on the sound sensation perceived by implant wearers because it controls the place and temporal information that are provided to the nerve fibres in the cochlea (Loizou, 1999). Cochlear implant stimulation strategies either transmit place information (vocoder type strategies, e.g. SPEAK (Loizou, 1999)) or mimic the temporal structure of auditory signals in addition to providing place information (i.e., the CIS strategy (Loizou, 1999) and the SAS strategy (Kessler, 1999)).

It has been proposed that improvement of the focussing ability of intracochlear electrodes could improve the performance of cochlear implants (Loizou, 1999; van den Honert & Stypulkowski, 1987). Moreover, research in cochlear implants has increasingly been focussed on ways to manipulate the excitation patterns of the cochlear nerve mainly by improving the electrode design, manipulating the electrode

configuration and varying the stimulus distribution[1] on the electrodes (Jolly, Spelman, & Clopton, 1996; Liang, Lusted, & White, 1999; Rodenhiser & Spelman, 1995; Ruddy & Loeb, 1995). The Clarion electrode array is designed to create focussed stimulation based on the requirement that spectral content must be preserved during transmission of the auditory signals to the nerve fibres (Kessler, 1999).

Traditionally, stimulation is not applied to more than one electrode pair at a time to ensure that the charges that are injected through the electrodes are balanced during the anodic and cathodic cycles (Brummer & Turner, 1975). Balanced charge injection prevents the occurrence of irreversible electrochemical reactions at the electrode-tissue interface (Donaldson & Donaldson, 1986; Huang et al., 1999). This is ultimately also the reason for current rather than voltage stimulation in cochlear implants (Robblee & Rose, 1990). However, it has been shown that bipolar type stimulation causes bimodal excitation patterns (Chapter 3; Frijns, de Snoo, & ten Kate, 1995; Jolly, Spelman, & Clopton, 1996) and that the focussing ability of monopolar stimulation with an electrode pair is limited although it has the advantage of activating only one region of nerve fibres (Chapter 3). Electrode configurations that focus stimulation and have unimodal excitation properties are required to augment excitation of independent neural populations.

Tripolar and quadrupolar electrode configurations have been investigated both with animal experiments and models (Kral et al., 1998; Miyoshi et al., 1999; Suesserman & Spelman, 1993). These stimulation modes proved to focus the excitation profile and eliminate bimodal excitation patterns that occur during stimulation with bipolar electrode configurations. Rodenhiser and Spelman (1995) used an inverse technique to determine the driving currents required for focussed stimulation in the cochlea.

[1] In this chapter the term "stimulus distribution" will be used in the context of the allocation of different stimulation currents for different electrodes, i.e one stimulus distribution could entail application of stimulation currents of -100, 200 and -100 A on the three electrodes in a tripolar electrode configuration, while another could entail the application of -100, -100 and 200 A currents on a similar electrode configuration.

They defined the stimulation pattern which was required in the Organ of Corti and calculated the stimulation currents on five electrodes necessary to produce the stimulation pattern.

One of the device objectives of the Clarion implant is increasing the transmission speed of auditory information to the nerve fibres (Kessler, 1999). The idea is thus to transmit all temporal and place information that are available to the normal auditory system via electrical stimulation to the nerve fibres in the deaf cochlea in such a way that the auditory centres in the brain cannot distinguish between the normal and electrically transmitted information. Preservation of the temporal structure of the speech signal (and thus the transmission speed of temporal information) could be improved if stimuli can be presented on several electrodes simultaneously. This is because nerve fibres at different locations in the cochlea frequently need to be activated synchronously (or pseudo-synchronously as implemented by the CIS strategy) to render understandable speech. To replicate the natural properties and normal physiological processing of sound, simultaneous analogue stimulation (SAS) on multiple electrodes has recently been reimplemented in the Clarion speech processor (Kessler, 1999). The SAS strategy has its roots in compressed analogue strategies (Kessler, 1999; Loizou, 1999), which implemented simultaneous bipolar analogue stimulation and were used in the Ineraid (Tye-Murray et al., 1992) and UCSF/Storz (Schindler & Kessler, 1989) devices.

Alternative electrode configurations that could improve the transfer of both place and temporal information are investigated in this chapter. The combined FE-nerve fibre model described in Chapter 2 is used to investigate 1) the focussing ability of quadrupolar and tetrapolar electrode configurations and 2) the simultaneous presentation of stimuli on multiple electrodes to provide more degrees of freedom in shaping the excitation profile and to preserve the temporal structure of the auditory signal that is transmitted to the nerve fibres in the cochlea.

2 EXCITATION PATTERNS OF MULTIPLE ELECTRODE CONFIGURATIONS

2.1 FE Model

The FE model (Chapter 2) was used to investigate four types of electrode configurations that are either not used or are in experimental use in cochlear implants: enhanced tripolar, quadrupolar, tetrapolar and pseudo-continuous electrode configurations. The medial electrode array was used to construct all the multipolar electrode configurations since it has been proved (both experimentally and through models of the implanted cochlea) that perimodiolar arrays render better selectivity than arrays further away from the modiolus (Chapter 3; Shepherd, Hatsushika, & Clark, 1993).

2.1.1 Enhanced tripolar electrode configurations

Table 5.1. Details of enhanced tripolar electrode configurations

Abbreviation	**Stimulation current ratio**	**Electrode geometry**	**Description**
TRI1	1:2:1	point	Three radial pairs spaced NBP
TRI2	1:2:3	point	
TRI3	2:4:3	point	

The enhanced tripolar electrode configuration described here is really a hexapolar mode because it comprises three electrode pairs. However, since the electrode pairs are in a radial configuration, only three degrees of freedom are available to shape neural excitation, similar to a true tripolar mode. Since localised activation can be achieved with radial electrode configurations (Chapter 3), the possibility of using this characteristic simultaneously on three electrode pairs to manipulate the shape of neural activation was investigated. Because each "pole" in the tripole has its own return electrode, the total current injected need not be balanced between the "poles", i.e. currents on the active electrodes (i.e. the electrodes closest to the nerve fibres)

may be in phase.

2.1.2 Quadrupolar electrode configurations

Table 5.2. Details of quadrupolar electrode configurations

Abbreviation	Stimulation current ratio	Electrode geometry	Description
QUAD1	2:1	banded	Three narrowly (NBP) spaced electrodes
QUAD2	1:-2:1	banded	Three normally (BP) spaced electrodes
QUAD3	1:-2:1	banded	Three widely (BP+1) spaced electrodes
QUAD4	1:-2:1	point	Three closely (NBP) spaced electrodes
QUAD5	1:-2:1	point	Three radial pairs spaced NBP
QUAD6	1:-1:-1:1	banded	Two sets of normally (BP) spaced electrodes separated by a BP+1 electrode separation

A quadrupolar electrode configuration consists of either three electrodes where the centre electrode carries twice the inverted current of the lateral electrodes (i.e. two dipoles with one common pole), or four electrodes forming two separate dipoles. The three-electrode quadrupole will hereafter be called an "overlapping" quadrupolar configuration, whereas a four-electrode quadrupole will be referred to as a "non-overlapping" quadrupole. The effects of the following parameters on the focussing ability of quadrupolar electrode sets were investigated: (1) proximity of the poles (QUAD1, QUAD2 and QUAD3), (2) the use of point electrodes instead of banded

electrodes (QUAD4 and QUAD5) and (3) separation of the central, combined pole into two poles (QUAD6). QUAD5 is similar to the enhanced tripolar configurations because it comprises three radially oriented electrode pairs.

2.1.3 Tetrapolar electrode configuration

Table 5.3. Details of tetrapolar electrode configurations

[1]The return electrode is a large electrode (comprising five FE model segments from segment 54 to segment 58) toward the apex inside the scala tympani.

[2]The return electrode is located somewhere outside the cochlea.

[3] The return electrode is a common ground type configuration where the part of the electrode that is not used is short-circuited and used as the return electrode.

Abbreviation	**Stimulation current ratio**	**Electrode geometry**	**Description**
TET1	1:1:-4:1:1	banded	Five NBP spaced electrodes
TET2	1:1:-4:1:1	banded	Five BP spaced electrodes
TET3	-4:-3:-1:-3:-4	banded	AR[1], MONO[2], CGND[3]
TET4	-1:-3:-4:-3:-1		

A tetrapolar electrode configuration comprises five electrodes. Focussing and shaping of excitation patterns were individually investigated. Focussing of the excitation pattern was investigated by spreading the stimulation current on the lateral electrodes in an overlapping quadrupolar electrode configuration over two lateral electrodes on each side of the central electrode (TET1) while keeping the current on the central electrode fixed. The surface area of the side poles was thus increased thereby decreasing the current density from these poles. The effect of interelectrode separation was also investigated (TET2).

Shaping of the neural activation pattern was investigated by a simultaneously activated set of five electrodes (TET3 and TET4). Two "inverse" stimulus

distributions were selected: the first (TET3) had its strongest activating ability (i.e. highest absolute stimulation current) on the two outer electrodes and the weakest activating ability (i.e. lowest absolute stimulation current) on the centre electrode, while the second stimulus distribution (TET4) had its strongest activating ability on the centre electrode and the weakest on the outside electrodes. The objective was thus to obtain -shaped (TET3) and V-shaped (TET4) neural activation patterns. A banded electrode geometry was selected because the Nucleus electrode could potentially be used in this configuration (although the implanted hardware of the Nucleus device does not currently allow stimulation on more than one electrode pair).

2.1.4 Pseudo-continuous electrode configurations

Table 5.4. Functions implemented over CON1 and CON2 electrode configurations. The shapes of the functions are shown in Figure 5.9.

Function	Expression	Scaled stimulation currents in A applied on the FE model sections indicated below.										
		9	10	11	12	13	14	15	16	17	18	19
CON1	$f_1(x) = \sin(x) + \sin(2x)$	-46	-55	-60	-59	-54	-48	-42	-39	-42	-49	-60
CON2	$f_2(x) = \sin(0.9x) + \sin(2.5x)$	0	-11	-28	-47	-62	-69	-67	-60	-50	-43	-43

The possibility to shape the potential distribution at the nerve fibres in a continuous fashion was investigated by activating a large number of electrodes simultaneously. Two arbitrary stimulus distributions were investigated and their details are given in Table 5.4. The electrode configuration comprises 11 "line" electrodes defined on the perimeter of the electrode carrier on the boundaries of each segment of the FE model. Three types of return electrodes were modelled: AR, MONO and CGND. Details of the return electrodes are given in Table 5.3.

2.2 Modelling of auditory nerve excitation

Neural excitation patterns were again calculated with the GSEF model by determining the threshold current at which a specific modelled nerve fibre will generate a propagating action potential. However, since stimulation currents were not equal on all electrodes, scaling of potential distributions were performed relative to the maximum current applied on any one of the electrodes. Consequently, only relative thresholds were determined, i.e. spatial tuning curves relative to the minimum threshold current (dB above threshold) were calculated. A relative indication of threshold currents was obtained from AF contours where a higher absolute value of the activating function indicates lower threshold currents.

2.3 Focussing and shaping ability of multi-electrode systems

Because the CFI defined in Chapter 2 is not clearly visible or does not exist in the excitation patterns of most multi-electrode systems, an alternative measure had to be defined to quantify the focussing ability of multi-electrode systems. If multimodal excitation exists for an electrode set, the *unimodal* focussing ability *UF* of an electrode set and associated stimulus pattern is defined as follows: If *W* is the projection of the electrode contacts on the basilar membrane, *P* is spread of excitation of the primary peak in the excitation profile at the current intensity relative to the threshold current (dB above threshold) *L* where the lowest side-lobe in the excitation pattern appears, the focussing ability of the electrode set is defined as

$$UF = \frac{W}{P} \cdot \frac{L}{20} \tag{5.1}$$

for a given stimulus pattern (Figure 5.1). A "perfectly" focussed excitation pattern is defined to have P=W and L = 20 dB. The value of L is limited to 20 dB, i.e. if L is found to be greater than 20 dB, its value would be set equal to 20 dB. This facilitates calculation of *UF* for electrode configurations that do not display side-lobes in the electrical tuning curves, e.g. monopolar electrode configurations. 20 dB was selected because this is approximately the maximum dynamic range for a cochlear implant wearer (Shannon, 1983). A *UF* value equal to 1 describes a perfectly

focussed electrode according to this definition. In other words, the closer to 1 an electrode set's *UF* value, the better its focussing ability. Typically, electrode sets would exhibit *UF* values far less than 1 because, even though the lowest side-lobes might approach 20 dB above threshold, the spread of excitation at high stimulus intensities is always wider than the projection of the electrode contacts along the length of the basilar membrane if the electrodes are separated from the nerve fibres. Since the equation does not compensate for distance from the electrodes to the target nerve fibres, electrodes that are located further away from the nerve fibres will (correctly) exhibit less focussed excitation because of current spread in the volume conductor. *UF* essentially gives an indication of how the spread of excitation at a specific stimulus intensity compare for different electrode and stimulus configurations. *UF* is defined only over the stimulus intensities below where the first side-lobe in each neural response appears.

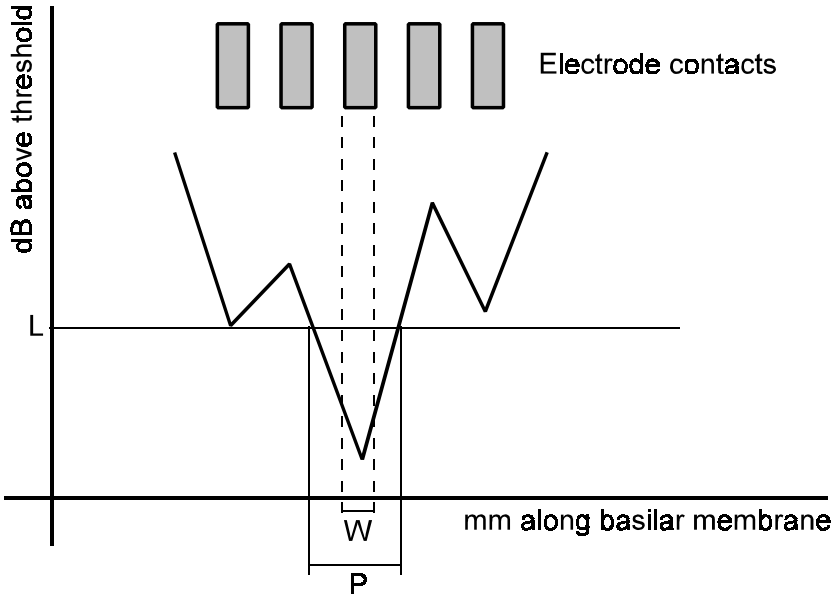

Figure 5.1. Schematic representation of parameters in definition of UF.

Although *UF* cannot be measured in implant wearers, it could potentially be measured in animals. Kral et al. (1998) measured electrically evoked spatial tuning curves in cats for a number of electrode configurations. Spatial tuning curves were measured by recording thresholds of single units in the internal auditory meatus as a result of electrical stimulation.

To quantify the shaping ability of electrode sets, the correlation coefficient between the stimulus distribution on the electrodes and the electrical tuning curve was calculated and the threshold data were plotted versus stimulation current. This gave an indication of the linearity of the relationship between the stimulus distribution and the neural response profile and of the deviation of this relationship from linearity.

3 RESULTS

3.1 Focussing of neural excitation patterns

AF contours of the potential distributions generated with various electrode configurations and stimulus distributions (Figure 5.2) show that (1) trimodal excitation could occur for overlapping quadrupolar electrode configurations, (2) the central region of excitation of overlapping quadrupolar configurations is likely to be excited at lower stimulus intensities than the lateral regions, since the intensity of the activating function is much higher for the central region than for the lateral regions, (3) narrowly spaced quadrupoles will exhibit higher minimum threshold currents than widely spaced quadrupoles because the absolute maximum intensity of the activating function is lower for narrowly spaced quadrupoles (e.g. QUAD1) than for more widely spaced quadrupoles (e.g. QUAD3), (4) increasing the interelectrode separation has a defocussing effect on the central (and lateral) regions of excitation (compare QUAD1 to QUAD3), (5) similar to bipolar and monopolar stimulation (Chapter 3), point electrode geometries are expected to require lower stimulus current intensities to elicit a response than banded electrode geometries (compare QUAD1, QUAD4 and QUAD5), and (6) there should not be much difference in either minimum threshold currents or focussing ability between using point electrodes and radially oriented point electrode pairs to create a quadrupole (compare QUAD4 and QUAD5).

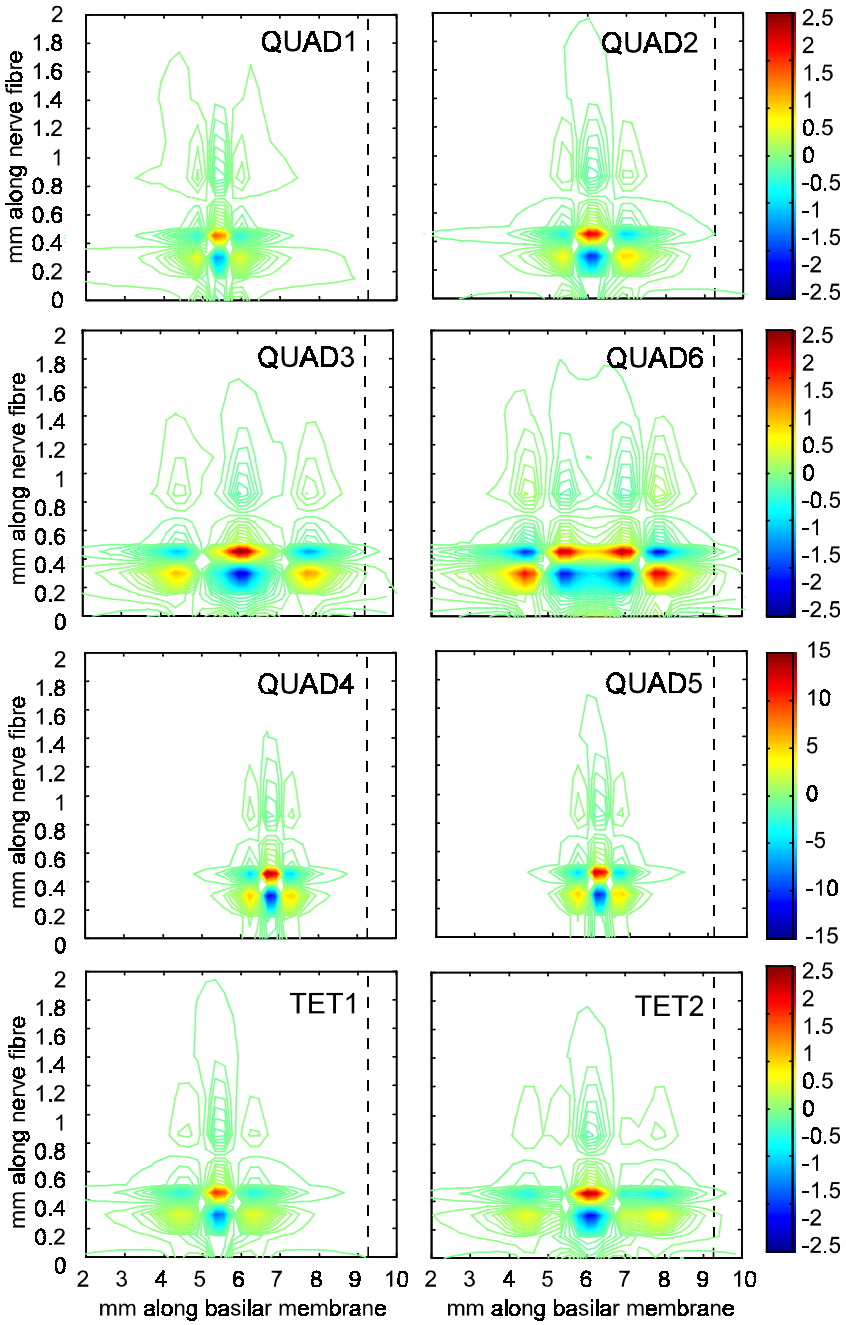

Figure 5.2. AF contour plots showing possible regions and spread of excitation along the basilar membrane as a result of stimulation with different quadrupolar and tetrapolar electrode configurations. The spatial scales of all the graphs are the same and are indicated for the left graphs (ordinate) and for the lower graphs (absisca). The colourbar multiplication factor is 10^4 mV/ms.

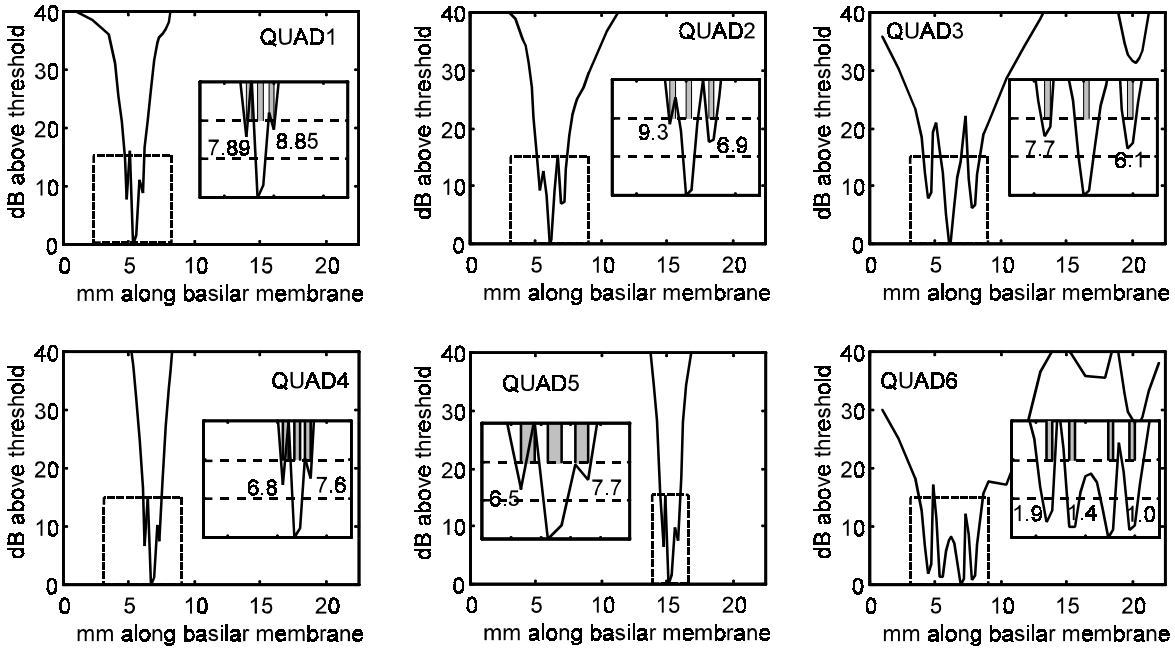

Figure 5.3. Electrical tuning curves for quadrupolar electrode configurations. An enlargement of the primary region of activation (dashed block) is shown as an inset in each figure. Shaded blocks indicate the location of the stimulating electrode pairs. Numbers next to minima in insets indicate dB above threshold for side lobes.

Non-overlapping quadrupolar stimulation (QUAD6) creates four regions of excitation which are expected to occur at approximately the same stimulus intensity. This observation is based on similar absolute intensities of the activating function across al four regions of excitation. The tetrapolar configurations show similar trends with regard to minimum threshold currents and spread of excitation as a function of electrode separation than the quadrupolar modes. However, there is an even greater difference between the absolute activating function intensities at the central and lateral regions of excitation, suggesting that the lateral excitation will occur at higher stimulus intensities relative to the minimum threshold current than for the QUAD modes.

Electrical tuning curves for the different electrode configurations confirm the qualitative observations based on AF contours. Overlapping quadrupolar stimulation creates trimodal excitation patterns (QUAD1 to QUAD5 in Figure 5.3). Four minima

are created in the electrical tuning curve when the poles are individually placed (QUAD6 in Figure 5.3). The lateral lobes in the trimodal excitation pattern appear at a few dB above threshold in contrast to the almost equal threshold values of the bimodal peaks created with bipolar electrode configurations and with the non-overlapping quadrupolar configuration. The stimulus intensities where side lobes appear in the electrical tuning curves are given in the insets in Figure 5.3. For the tetrapolar configurations where the lateral poles are spread over two electrodes, the side lobes in the electrical tuning curves are more suppressed (0.9 to 1.65 dB) than for the quadrupolar configurations (Figure 5.4). UF was calculated for all electrode configurations and is shown in Figure 5.5 as a function of electrode configuration in the order of best to worst focussing ability. UF is somewhat less for tetrapolar configurations than for quadrupolar configurations with corresponding interelectrode separation. QUAD1 displays the best focussing ability of all the QUAD modes.

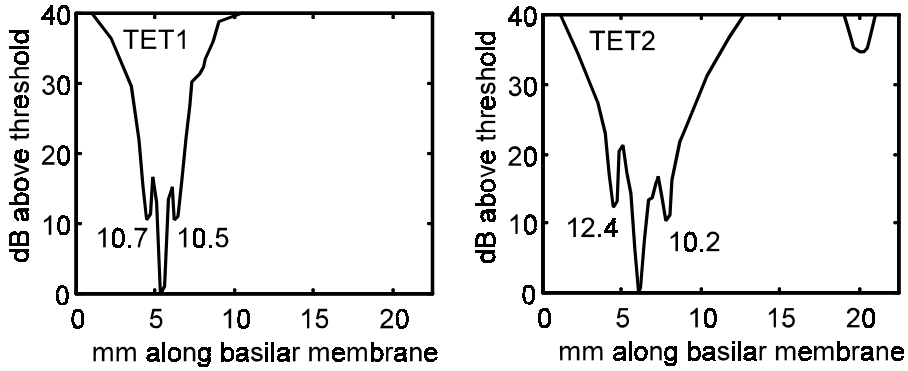

Figure 5.4. Electrical tuning curves for tetrapolar electrode configurations TET1 and TET2. Numbers next to minima indicate dB above threshold for side lobes.

No ectopic excitation of nerve fibres originating from superior cochlear canals is predicted below 40 dB above threshold for narrowly spaced (NBP and BP for quadrupolar and NBP for tetrapolar) electrode configurations. Ectopic stimulation is, however, present for more widely spaced electrode configurations (BP+1 separation for quadrupolar and BP separation for tetrapolar) and also for the non-overlapping quadrupolar configuration (QUAD6).

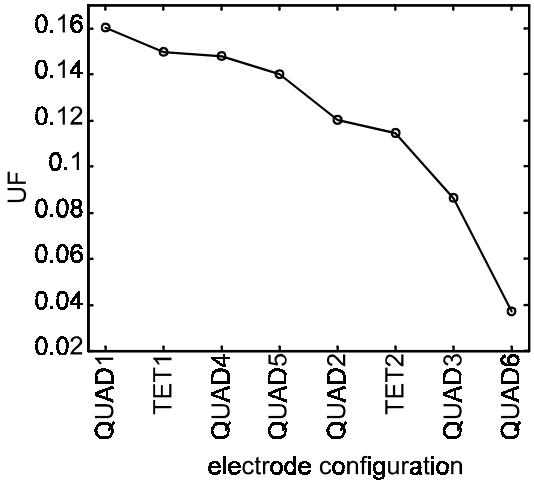

Figure 5.5. UF as a function of electrode configuration.

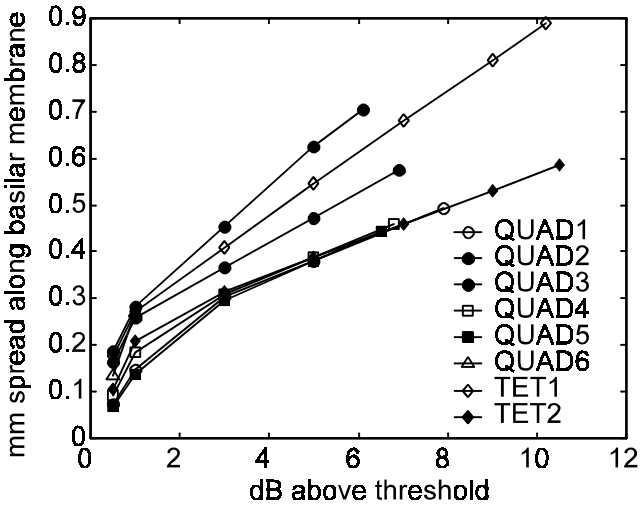

Figure 5.6. Focussing of multipolar electrode configurations. The datum point at the highest stimulus intensity (dB level) of each curve corresponds to the stimulus intensity where the lowest sidelobe in the electrical tuning curve appears.

Figure 5.6 shows spread along the basilar membrane as a function of stimulus intensity up to current intensities where side lobes appear in the electrical tuning curves. Results for QUAD6 could not be calculated above 1 dB above threshold because of side-lobes appearing at approximately 1 dB above threshold.

The slope of the lines give an indication of the rate of change in the spread of excitation as a function of stimulus intensity. The shallower the slope of the line, the less the increase in spread of excitation as a result of increasing stimulus intensity. The initial steep slopes of the curves indicate that the spread of excitation increases rapidly at very low relative stimulus intensities. In the model, this slope mostly reflects the difference in excitation threshold current between the two nerve fibres opposite the boundaries of the exciting electrode. Narrower electrode configurations (QUAD1, QUAD4, QUAD5 and TET1) display the shallowest slopes overall, indicating less widening of the region of excitation with increasing stimulus intensity than when wider spaced electrode configurations are used.

The interpretation of UF is clear in Figure 5.6 where curves corresponding to lower values of UF (and therefore exhibiting lower unimodal focussing ability) are located towards wider spread of activation values on the ordinate and vice versa.

3.2 Shaping of neural excitation

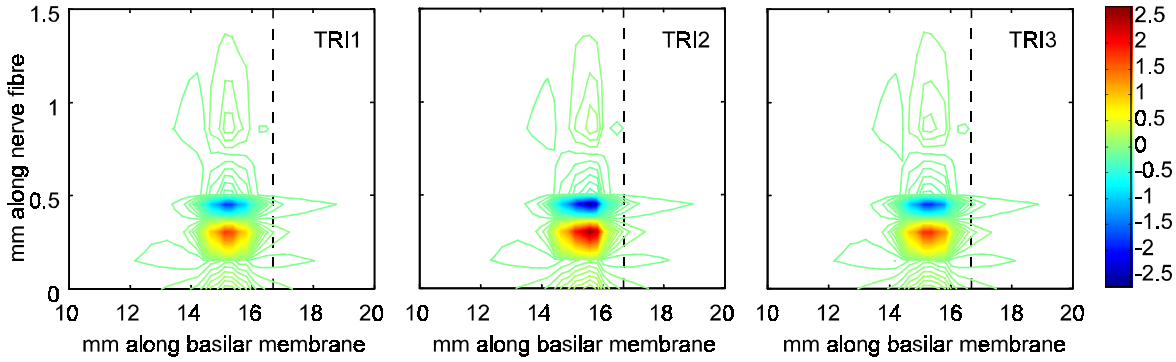

Figure 5.7. AF contours of enhanced tripolar electrode configurations showing the shaping properties of the potential fields. The multiplication factor scale on the colourbar is 10^5 mV/ms.

For tetrapolar and pseudo-continuous electrode configurations (Figure 5.9), AF contours show that different stimulus distributions will activate the nerve fibre population in different ways. Similar to enhanced tripolar configurations, lower

threshold currents are predicted for nerve fibres close to electrodes carrying higher stimulus currents relative to their neighbours, i.e. lateral electrodes in TET3 and central electrode in TET4 (Figure 5.9). This is confirmed by AF contours for the same stimulus distributions created with the analytical model (right graphs in Figure 5.9).

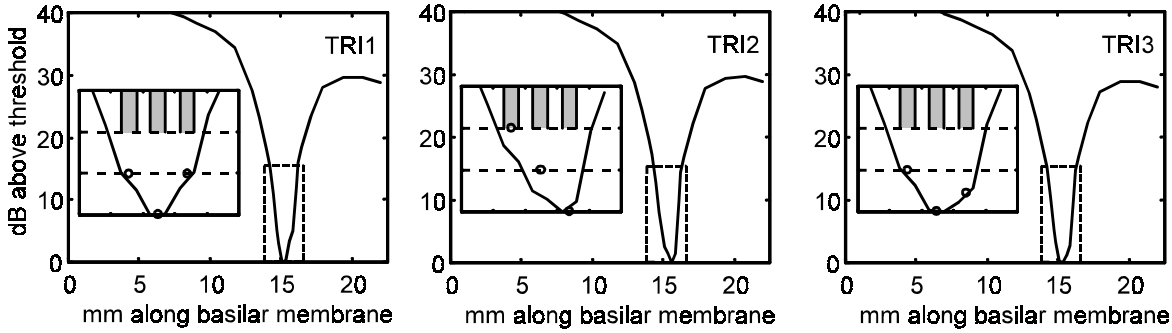

Figure 5.8. Electrical tuning curves for enhanced tripolar electrode configurations. An enlargement of the primary region of activation (dashed block) is shown as an inset in each figure. Shaded blocks indicate the location of the stimulating electrode pairs. An inverted representation (i.e. highest stimulus intensity is located at 0 dB and lower stimulus intensities are placed towards higher thresholds) of the stimulus distribution on the electrodes is shown with open circles in each inset.

The effect of the 3-D structure of the cochlea on excitation patterns is clearly visible in Figure 5.9 where the AF contours obtained with the FE model show a possible region of excitation in the third half-turn of the cochlea model for the TET configurations.

The open circles in Figure 5.10 give an indication of the shape of the stimulus distribution and of the location of the electrodes along the length of the basilar membrane for multipolar shaping electrode configurations. When an AR return electrode is used, manipulation of the excitation profile is relatively well achieved in the vicinity of the electrode set. However, the accumulated current at the return electrode causes excitation of nerve fibres at lower stimulus currents than those required for excitation at the active electrodes (solid lines in graphs of TET configurations in Figure 5.10) (not shown for the pseudo-continuous electrode sets).

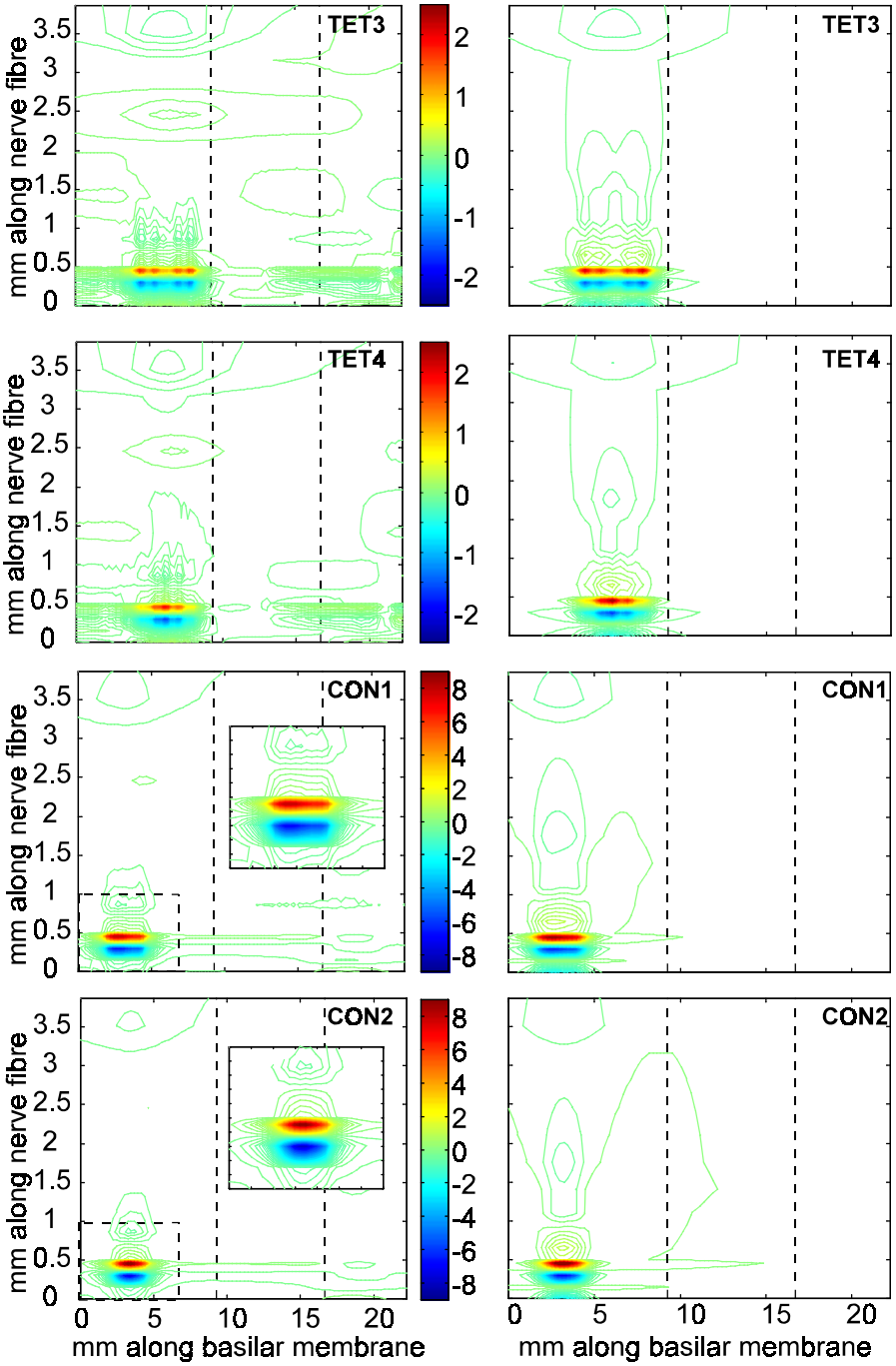

Figure 5.9. AF contours with a distant return electrode (MONO) generated with the FE model (left graphs) and the analytical model (right graphs). The multiplication factor of the scale on the colourbar is 10^4 mV/ms.

To suppress the excitation of nerve fibres around the return electrode, MONO and CGND return electrodes were used. When a remote (MONO) return electrode is used, the shaping ability of the electrode set is less pronounced but still visible. This is evident from Figure 5.10 where the region of activation is broader and exhibits less localised variations when a remote (MONO) return electrode is used than when an AR or a CGND return electrode is used. A CGND return electrode maintains the shaping profile at the active electrodes in a more localized manner than a MONO return electrode, but creates widespread excitation through all cochlear canals at stimulus intensities below 15 dB above threshold. The dynamic range over which a CGND return electrode will allow selective activation of nerve fibres is thus limited relative to that of a MONO return electrode.

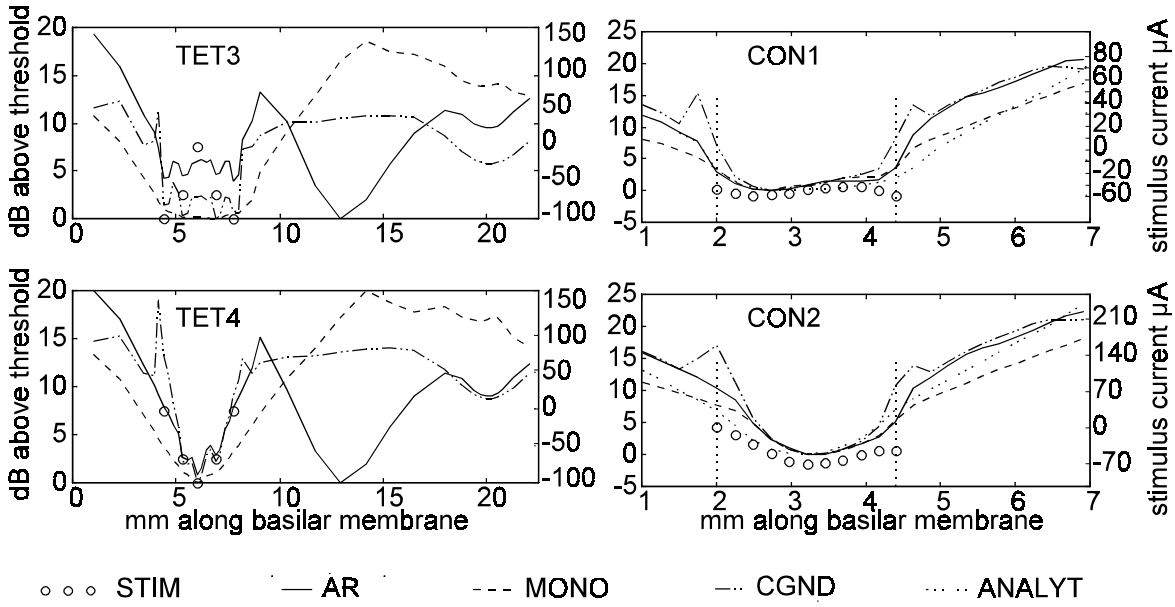

Figure 5.10. Electrical tuning curves for tetrapolar electrode configurations are shown in the left graphs while the same are shown for pseudo-continuous electrode configurations in the right graphs. Open circles indicate the stimulus intensity in A at the location of the active electrodes (scale on the right ordinate).

Figure 5.11 (threshold versus stimulus current) shows that there is a definite, almost linear relationship between the stimulus distribution on an electrode set and the excitation profile of the nerve fibres. The correlation coefficient is mostly greater than

0.9 and approaches 1 in many cases. The greatest deviations are seen when the stimulus distribution is increasing in magnitude at the boundaries of an electrode set relative to the neighbouring electrodes in the set, e.g. TET3 and CON1.

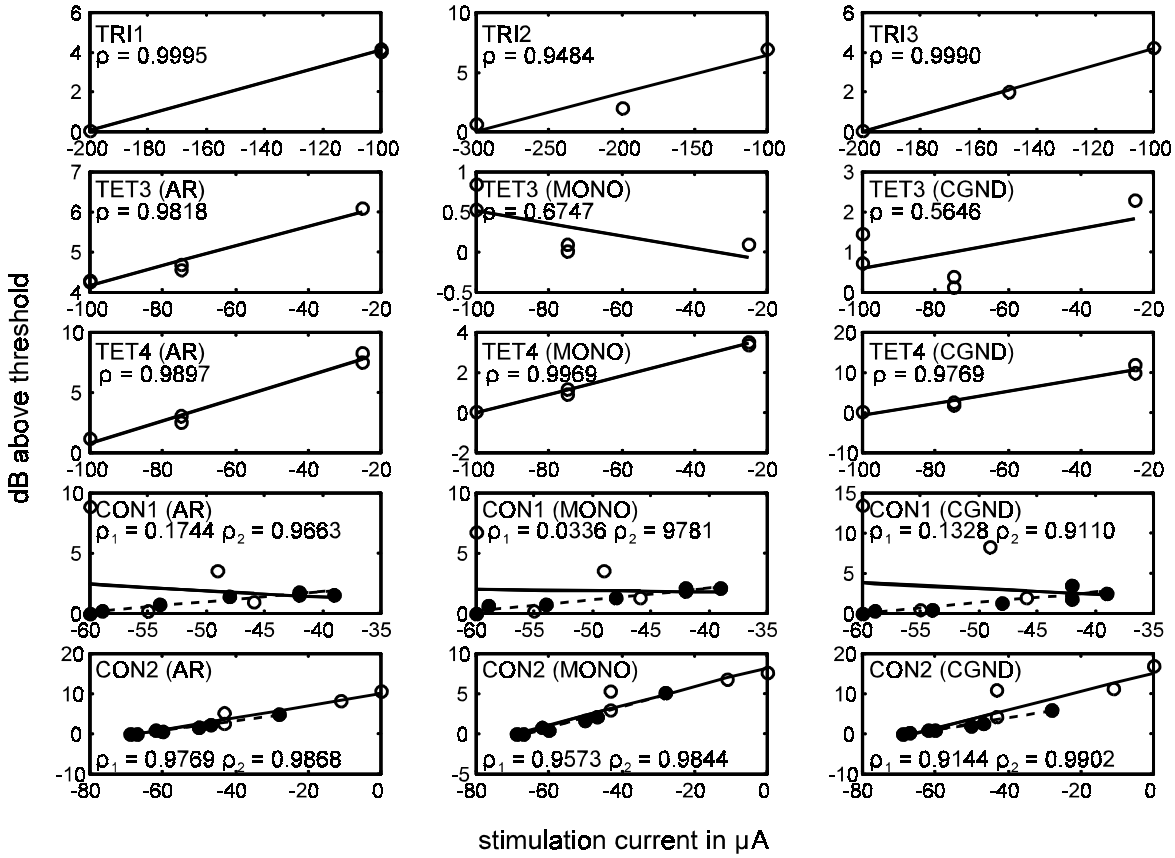

Figure 5.11. Shaping properties of electrode sets characterized by correlation coefficient and distribution of data points relative to linear fit through data points. Two correlation coefficients are given for the pseudo-continuous electrode configurations: $_1$ is for the complete data set while $_2$ is for the data set excluding data for the first and last two electrodes of the set. Solid lines show a linear least squares fit through the data while dotted lines show the same for the limited data set for the pseudo-continuous electrode configurations.

The linear relationship between stimulus distribution and excitation profile also breaks down at the boundaries of the pseudo-continuous electrode sets. If, however, the excitation profile on nerve fibres next to the lateral two electrodes on each side of the electrode set is disregarded, the linear relationship between stimulus distribution and excitation profile becomes very strong (correlation coefficient greater than 0.9) for all types of return electrodes used.

4 DISCUSSION

4.1 Focussing of neural excitation patterns

Model results confirm the focussing ability of overlapping quadrupolar electrode configurations as reported by other researchers (Jolly, Spelman, & Clopton, 1996; Kral et al., 1998). It was also shown that spreading the current of the lateral poles in the quadrupole over two electrodes on both sides of the central pole could suppress side-lobes in the excitation profile. This approach is similar to the approach of Kral et al. (1998) who used an additional remote electrode to return some of the current injected from the central electrode that would otherwise be returned by the lateral electrodes. QUAD5, which is configured from an enhanced tripolar electrode set, is also similar to the electrode configuration used by Kral et al.

The resolution of the data that Kral et al. (1998) measured in cats is not sufficient to calculate *UF*. Also, the measured electrical tuning curves do not show definite lateral minima as displayed by results from the model. All the same, *UF* was estimated as 0.043 for an electrical tuning curve measured *in vivo* for a tripolar configuration where the current intensity on the lateral electrodes was suppressed by 10 dB from that injected by the central electrode. This low value of UF compared to the values calculated for the modelled electrode configurations could be because uncurved banded electrode arrays (similar to the arrays used in the Nucleus implant) were used for the measurements. This type of array is frequently located distal from the nerve fibres (Roland et al., 2000). Spread of excitation is larger for arrays located further

from the nerve fibres (Chapter 3), which could cause less pronounced trimodal excitation patterns. However, both the modelled and the measured electrical tuning curves show suppression of the side-lobes in the excitation profile because the lateral poles do not carry the full complement of the current injected by the central pole. Also, measured data (Kral et al., 1998) confirm the findings that (1) spread of excitation is less for the focussing electrode configurations than for monopolar electrode configurations and (2) unimodal focussing can be achieved through excitation with multiple electrode configurations.

It has been shown that narrowly spaced electrode sets possess better focussing ability than more widely spaced electrode sets. The implication for the design of intracochlear electrodes is that focussing of excitation patterns could be improved by a combination of increasing the lateral electrode density, i.e. include more electrode contacts per unit length, and using quadrupolar or tetrapolar electrode configurations. Although the side-lobes generated with quadrupolar and tetrapolar electrode configurations could be suppressed even further by using a common ground electrode configuration as return instead of one or two lateral electrodes, the advantage of quadrupolar or tetrapolar configurations is that several regions of focussed excitation can be created simultaneously in SAS (Kessler, 1999) or simultaneous pulsatile (Kessler, 1999) type strategies.

Slightly lower values of UF for the overlapping quadrupolar electrode configurations compared to the tetrapolar configurations suggest that there could be a tradeoff between suppression of side lobes and focussing ability of an electrode set. The ultimate example would be excitation profiles created with monopolar stimulation versus those created with overlapping quadrupolar stimulation. With monopolar stimulation no side-lobes exist in the excitation profile, but the focussing ability of the configuration is low. On the other hand, the focussing ability of overlapping quadrupolar configurations is high but side-lobes exist in the excitation profile within the dynamic range of many cochlear implant users.

A high lateral electrode density could allow patient-specific electrode configurations with high focussing ability. At locations in the cochlea where low threshold currents are sufficient to excite nerve fibres, narrowly spaced electrode configurations could be used to create electrode sets. An increased number of discrete regions of excitation (relative to the number of regions of excitation created with electrode arrays having a low lateral electrode density) could thus be created in such areas of the cochlea. On the other hand, at locations in the cochlea where surviving nerve fibres are sparse or higher stimulation currents are required to elicit a response, electrode sets could be configured in a BP+x (where x is the number of electrodes separating active electrodes) configuration to lower threshold currents (Figure 5.2). Moreover, electrode sets can be configured to use more than one neighbouring electrode contact to form an "electrode". This could be advantageous when larger stimulation currents are required since an increased electrode surface area will lower the current density on the electrode surface and thus protect the electrode metal from corrosion (Brummer & Turner, 1977).

Curves showing spread of excitation along the basilar membrane as a function of stimulus intensity (in dB) above threshold (Figure 5.5) are equivalent to input-output functions. Recruitment properties of nerve fibres with different diameters are not reflected in the model, i.e. in the current model a homogeneous nerve fibre population is assumed. The approximately linear relationship between relative stimulus intensity and spread of excitation for the focussing electrode configurations show that, up to where side-lobes appear in the excitation profile, the size of the excited nerve population is proportional to the stimulus intensity.

4.2 Shaping of neural excitation patterns

Miyoshi et al. (1999) experimented with shaping of the excitation profile using a tripolar electrode configuration (similar to the overlapping quadrupolar configurations described in this chapter). Monophasic current stimuli were used with the central electrode serving as the cathode and the lateral electrodes as the anodes. It was found that it might be possible to limit the region of excitation and to vary the spatial

location of the stimulation site by controlling the current on the lateral electrodes. Although the results of Miyoshi et al. do not include the effect of biphasic stimuli (Chapter 3), their results are similar to results obtained with the enhanced tripolar electrode configuration in this chapter. The use of enhanced tripolar configurations rather than normal tripolar or quadrupolar configurations to shape neural excitation profiles is advantageous since no phase reversals that cause irregularities in the excitation profile occur. This is useful when a continuous excitation profile is desired. With the enhanced tripolar electrode configuration side-lobes were thus eliminated by the use of three radially oriented electrode pairs versus the use of monophasic stimuli by Miyoshi et al. to produced the same effect. Results presented in this chapter, based on excitation profiles calculated with biphasic stimuli, support the findings of Miyoshi et al. Firstly, the region of excitation can be limited if a tripole is used in an overlapping quadrupolar configuration (QUAD5). Secondly, the location of the region of excitation can be manipulated (possibly in a continuous fashion as claimed by Miyoshi et al.) by controlling the currents injected from the lateral electrodes relative to that injected by the central electrode.

Model results suggest that the excitation profile could be shaped continuously on nerve fibres covering a larger region of the cochlea through multipolar banded electrode configurations (TET3 and TET4) and pseudo-continuous electrode configurations. Monopolar and common ground return electrodes are more suitable to create continuous excitation profiles than an AR return electrode, but cannot provide the same degree of selectivity and focussing offered by radially oriented electrode pairs. It could thus be advantageous if an electrode array with a large number of radially oriented electrode pairs could be used to create continuous excitation patterns. Such an electrode could provide localised excitation around each electrode pair which could also limit ectopic excitation of nerve fibres originating from other cochlear regions.

The pseudo-continuous electrode configuration of the Clarion implant that exists when the SAS strategy is used, is similar to a low electrode density implementation

of the shaping electrode configurations discussed in this chapter. Therefore, model results suggest that the Clarion implant could effectively deliver auditory information simultaneously to different nerve fibre populations in the cochlea by using the SAS strategy.

The best electrode configuration for a specific person would once again be determined by the nerve survival pattern in the deaf cochlea as well as the location of the array relative to the surviving nerve fibres. Unfortunately, these parameters cannot be measured or calculated preoperatively. A perimodiolar electrode design could limit variations in array location between cochlear implant users, but nerve survival cannot be controlled. Similar to focussing electrode configurations, an electrode array with a high lateral electrode density could facilitate customization of an electrode array for individual persons by activation of a custom selection of electrodes depending on nerve survival patterns.

5 CONCLUSION

Model results confirm that focussing of excitation around intracochlear electrodes could be improved by using overlapping quadrupolar electrode configurations. These electrode and stimulus configurations create trimodal excitation pattens. The suppression of the side-lobes in trimodal excitation patterns depends largely on the electrode separation and the stimulus distribution. If the stimuli on the lateral electrodes are spread over two neighbouring electrodes, side-lobes in the excitation profile could be suppressed even further. A trade-off could, however, exist between focussing ability of electrode configurations and suppression of side-lobes in the excitation profile.

Results also suggest that the excitation profile could be shaped continuously with enhanced tripolar electrode configurations, multipolar banded electrode configurations and pseudo-continuous electrode configurations. Based on model

results obtained with shaping electrode configurations, it is concluded that the SAS strategy implemented in the Clarion processor could effectively deliver auditory information in a simultaneous fashion to different nerve fibre populations in the cochlea.

An improved electrode array that facilitates focussing and continuous shaping of neural excitation profiles could be constructed by including a large number of electrode contacts. Banded electrode geometries could provide focussing and shaping of the excitation profile. However, the use of a remote return electrode (which is required if irregularities in the excitation profile are unwanted) could potentially degrade the shaping ability of electrode sets because of current spread. Radially oriented electrode pairs address the return electrode problem by providing a local current return path that limits spread of excitation and facilitates in-phase stimulation on the active electrodes. An array with high lateral electrode density could furthermore facilitate customization of the array for individual implant users by selecting subsets of electrodes based on surviving nerve fibre patterns.

Chapter 6
GENERAL DISCUSSION

1 RESEARCH PROBLEM AND APPROACH

Accurate models of the implanted cochlea are required to gain a better understanding of the functioning of cochlear implants and to be used as tools during the development of new generation cochlear implants (Briaire & Frijns, 2000). Such models could focus on the nerve-implant interface or on processing of auditory information by the higher auditory system. In this thesis the focus was on modelling of the nerve fibre-implant interface. The objective was to introduce an accurate model of the implanted cochlea with which potential distributions and neural excitation patterns around cochlear implant electrodes could be determined.

To gain an appreciation of the effects of the 3-D structure of the implanted cochlea and of array and model variations, a 3-D model was required. Although a number of 3-D volume conduction models of the cochlea exist, a model that could effortlessly facilitate simulation of array variations and could therefore also be used to experiment with new arrays has not yet been constructed. The definition and construction of a detailed 3-D spiralling FE model of the implanted cochlea have been discussed. The model was extruded from a 2-D geometry representing a section through one turn of the cochlea into three dimensions around a central axis. The model incorporates the effect of neighbouring canals and conduction along the fluid-filled scalae of the cochlea. To create different array locations, electrode geometries and electrode configurations without remeshing the volume containing the electrode array, two electrode arrays were included in the original model. To activate or deactivate a specific array the resistivities of its elements were changed to those of an insulator

or a conductor while the resistivity of the other array's elements was set to that of perilymph. Model generation, choice of model parameters and model verification methods have been discussed in detail in Chapter 2. Potential distributions generated with the FE model have been coupled to a nerve fibre model to facilitate the investigation of auditory nerve fibre excitation patterns around intracochlear electrode arrays. The GSEF nerve fibre model was used to calculate the neural response to excitation. The nerve fibre model is coupled to the FE model by defining the location of an array of nerve fibre models as a curved plane in the FE model. The nerve fibre model and also the FE-nerve fibre model interface have been discussed in full in Chapter 2.

2 RESULTS AND CONCLUSIONS

This study mainly endeavoured to explain four aspects influencing neural excitation patterns as a result of intracochlear stimulation: (1) the effect of array variations and nerve fibre degeneration (Chapter 3), (2) the effect of model variations (Chapter 3), (3) the effect of scar tissue around implanted electrodes (Chapter 4), and (4) focussing and shaping of excitation profiles with nonstandard electrode configurations (Chapter 5). In all cases the 3-D FE model described in Chapter 2 was used to calculate potential distributions as a result of current injection from different array variations with and without variations in the model structure. Activating function contours were frequently used to obtain a preliminary estimate of excitation profiles that can be expected as a result of a specific potential distribution. A nerve fibre model was used to translate potential distributions into excitation profiles that could be interpreted in terms of data measured in animals and humans.

In general it was found that the spiralling geometry of the cochlea causes asymmetry in potential distributions and that the location of electrodes along the length of the basilar membrane has a stronger influence on the location of excitation along the basilar membrane than the polarity of the leading phase of the stimulus.

Variation in array location indicated that threshold currents and the effect of postsurgical neural degeneration (and also ongoing loss of peripheral dendrites) on threshold currents can be limited by placing arrays close to the modiolus. It was also shown that array location is the primary parameter that controls excitation spread, although electrode separation can be used to a lesser extent to do the same. Subsequent variations in electrode geometry showed that point electrode geometries are recommended above banded electrode geometries only when the array can be placed close to the modiolus.

The critical focussing intensity of an electrode configuration was defined as the lowest stimulus intensity relative to the minimum threshold current where the excitation profile displays a discontinuity in slope. This discontinuity in the excitation profile indicates the point where spread of excitation becomes unfocussed. It was shown that CFI is a function of electrode separation.

The existence of bimodal excitation patterns at comfortable stimulus intensities for longitudinal bipolar electrode configurations were confirmed. The threshold minimum around the electrode that should act as the return electrode (and not as stimulating electrode) is regarded as an ectopic region of excitation. It was shown that NBP electrode configuration can be used besides radial, offset radial and monopolar electrode configurations to create unimodal excitation patterns. The CFI indicated that the focussing ability of monopolar stimulation is approximately the same as that of widely spaced bipolar electrode configurations. This finding is significant since widely spaced electrode configurations are frequently used to excite nerve fibres when closely spaced electrode configurations fail to do so. Given the advantage of unimodal excitation patterns when using monopolar electrode configurations, monopolar electrode configurations should be favoured above widely spaced bipolar configurations if the option is available. Based on current spread versus electrode configuration curves, and CFI values, it is believed that monopolar stimulation could be advantageous when BP+2 stimulation is required.

Evidence of electrode discrimination ability by implant wearers for overlapping regions of excitation exists (Hanekom & Shannon, 1996). In addition, simulation results indicated that neighbouring, narrowly spaced electrode pairs create overlapping but different excitation patterns. These observations suggest that the stimulation resolution of cochlear implant electrode arrays can potentially be improved by increasing the number of electrode contacts in an array.

Model results indicated that there is a tradeoff between array location and the degree of ectopic stimulation caused by a specific array location. Perimodiolar arrays, which are the arrays of choice when focussed excitation is required, are more prone to cause ectopic excitation than arrays further away from the nerve fibres. A precautionary measure that could be taken to prevent ectopic excitation is to use the *narrowest* possible spaced electrode pair that would elicit a response and allow sufficient loudness growth. This could mean that several different electrode configurations should be used in one implant wearer to obtain the best results.

The effects of various cochlear structures in the model on excitation profiles were investigated. It was shown that, at least in this model, the effects of the helicotrema, stria vascularis and Organ of Corti were negligible. Structures that did have a noticeable effect and should consequently be included in future models, are the spiral lamina, Reissner's membrane and the basilar membrane. Simulated tapering of the perilymphatic spaces in the cochlear model also had a marked effect on mainly minimum threshold currents. Narrowing of the cochlear canals towards the apex causes an increase in the resistivity of the volume surrounding the electrodes which, in turn, causes threshold currents to decrease towards the apex. Evidence of more focussed excitation towards the apex as a result of tapering of the canals is vaguely displayed by the model and could be more pronounced in a real cochlea.

The effect of electrode encapsulation by fibrous scar tissue on electrical potential distributions and auditory nerve fibre excitation patterns was investigated by creating a thin layer of encapsulation tissue around the modelled electrodes in the FE model.

An LP model of the implanted cochlea incorporating encapsulation tissue around the electrode array was created to explain threshold changes predicted by the FE-nerve fibre model in the presence of encapsulation tissue. Both the LP and the FE models show that electrical potentials at the target nerve fibres and the electrode contacts increase in the presence of encapsulation tissue. This leads to a decrease in threshold currents and spread of excitation. Narrowly spaced electrode configurations and array locations close to the modiolus are influenced most by the presence of encapsulation tissue. It was concluded that the effect of electrode encapsulation on threshold currents and spread of excitation is a function of electrode configuration and array location. Although compliance problems could occur if the resistance of encapsulation tissue becomes very high, advantages of electrode encapsulation could be a decrease in threshold current and an increase in dynamic range.

In Chapter 4 it was observed that a local increase in the resistivity of the volume in contact with the electrodes can cause a decrease in threshold currents, as well as an increase in the focussing ability of an electrode configuration. Some evidence that the same effects are caused by tapering of the cochlear canals (i.e. an increase in the resistance of the cochlear volume surrounding the electrodes) was also found in Chapter 3. These observations suggest that the electrode carrier might also serve to lower threshold currents and could even focus excitation. This statement was verified with simulations where the electrode carrier was deactivated[1] (i.e. its resistivity was set equal to that of perilymph) and has also been proposed by Suesserman and Spelman (1993). It has been suggested that an electrode carrier that replaces much of the perilymph in the scala tympani could compensate for electrode to nerve fibre distance variations (Seldon et al., 1994; Zrunek et al., 1980). Such variations are known to cause threshold current variations and also variations in the focussing of neural excitation patterns around electrodes (Chapter 3, Shepherd et al., 1993). A variation on the scalar filling approach has recently been introduced

[1]These results have not been presented elsewhere in this thesis.

by which a straight array (e.g. the electrode array of the Nucleus implant) is placed in a perimodiolar position (Tykocinski et al., 2000). This is done by an electrode positioner that is inserted into the scala tympani lateral to the electrode array and distal from the modiolus, forcing the array into a perimodiolar position. Based on model results this technique should reduce threshold currents and spread of excitation as hoped. However, whether sufficient flow of perilymph will be possible to assure minimal cochlear damage over the long term, e.g. survival of the hair cells (Leake, Kessler & Merzenich, 1990), is not clear.

Finally, the focussing and shaping ability of various multi-electrode configurations was investigated. Electrode configurations modelled included enhanced tripolar, quadrupolar, tetrapolar and pseudo-continuous configurations. It was confirmed that focussing of excitation around intracochlear electrodes could be improved by using overlapping quadrupolar electrode configurations. Side-lobes in the excitation profile, which occur at relatively higher stimulus intensities relative to the stimulus intensity required to excite the target nerve fibres, can be further suppressed if the currents that are returned to the lateral electrodes are spread over multiple electrodes. The ultimate lateral spread would occur for a common ground return electrode. Simulation results suggest that a tradeoff could exist between focussing ability of electrode configurations and suppression of side-lobes in the excitation profile.

It has been shown that it could be possible to shape the excitation profile continuously with enhanced tripolar electrode configurations, multipolar banded electrode configurations and pseudo-continuous electrode configurations. Model results obtained with shaping electrode configurations suggest that the SAS strategy implemented in the Clarion processor could effectively deliver auditory information in a simultaneous fashion to different nerve fibre populations in the cochlea.

Results from Chapter 3 suggest that electrode pairs might be discriminable even though their respective regions of excitation might overlap. Furthermore, results from Chapter 5 that show that continuous shaping of the excitation profile might be

possible with an array with high lateral electrode density and that the focussing ability of multipolar electrode configurations is improved if electrode separation is decreased. These results provide some evidence in favour of increasing the lateral electrode density of intracochlear electrode arrays. An array with high lateral electrode density could also facilitate customization of the array for individual implant users by selecting subsets of electrodes based on surviving nerve fibre patterns.

3 RESEARCH CONTRIBUTION

The most important research contributions made by this study are the following:

1) The creation of a detailed 3-D model of the implanted cochlea that accurately predicts measurable effects in cochlear implant wearers and facilitates effortless implementation of existing and new array variations.
2) The establishment of the important fine anatomical structures required in a 3-D representation of the implanted cochlea.
3) Establishment of evidence that array location is the primary parameter that controls spread of excitation.
4) Confirmation that monopolar stimulation could deliver focussed stimulation to approximately the same degree than that delivered by widely spaced electrode configurations and that the use of monopolar configurations over bipolar configurations is advantageous under certain conditions.
5) Explanation of the effect that encapsulation tissue around cochlear implant electrodes could have on neural excitation profiles.
6) Extension on the information available on the focussing ability of multipolar electrode configurations.
7) Establishment of evidence that excitation profiles could be shaped in a continuous fashion using multiple radially oriented electrode pairs and also longitudinally oriented electrode sets operating in a non-bipolar fashion.
8) Confirmation that the SAS strategy could effectively deliver auditory information to different neural populations along the length of the cochlea.

9) Establishment of evidence that a higher lateral electrode density could facilitate better focussing of excitation, continuous shaping of excitation profiles and postoperative customization of electrode arrays for individual implant wearers.

4 FUTURE RESEARCH DIRECTIVES

Much valuable information has been gathered from the representation of an implanted cochlea has been presented in this thesis. Although the model does not incorporate the tapering of the cochlea toward the apex, simulations that were performed in a restricted region of the cochlea (e.g. simulation of NBP to BP+3 electrode configurations confined to the region halfway through the first half-turn of the modelled cochlea) are not significantly influenced by the untapered geometry. The present model lies the foundation for development of a tapered, high resolution, detailed model of the human cochlea and the use of a more accurate human nerve fibre model that includes fine details such as the soma region of the fibre (Rattay, 1999).

However, although the information gained by the above-mentioned improvements could provide some additional insights into the nerve fibre-implant interface, results are nonspecific, i.e. only general trends in cochlear implant patients can be predicted. It is proposed that the next quantum step in modelling of the auditory nerve-implant interface would be to model individual cochleas. This could facilitate preoperative evaluation of potential cochlear implant candidates, estimation of the potential benefits of implantation for an individual and ultimately, estimation of what a person could expect to hear with his or her implant. To facilitate modelling of individual cochleas, research presented in this thesis should be extended to include the development of high resolution imaging techniques whereby an accurate numerical representation of the shape of an individual's cochlea can be obtained. Automatic model generation software and atraumatic techniques to estimate nerve survival

patterns inside the deaf cochlea should also be developed. The model presented in this thesis can provide a basic geometry which could be adapted according to the additional information gained from imaging, e.g. by scaling each model segment according to the dimensions provided by the imaging technique.

The model provided evidence that a high density electrode array could increase the amount of auditory information that can be transferred to the auditory nerve fibres. Research required to complement the findings in this thesis regarding high density electrode arrays should include *in vitro* characterization of the potential fields generated by such an array in an electrode tank and also measurements in cadaver cochleas and animals to assess the functionality and effectiveness of such an array.

REFERENCES

Advanced Bionics Corporation (8-21-2000). *Clarion system: Hifocus electrode* [online]. Available: http://www.cochlearimplant.com/shortcut_hifocus.html.

Allen, J. B. (1985). Cochlear modelling. *IEEE ASSP Magazine,* 3-29.

ANSYS (1997). *ANSYS Modelling and Meshing Guide* USA: SAS IP, Inc.

ANSYS (1999). *ANSYS Electromagnetic Field Analysis Guide (pp. 13-1-13-8).* USA: SAS IP, Inc.

Bertoluzza, A., Fagnano, C., Monti, P., Simoni, R., Tinti, A., Tosi, M. R., & Caramazza, R. (1992). Raman spectroscopy in the study of biocompatibility. *Clinical Materials, 9,* 49-68.

Black, R. C., & Clark, G. M. (1980). Differential electrical stimulation and the auditory nerve. *Journal of the Acoustical Society of America, 67*.

Black, R. C., Clark, G. M., & Patrick, J. F. (1981). Current distribution measurements within the human cochlea. *IEEE Transactions on Biomedical Engineering, BME-28,* 721-724.

Briaire, J. J., & Frijns, J. H. M. (2000). 3D mesh generation to solve the electrical volume conduction problem in the implanted inner ear. *Simulation Practice and Theory, 8,* 57-73.

Brown, C. J., Abbas, P. J., Bertschy, M., Tyler, R. S., Lowder, M., Takahashi, G., Purdy, S., & Gantz, B. J. (1995). Longitudinal assessment of physiological and psychophysical measures in cochlear implant users. *Ear and Hearing, 16(5),* 439-449.

Brummer, S. B., & Turner, M. J. (1975). Electrical stimulation of the nervous system: The principle of safe charge injection with noble metal electrodes. *Bioelectrochemistry and Bioenergetics, 2,* 13-25.

Brummer, S. B., & Turner, M. J. (1977). Electrical stimulation with Pt electrodes:II-Estimation of maximum surface redox (theoretical non-gassing) limits. *IEEE Transactions on Biomedical Engineering, BME-24,* 440-443.

Busby, P. A., Whitford, L. A., Blamey, P. J., Richardson, L. M., & Clark, G. M. (1994).

Pitch perception for different modes of stimulation using the Cochlear multiple-electrode prosthesis. *Journal of the Acoustical Society of America, 95(5),* 2658-2669.

Clark, G. M. (1996). Electrical stimulation of the auditory nerve: the coding of frequency, the perception of pitch and the development of cochlear implant speech processing strategies for profoundly deaf people. *Clinical and Experimental Pharmacology and Physiology, 23,* 766-776.

Clark, G. M., Shute, S. A., Shepherd, R. K., & Carter, T. D. (1995). Cochlear implantation: Osteoneogenesis, electrode-tissue impedance, and residual hearing. *Annals of Otology, Rhinology and Laryngology Supplement (United States), 166 ,* 40-42.

Clark, G. M., Tong, Y. C., & Patrick, J. F. (1990). *Cochlear Prostheses* Great Britain: Churchill Livingston.

De Sauvage, R. C., da Costa, D. L., Erre, J.-P., & Aran, J. M. (1997). Electrical and physiological changes during short-term and chronic electrical stimulation of the normal cochlea. *Hearing Research, 110,* 119-134.

Donaldson, N. d. N., & Donaldson, P. E. K. (1986). When are actively balanced ('Lilly') stimulating pulses necessary in a neurological prosthesis? II pH changes; Noxious products; Electrode corrosion; Discussion. *Medical and Biological Engineering and Computing, 24,* 50-56.

Dorman, M. F., Smith, L. M., Dankowski, K., McCandless, G., & Parkin, J. L. (1992). Long-term measures of electrode impedance and auditory thresholds for the Ineraid cochlear implant. *Journal of Speech and Hearing, 35,* 1126-1130.

Eddington, D., Dobelle, W., Brackmann, D. E., Mladejousky, M., & Parkin, J. L. (1988). Auditory prosthesis research with multiple channel intracochlear stimulation in man. *Annals of Otology, Rhinology and Laryngology Supplement, 87,* 5-39.

Finley, C. C., Wilson, B. S., & White, M. W. (1990). Models of neural responsiveness to electrical stimulation. In Miller, J. M. and Spelman, F. A., *Cochlear Implants* (pp. 55-96). New York: Springer-Verlag Inc.

Frankenhaeuser, B., & Huxley, A. F. (1964). The action potential in the myelinated

nerve fibre of Xenopus Laevis as computed on the basis of voltage clamp data. *Journal of Physiology, 171,* 302-315.

Frijns, J. H. M. (1995). *Cochlear implants: A modelling approach*. Ph.D Thesis, Rijksuniversiteit, Leiden, The Netherlands.

Frijns, J. H. M., Briaire, J. J., & Schoonhoven, R. (2000). Integrated use of volume conduction and neural models to simulate the response to cochlear implants. *Simulation Practice and Theory, 8,* 75-97.

Frijns, J. H. M., de Snoo, S. L., & Schoonhoven, R. (1995). Potential distributions and neural excitation patterns in a rotationally symmetric model of the electrically stimulated cochlea. In Frijns, J. H. M., *Cochlear Implants. A Modelling Approach* (pp. 93-124). Den Haag: CIP-Data Koninklijke Bibliotheek.

Fu, Q.-J., & Shannon, R. V. (1999a). Effects of electrode location and spacing on phoneme recognition with the nucleus-22 cochlear implant. *Ear and Hearing, 20,* 321-331.

Fu, Q.-J., & Shannon, R. V. (1999b). Effects of electrode configuration and frequency allocation on vowel recognition with the nucleus-22 cochlear implant. *Ear and Hearing, 20,* 332-344.

Fujita, S., & Ito, J. (1999). Ability of nucleus cochlear implantees to recognize music. *Annals of Otology, Rhinology and Laryngology, 108,* 634-640.

Girzon, G. (1987). *Investigation of current flow in the inner ear during electrical stimulation of intracochlear electrodes*. MS Thesis in EE&CS, MIT, Cambridge, Massachusetts.

Golden, B. (2-1-1997). *Cochlea* [online]. Available: http://www.yavapai.cc.az.us/division/sci_math/biology/golden/a&p/AP112-22.HTM.

Gonzalez, G., & Huerta, M. A. (1979). Surface potentials of spheroidal volume conductors excited by an electric dipole source. *International Journal of Electronics, 47,* 213-220.

Grill, W. M., & Mortimer, J. T. (1994). Electrical properties of implant encapsulation tissue. *Annals of Biomedical Engineering, 22,* 23-33.

Gstoettner, W., Franz, P., Hamzavi, J., Plenk, H. Jr., Baumgartner, W., & Czerny,

C. (1999). Intracochlear position of cochlear implant electrodes. *Acta Oto-Laryngologica, 119,* 229-233.

Hanekom, J. J., & Shannon, R. V. (1996). Place pitch discrimination and speech recognition in cochlear implant users. *The South African Journal of Communication Disorders, 43,* 27-40.

Hanekom, J. J., & Shannon, R. V. (1998). Gap detection as a measure of electrode interaction in cochlear implants. *Journal of the Acoustical Society of America, 104(4),* 2372-2384.

Hatsushika, S.-I., Shepherd, R. K., Tong, Y. C., Clark, G. M., & Funasaka, S. (1990). Dimensions of the scala tympani in the human and cat with reference to cochlear implants. *Annals of Otology, Rhinology and Laryngology, 99,* 871-876.

Hirsch, H. G. (1993). Intelligibility improvements of noisy speech for people with cochlear implants. *Speech Communication, 12,* 261-266.

Huang, C. Q., Shepherd, R. K., Carter, P., Seligman, P., & Tabor, B. (1999). Electrical stimulation of the auditory nerve: Direct current measurement *in vivo*. *IEEE Transactions on Biomedical Engineering, 46,* 461-470.

Johnstone, B. M., Johnstone, J. R., & Pugsley, I. D. (1966). Membrane resistance in endolymphatic walls of the first turn of the guinea-pig cochlea. *Journal of the Acoustical Society of America, 40(6),* 1398-1404.

Jolly, C. N., Spelman, F. A., & Clopton, B. M. (1996). Quadrupolar stimulation for cochlear prostheses: Modeling and experimental data. *IEEE Transactions on Biomedical Engineering, 43,* 857-865.

Jolly, C. N., Clopton, B. M., Spelman, F. A. & Lineaweaver, S. K. (1997). Guinea pig auditory nerve response triggered by a high density electrode array. *Medical Progress through Technology, 21 (suppl.),* 13-23.

Kessler, D. K. (1999). The Clarion multi-strategy cochlear implant. *Annals of Otology, Rhinology and Laryngology, 108 (Suppl 177),* 8-16.

Kou, B. S., Shipp, D. B., & Nedzelski, J. M. (1994). Subject benefits reported by adult Nucleus 22-channel cochlear implant users. *Journal of Otolaryngology (Canada), 23(1),* 8-14.

Kral, A., Hartmann, R., Mortazavi, D., & Klinke, R. (1998). Spatial resolution of

cochlear implants: the electrical field and excitation of auditory afferents. *Hearing Research, 121,* 11-28.

Leake, P. A., Kessler, D.K., & Merzenich, M.M. (1990). Application and safety of cochlear prostheses. In Agnew F.A. & McCreery, D.B., *Neural Prosthses. Fundamental Studies.* (pp.253-296). New Jersey: Prentice Hall.

Leake, P. A., Snyder, R. L., Hradek, G. T., & Rebscher, S. J. (1992). Chronic intracochlear electrical stimulation in neonatally deafened cats: Effects of intensity and stimulating electrode location. *Hearing Research, 64(1),* 99-117.

Leeson, T. S. & Leeson, C. S. (1981). *Histology (pp. 572-581).* Philadelphia: W.B. Saunders Company.

Liang, D. H., Lusted, H. S., & White, R. L. (1999). The nerve-electrode interface of the cochlear implant: Current spread. *IEEE Transactions on Biomedical Engineering, 46,* 35-43.

Lim, H. H., Tong, Y. C., & Clark, G. M. (1989). Forward masking patterns produced by intracochlear electrical stimulation of one and two electrode pairs in the human cochlea. *Journal of the Acoustical Society of America, 86(3),* 971-980.

Linthicum, F. H. Jr., Fayad, J., Otto, S. R., Galey, F. R., & House, W. F. (1991). Cochlear implant histopathology. *American Journal of Otology, 12(4),* 245-311.

Loizou, P. C. (1999). Signal-processing techniques for cochlear implants. *IEEE Engineering in Medicine and Biology, 18(3),* 34-46.

Marsh, M. A., Coker, N. J., & Jenkins, H. A. (1992). Temporal bone histopathology of a patient with a nucleus 22-channel cochlear implant. *The American Journal of Otology, 13,* 241-248.

McKay, C. M., O'Brien, A., & James, C. J. (1999). Effect of current level on electrode discrimination in electrical stimulation. *Hearing Research, 136,* 159-164.

Miller, A. L., Morris, D. J., & Pfingst, B. E. (2000). Effects of time after deafening and implantation on guinea pig electrical detection thresholds. *Hearing Research, 144,* 175-186.

Miller, J. F. & Spelman, F. A. (1990). Fundamental research for development of cochlear research . In Miller, A. L. and Spelman, F. A., *Cochlear Implants: Models of the Electrically Stimulated Ear* (pp. 413-418). New York: Springer-

Verlag.

Miyoshi, S., Shimizu, S., Matsushima, J., & Ifukube, T. (1999). Proposal for a new method for narrowing and moving the stimulated region of cochlear implants: Animal experiment and numerical analysis. *IEEE Transactions on Biomedical Engineering, 46,* 451-460.

Nanas, J. M. (1988). Biocompatibility overview: Classes of materials, inflammation, infection. In Webster, J. G., *Encyclopedia of Medical Devices and Instrumentation* (pp. 181-194).Wiley.

National Institutes of Health (1995). Cochlear implants in adults and children. NIH Consensus Statement. 1-30.

Pfingst, B. E. (1990). Changes over time in thresholds for electrical stimulation of the cochlea. *Hearing Research, 50(1-2),* 225-236.

Pfingst, B. E., Morris, D. J., & Miller, A. L. (1995). Effects on electrode configuration on threshold functions for electrical stimulation of the cochlea. *Hearing Research, 85,* 76-84.

Pfingst, B. E., Holloway, L. A., Zwolan, T. A., & Collins, L. M. (1999). Effects of stimulus level on electrode-place discrimination in human subjects with cochlear implants. *Hearing Research, 134,* 105-115.

Plonsey, R. (1969). *Bioelectric Phenomena. McGraw-Hill series in Bioengineering.* New York: McGraw-Hill Book Company.

Rattay, F. (1990). *Electrical Nerve Stimulation. Theory, Experiments and Applications.* Vienna: Springer-Verlag.

Rattay, F. (1999). The basic mechanism for the electrical stimulation of the nervous system. *Neuroscience, 89,* 335-346.

Rattay, F., Leao, R. N., & Felix, H. (2001). A model of the electrically excited human cochlear neuron. II. Influence of the 3-dimensional cochlear structure on neural excitability. *Hearing Research, 153,* 64-79.

Rebscher, S. J., Talbot, N., Bruszewski, W., Heilmann, M., Brasell, J., & Merzenich, M. M. (1996). A transparent model of the human scala tympani cavity. *Journal of Neuroscience Methods, 64,* 105-114.

Reilly, J. P., Freeman, V. T., & Larkin, W. D. (1985). Sensory effects of transient

electrical stimulation. Evaluation with a neuroelectric model. *IEEE Transactions on Biomedical Engineering, BME-32(12),* 1001-1011.

Robblee, L. S. & Rose, T. L. (1990). Electrochemical guidelines for selection of protocols and electrode materials for neural stimulation. In Agnew, W. F. and McCreery, D. B., *Neural prosteses. Fundamental studies* (pp. 25-66). Englewood Cliffs, New Jersey: Prentice-Hall, Inc.

Rodenhiser, K. L., & Spelman, F. A. (1995). A method for determining the driving currents for focused stimulation in the cochlea. *IEEE Transactions on Biomedical Engineering, 42(4),* 337-342.

Roland, J. T., Fishman, A. J., Alexiades, G., & Cohen, N. L. (2000). Electrode to modiolus proximity: A fluoroscopic and histologic analysis. *American Journal of Otology, 21,* 218-225.

Rubinstein, J. T., Soma, M., & Spelman, F. A. (1985). Mixed boundary value problems in the implanted cochlea: An analytical model of a cylindrical banded electrode array. *IEEE Seventh Annual Conference of the Engineering in Medicine and Biology Society,* 1120-1123.

Rubinstein, J. T. (1988). *Quasi-static analytical models for electrical stimulation of the auditory nervous system*. Ph.D. Thesis, University of Washington.

Ruddy, H. A., & Loeb, G. E. (1995). Influence of materials and geometry on fields produced by cochlear electrode arrays. *Medical and Biological Engineering and Computing, 33,* 793-801.

Schindler, R. A., & Kessler, D. K. (1989). State of the art cochlear implants: The UCSF experience. *American Journal of Otology, 10(2),* 79-83.

Schwartz, J. R., & Eikhof, G. (1987). Na currents and action potentials in rat myelinated nerve fibres at 20 and 30 degrees C. *Pflügers Archiv, 409,* 569-577.

Seldon, H. L., Dahm, M. C., Clark, G. M., & Crowe, S. (1994). Silastic with polyacrylic acid filler: Swelling properties, biocompatibility and potential use in cochlear implants. *Biomaterials, 15,* 1161-1169.

Shannon, R. V. (1983). Multichannel electrical stimulation of the auditory nerve in man. I. Basic psychophysics. *Hearing Research, 11,* 157-189.

Shepherd, R. K., Clark, G. M., Pyman, B. C., & Webb, R. L. (1985). Banded

intracochlear electrode array: Evaluation of insertion trauma in human temporal bones. *Annals of Otology, Rhinology and Laryngology, 94,* 55-59.

Shepherd, R. K., Hatsushika, S.-I., & Clark, G. M. (1993). Electrical stimulation of the auditory nerve. The effect of electrode position on neural excitation. *Hearing Research, 66,* 108-120.

Skinner, M. W., Ketten, D. R., Vannier, M. W., Gates, G. A., Yoffie, R. L., & Kalender, W. A. (1994). Determination of the position of Nucleus cochlear implant electrodes in the inner ear. *The American Journal of Otology , 15(5),* 644-651.

Spelman, F. A., Clopton, B. M., & Pfingst, B. E. (1982). Tissue impedance and current flow in the implanted ear. Implications for the cochlear prosthesis . *Annals of Otology, Rhinology and Laryngology Supplement (United States), 91(Suppl 98),* 3-8.

Spelman, F. A., Pfingst, B. E., Miller, J. M., Hassul, M., & Powers, W. E. (1980). Biophysical measurements in the implanted cochlea. *Oto-Laryngology: Head-Neck Surgery, 88,* 183-187.

Spoendlin, H., & Schrott, A. (1989). Analysis of the human auditory nerve. *Hearing Research, 43,* 25-38.

Steele, C. W. (1987). *Numerical Computation of Electric and Magnetic Fields* New York: Van Nostrand Reinhold Company Inc.

Strelioff, D. (1973). A computer simulation of the generation and distribution of cochlear potentials. *Journal of the Acoustical Society of America, 54(3),* 620-629.

Suesserman, M. F., & Spelman, F. A. (1993). Lumped-parameter model for *in vivo* cochlear stimulation. *IEEE Transactions on Biomedical Engineering, 40(3),* 237-245.

Tye-Murray, N., Tyler, R. S., Woodworth, G. G., & Gantz, B. J. (1992). Performance over time with Nucleus or Ineraid cochlear implant. *Ear and Hearing, 13(3),* 200-209.

Tykocinski, M., Cohen, L. T., Pyman, B. C., Roland, J. T. Jr., Treaba, C. G., Palamara, J., Dahm, M. C., Shepherd, R. K., Xu, J., Cowan, R. S., Cohen, N.

L., & Clark, G. M. (2000). Comparison of electrode position in the human cochlea using various perimodiolar electrode arrays. *American Journal of Otology, 21,* 205-211.

Ulehlova, L., Voldrich, L., & Janisch, R. (1987). Correlative study of sensory cell density and cochlear length in humans. *Hearing Research, 28,* 149-151.

Van den Honert, C., & Stypulkowski, P. H. (1987). Single fiber mapping of spatial excitation patterns in the electrically stimulated auditory nerve. *Hearing Research, 29,* 195-206.

Wang, G., Vannier, M. W., Skinner, M. W., Kalender, W. A., Polacin, A., & Ketten, D. R. (1996). Unwrapping cochlear implants by spiral CT. *IEEE Transactions on Biomedical Engineering, 43(9),* 891-900.

Webb, R. L., Clark, G. M., Shepherd, R. K., Franz, B. K., & Pyman, B. C. (1988). The biological safety of the Cochlear Corporation multiple-electrode intracochlear implant. *American Journal of Otology, 9(1),* 8-13.

Welling, D. B., Hinojosa, R., Gantz, B. J., & Lee, J. T. (1993). Insertional trauma of multichannel cochlear implants. *Laryngoscope, 103(9),* 995-1001.

White, J. A., Burgess, B. J., Hall, R. D., & Nadol, J. B. (2000). Pattern of degeneration of the spiral ganglion cell and its processes in the C57BL/6J mouse. *Hearing Research, 141,* 12-18.

Wilson, B. S., Lawson, D. T., & Zerbi, M. (1996). Speech processors for auditory prostheses. *NIH Progress Report (2nd quarterly)*.

Zappia, J. J., Niparko, J. K., Oviat, D. L., Kemink, J. L., & Altschuler, R. A. (1991). Evaluation of the temporal bones of a multichannel cochlear implant patient. *Annals of Otology, Rhinology and Laryngology, 100,* 914-921.

Zrunek, M., Lischka, M., Hochmair-Desoyer, I. J., & Burian, K. (1980). Dimensions of the scala tympani in relation to the diameters of multichannel electrodes. *Archives of Oto-Laryngology, 229,* 159-165.

Errata

1. Legend figure 2.3:
   "mammalian cochlea" should be replaced with "guinea pig cochlea"

2. The following sentence should be added to the end of the first paragraph of Chapter 2, section 2.2.4 on page 18:
   This is because the model is a purely resistive model and because of the change in the distance between the stimulation electrodes and the target neural elements. Also refer to Errata 4 and Chapter 2, section 2.2.5.

3. Legend Figure 2.4:
   The following sentence should be added at the end of the legend: "Note that the location of the modelled spiral ganglion corresponds with the location of the spiral ganglion in Figure 2.3."

4. The following paragraph should be added after the first line on page 24:
   Scaling of the resistivity to compensate for increased membrane thickness is based on the equation

$$\boldsymbol{J} = \frac{1}{\rho}\boldsymbol{E} = \frac{1}{\rho}\frac{V}{\boldsymbol{d}} \qquad \text{(E1)}$$

   where $\boldsymbol{d}$ is a distance vector from the source $\boldsymbol{J}$ to the location where the potential V is to be calculated. Equation E1 shows that when the product of and $|\boldsymbol{d}|$ is kept constant, V will be unique for a specific $\boldsymbol{J}$. This principle is also used to scale the resistivities of the perilymph to simulate tapering of the cochlea (Chapter 3, section 2.2.1).

5. The following sentence should be added before the sentence starting on line 5 on page 22:
   This observation is based on equation E1 that shows that, given a fixed distance and a fixed resistivity of the tissues between the electrode and the nerve fibres, lower current density (for the larger electrode) will result in a lower potential at the target neural elements (and therefore an increase in threshold current relative to the threshold current of the other electrode in the pair).

6. Legend Table 2.3:
   Add the following reference to the legend: (Schwartz & Eikhof, 1987)

7. Table 2.4
   The symbols and units for the parameters *Faraday's constant* and *Gas constant* are interchanged.